EXPERIMENTAL/ANALYTICAL PREDICTIVE MODELS OF DAMPED STRUCTURAL DYNAMICS

by

Etienne Balmès

S.M., Massachusetts Institute of Technology (1991)

D.E.A. UPMC, Paris VI (1990)

Ingénieur de l'Ecole Polytechnique (1989)

Submitted to the Department of
Aeronautics and Astronautics
in partial fulfillment of the
requirements for the degree of

Doctor of Philosophy

at the

Massachusetts Institute of Technology

May, 1993

Signature of Author_____
Department of Aeronautics and Astronautics
May 10, 1993

Certified by_____
Professor Edward F. Crawley
Thesis Supervisor, Professor of Aeronautics and Astronautics

Certified by_____
Professor Michael Athans
Professor of Electrical Engineering

Certified by_____
Professor John Dugundji
Professor of Aeronautics and Astronautics

Accepted by_____
Professor Harold Y. Wachman
Chairman, Department Graduate Committee

EXPERIMENTAL/ANALYTICAL PREDICTIVE MODELS OF DAMPED STRUCTURAL DYNAMICS

by

Etienne Balmès

Submitted to the Department of Aeronautics and Astronautics
on May 5, 1993 in partial fulfillment of the requirements for the
Degree of Doctor in Philosophy at the Massachusetts Institute of Technology

Abstract

Traditional analytical design and validation tools, such as the finite element method, do not generally allow an accurate representation of damping mechanisms. Identified experimental models accurately model the true system properties, but existing methods do not provide efficient ways to separately identify the contributions of the mass/stiffness distribution and those of damping mechanisms. The new solutions developed in this research resolve these difficulties and show how experimental and analytical results can be combined to create high-fidelity predictive models of damped structural dynamics.

A new algorithm for the identification of scaled complex modes from frequency domain experimental data is shown to be effective for the analysis of tests with large numbers of sensors and structures with high modal densities, local modes and significant effects of non-proportional damping. It is then shown that the enforcement of a properness condition on the identified complex modes allows an accurate determination of normal modes and of a non-proportional damping matrix. The application of the method on the case of the MIT/SERC interferometer testbed leads to the first experimental characterization of non-proportional damping.

Parameters of initial FE models are usually inaccurate and the system test data, used to determine experimental models, can also be used to update these parameters. A new classification of FE update methods is proposed and inherent limitations of such procedures are analyzed. For this analysis the case of the interferometer testbed and a new FE update algorithm, based on the use of truncated modal models and the comparison of measured and predicted transfer functions, are used.

The creation of high accuracy predictive models by a combined use of experimental damped normal mode models and updated undamped FE models is then discussed. Using such models of the interferometer testbed, the accuracy of predictions for arbitrary actuator/sensor architectures after known mass, damping or stiffness modifications, and the quality of parametric descriptions of model error are evaluated.

Thesis Supervisor: Dr. Edward Crawley

Title: Professor of Aeronautics and Astronautics

Acknowledgments

I would like to thank the DGA, Direction Générale de l'Armement, and Mr. Alain Quenzer, Directeur de l'Option Recherche, for supporting my research over the past four years.

I am deeply grateful to Professor Edward Crawley, for giving me the support of the Space Engineering Research Center, and for his willingness to become my thesis supervisor, thereby giving me so much of his time. He always provided interesting advice and taught me a lot about engineering practice.

I am also grateful to Professors Michael Athans, John Dugundji, and Andreas von Flotow for all the interesting ideas we discussed together. Special thanks to Larry Leier, for the many times when he has been my proof-reader, and to the members of the Interferometer team, Gary Blackwood, Eric Anderson, Dina Perry, Sam Crawford, John How, and all the others, for making the testbed what it is. Thanks to everyone at SERC who helped me have a good time, specially Brett Masters and Daniel Rey for many shared coffee breaks.

Finally, I dedicate this thesis to my wife, Gwénaëlle, with whom I shared many happy moments during our stay in Boston.

Biography

Degrees

M.S. in Aeronautics and Astronautics at the Massachusetts Institute of Technology, 1991

D.E.A. de Mécanique à l'Université Pierre et Marie Curie (Paris VI), 1990

Ingénieur de l'Ecole Polytechnique, Paris, 1989

Publications

Balmès, E., *Modeling Structural Dynamics for Control*, MIT MS Thesis, SERC report #14-91, 1991

Balmès, E., "High Modal Density, Curve Veering, Localization: A Different Perspective on the Structural Response," *Journal of Sound and Vibration*, 1993, **161**-2

Balmès, E., Crawley, E.F., "Designing and Modeling Structural Dynamics for Control. Applications to the MIT/SERC interferometer testbed," *1st SMAC conference*, Nice (France), December, 1992

Balmès, E., "Integration of Existing Methods and User Knowledge in a MIMO identification algorithm for structures with high modal densities," *IMAC*, 1993, pp. 613-619

Balmès, E., "A Finite Element Updating Procedure Using Frequency Response Functions. Applications to the MIT/SERC Interferometer Testbed.," *IMAC*, 1993, pp. 176-182

Balmès, E., "Hybrid Experimental/Analytical Models of Structural Dynamics: Creation and Use for Predictions," *SDM Conference*, April 1993

Balmès, E., "Experimental and Analytic Structural Dynamic Analysis Toolbox," *(A toolbox for MATLAB™, The MathWorks, Inc., 21 Eliot St., South Natick, MA 01760, USA)*, (to be released)

Table of Contents

NOMENCLATURE

An effort was made to comply with the proposed standard notation of the International Modal Analysis Conference (IMAC) available in Ref. [lie1].

b	actuator input shape matrix (location, direction, calibration)
$\phi_j^T b,\ \psi_j^T b$	modal controllability matrix (of the j^{th} normal / complex mode)
c	sensor output shape matrix (location, direction, calibration)
$c\phi_j,\ c\psi_j$	modal observability matrix (of the j^{th} normal / complex mode)
$\Delta M,\ \Delta C,\ \Delta K$	additive modifications of the mass, damping and stiffness matrices
$\Delta\mu,\ \Delta\Gamma,\ \Delta\Omega$	additive modifications of the modal mass, damping and stiffness matrices
E	correction matrix for high frequency modes
F	correction matrix for low frequency modes
ϕ	real or normal mode of the undamped system
ϕ_T	truncated set of low frequency normal modes (eventually augmented)
Γ	non-diagonal modal damping matrix
η	complex mode modal states
$H(s)$	transfer function matrix
$H(\omega)$	frequency response function matrix
λ_j	complex pole
$M,\ C,\ K$	mass, damping and stiffness matrices
N	number of degrees of freedom of the full finite element model
N_A	number of actuators
N_S	number of sensors
N_T	number of modes in a truncated modal model
p	normal mode pseudo-modal states
θ	complex mode of first order symmetric structural model
q	FE degree of freedom states
s	Laplace variable
$R_j = c\psi_j\psi_j^T b$	residue matrix of the j^{th} complex mode
$T_j = c\phi_j\phi_j^T b$	residue matrix of the j^{th} normal mode (ONLY useful for proportionally damped systems)
u	actuator input
Ω	diagonal modal stiffness matrix (modal frequencies squared)
ψ	complex mode of damped system
y	sensor output
z^{-1}	unit delay operator
$(\,)_I$	identified quantity

STANDARD ABBREVIATIONS

CMIF	complex mode indicator function
DOF(s)	degree(s) of freedom
FD	frequency domain
FE	finite element
I/O	input / output
IT	MIT/SERC interferometer testbed
logLS	logarithmic least squares cost function (see section 3.1.3)
MAC	modal assurance criterion (see section 4.1.2)
MIMO	multi-input, multi-ouput
Re, Im	real part, imaginary part
RMS	root-mean-square
SISO	single-input, single-output
TD	time domain

Chapter I

Introduction

1.1. MOTIVATION

The use of control loops to improve the dynamic characteristics of structures has recently found a number of applications in many different fields. This development, answering an increasing demand for tailored dynamic environments for sensitive instruments, requires at different design and validation stages the availability of high-accuracy structural dynamic models [ball]. The present research introduces a complete framework (see Figure 1.1) allowing the creation of high-fidelity predictive models of structural dynamics, with an original focus on the representation of damping, the use of reduced models, and the combination of experimental and analytical predictions.

The broad objective of high-fidelity structural modeling is achieved through a simultaneous use of two descriptions in terms of local component properties and of global system response.

Local component properties are usually modeled by finite elements, whose parameters (called design parameters) are derived from detailed descriptions of the geometry and physical properties of structural components. These local models are then assembled into a finite element model, which can be used to make predictions of system response for any sensor/actuator architecture as well as for modified system configurations.

For accurate predictions, elements must qualitatively give a physically significant representation of the component behavior within the full frequency range of interest for the system, and they must quantitatively use design parameters that reproduce the actual component properties. Usually for initial FE models, a number of design parameters are not very accurate, so system test results are often used to estimate design parameters with higher accuracy.

Once the system is built, global system tests provide measurements of the system properties as seen through a particular actuator/sensor architecture. In the low frequency range, the response can be described in terms of complex mode contributions, which can be estimated (in a process called identification) using test data. Modes of true systems are

complex because the system is damped. On the other hand, FE model predictions are generally undamped. To combine these two types of models, it is necessary to experimentally determine the system normal modes (which characterize the mass and stiffness properties) and modal damping matrix (which characterizes the dissipation mechanisms).

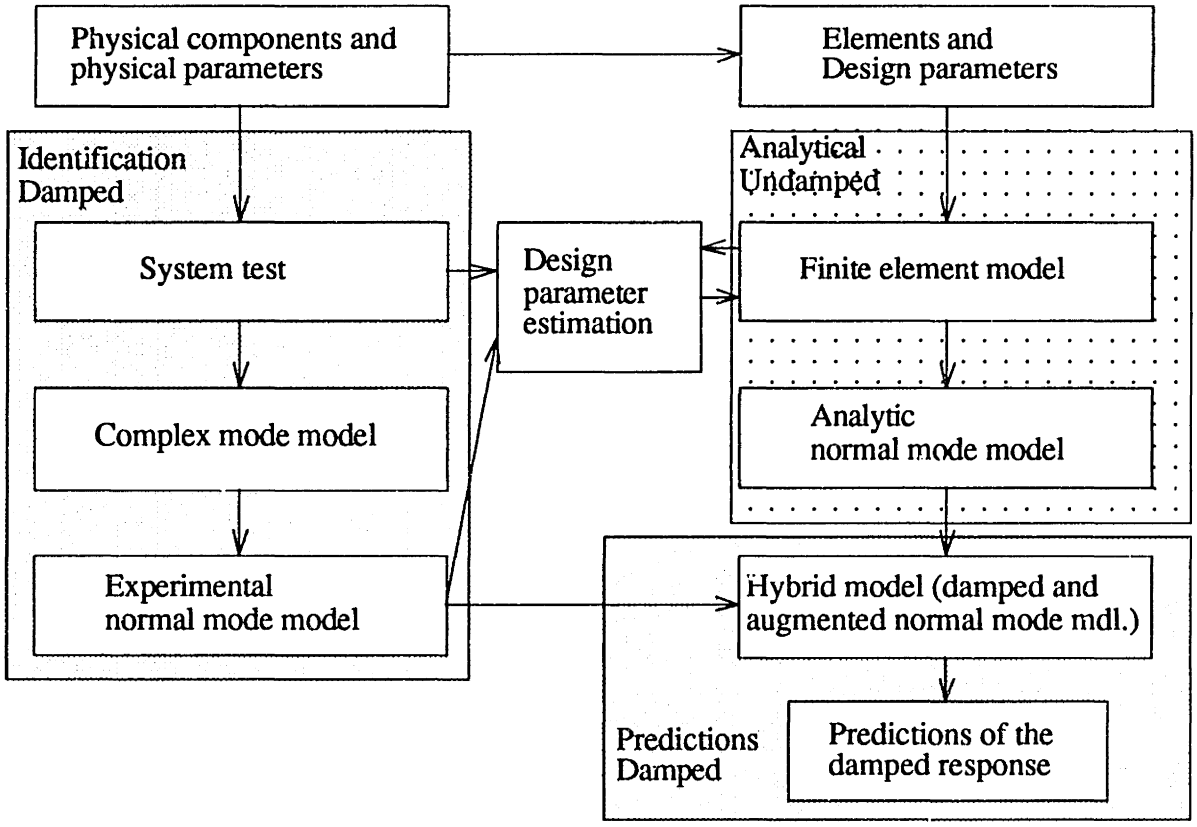

Figure 1.1.: Proposed methodology for the creation of predictive models of non-proportionally damped structures.

Identified normal mode models can be very accurate, but they can only be used to predict the effects of closing loops using the tested actuators and sensors. FE models allow many types of predictions, but are less accurate than identified models and do not in general allow a good representation of damping.

The objectives of this research will thus be to introduce new methods needed to accurately identify experimental normal mode models, to show how initial FE models can be updated using system test results, and to introduce models that combine the accurate but incomplete experimental models with the less accurate but detailed FE models to obtain high-fidelity and yet versatile predictions.

1.2. CONTRIBUTIONS

Experimental parametric models are often identified from system test results. Existing identification methods [full, all1, ewi1, lju1, lev1] are generally based on mathematical formulations of the problem which do not allow a user-guided iterative refinement of the models. Using broadband test data, the new methodology presented in this work alleviates these limitations and leads to extremely accurate identified models characterizing all the dynamics in the test bandwidth with no need for additional computational modes. It is further shown that the method correctly identifies complex modes of systems with high modal densities, local modes, and heavy non-proportional damping coupling.

To accurately represent damped structural dynamics, a clear distinction must be made between normal and complex modes. The relation between the two types of modes has been often studied, but results have remained of limited applicability [ses1]. A complete analysis of normal and complex mode properties is presented, and it is shown that the approximation of the identified complex modes by proper normal modes (corresponding to the truncated modal damping matrix) leads to very accurate normal mode models, even in cases with significant effects of non-proportional damping. The experimental results, obtained for the Interferometer Testbed (IT), mark the first experimental characterization of non-proportional damping.

Normal modes can also be predicted with a higher spatial resolution using finite element models. Parameters of initial FE models are however often inaccurate, so system test results have often been used to improve the estimation of different parameters [cae1, roy1, lin1, ber1, lev1]. FE update methodologies using direct comparisons of measured and predicted transfer functions have recently been introduced to alleviate difficulties of comparing inaccurate FE and identified parametric models. The present work introduces a new update algorithm using reduced predictive models and the log-least-squares cost function. Using this algorithm as an example, an analysis is done of inherent limitations of parameter updating procedures (not all parameters are "identifiable"; some parameters cannot be updated simultaneously).

Analytical and experimental normal mode models can be combined to form hybrid models allowing the prediction of the damped structural dynamics for arbitrary sensor/actuator architectures even after known modifications of the system mass, damping, and stiffness properties. The creation, use, and validity of such models is analyzed. Finally, a parametric description of model error based on these normal mode models is discussed, qualitatively for a simple two mode example, and quantitatively for the interferometer testbed model. This description leads to an original discussion of the

possibilities and limitations of parametric descriptions of model errors for real structural systems.

1.3. OUTLINE

Issues linked to different parametric representations of structural dynamic models are detailed in Chapter II. Properties of linear models of structural dynamics seen through a sensor/actuator architecture are discussed. The spectral decomposition of the response into normal and complex modes is reviewed. Finally, minimal representations of the system properties (dynamic modes, asymptotic contributions, dissipation) in a given low frequency bandwidth are addressed.

Experimental structural dynamic models can be identified from low frequency tests on existing systems. However, existing identification methods do not provide practical ways of handling difficulties linked to high modal densities and accurate damping modeling, so original solutions for the identification of parametric models are introduced in Chapter III. Using the minimal representations of Chapter II, a new algorithm is developed to identify the complex mode residues of the system. A method to obtain scaled complex modeshapes from the identified residue matrices is introduced. Then, in order to obtain a separate identification of mass/stiffness and damping properties, a new algorithm is introduced leading to identified models using the normal mode parametrization. Finally, errors linked to the model identification procedures are discussed.

Initial errors are often made on the values of FE model design parameters. Although component tests are clearly the most appropriate to correct these errors, it is often practical to use instead system test results in the form of normal modes or transfer functions. An analysis of the possibilities and limitations of such parameter updates is done in Chapter IV, using in particular an original algorithm based on the comparison of measured and predicted frequency response functions.

Finally, the creation of small but accurate predictive models (called hybrid since they combine experimental and FE models) is discussed in Chapter V. For non-tested sensor/actuator configurations, and for modifications of the mass, damping and stiffness properties, the accuracy of predictions made with such models is analyzed. These models also allow a simple description of the uncertainty in the system dynamics which is detailed.

The relevance and effectiveness of the present work is demonstrated using the MIT/SERC Interferometer Testbed (see the description in appendix) as a real experimental

case history. The applications of the proposed methods are done using a set of experimental measurements of the dynamic response of the interferometer testbed to external excitation at 6 different shaker locations and 28 accelerometers distributed on the truss structure (see Figure 7.3 in the appendix).

In Chapter III, complex and normal mode models of the testbed are identified, and their accuracy is evaluated. In Chapter IV are discussed the creation, refinement, and parametric update of the FE model of the interferometer testbed. Finally, in Chapter V, hybrid experimental/analytical models of the testbed are introduced. Their ability to predict non-tested sensor/actuator configurations as well as the response after mass, stiffness, or damping modifications is analyzed, and a description of uncertainty for these models is discussed.

Chapter II

Linear Models of Structural Dynamics

From a theoretical point of view, this chapter reviews and justifies different representations of linear models as well as underlying physical assumptions that will be used for throughout this report. Most of the points made have been previously considered by different authors, so that the objective this chapter is only to provide a complete and consistent treatment of all the aspects relevant to this research.

In section 2.1, assuming that exact (potentially infinite dimensional) descriptions of structural dynamics exist, physical assumptions implied in such models are first reviewed. Then, two forms of spectral decomposition of the dynamic response, using complex and normal modes respectively, are introduced and their properties detailed.

In section 2.2, experimental constraints are considered and finite dimensional models representing the response of the system in a restricted low frequency bandwidth are introduced. The model truncation process relating the ideal full order model to a minimal low order model for the considered bandwidth is detailed. Corrections for the effects of truncated dynamics are introduced. Finally, the validity of the representation of dissipation by a truncated viscous damping model is addressed.

2.1. IDEAL LINEAR MODELS FOR STRUCTURAL DYNAMICS

2.1.1. FUNDAMENTAL ASSUMPTIONS

In the present work, it is assumed that the low frequency response of the structure can be accurately represented by linear time-invariant models of the form

$$\begin{aligned} M\ddot{q} + C\dot{q} + Kq &= bu \\ y &= cq \end{aligned} \tag{2.1}$$

where u is the vector of inputs, y is a vector of displacement measurements, M, C, and K are respectively the mass, damping, and stiffness matrices of the system in the arbitrary set of coordinates q (the model is taken of order N which can be infinite for a continuous model). Outputs proportional to rate take the form $y_{vel.} = c\dot{q}$, which has not been shown

for clarity purposes. M is the system mass matrix in the coordinate system q, corresponding to a system kinetic energy of the form $U = \frac{1}{2}\dot{q}^T M\dot{q}$. Similarly K is the system stiffness matrix in the coordinate system q, corresponding to a system strain energy of the form $T = \frac{1}{2}q^T Kq$.

The actuator input shape matrix b and the sensor output shape matrix c are introduced here as a compact but complete notation allowing a characterization of the actuator and sensor properties. In the simplest case, a unit force input at a degree of freedom q_l, the input shape matrix is

$$b = \begin{bmatrix} \vdots \\ 1 \\ \vdots \end{bmatrix} \leftarrow l. \tag{2.2}$$

However, most actuators have inputs that are not in the direction of the initial model DOFs, that couple several DOFs, and that are not properly scaled (e.g. an active strut introduces a relative force input between to points in a direction that usually does not match the DOF directions and may use a voltage for u even though the product bu must be a force). Thus, for a system with N_A actuators b is a N by N_A matrix whose columns contain the location, direction and scaling information of the force patterns applied on each of the DOFs q for unit inputs in each of the actuators.

Similarly, for a system with N_S sensors, c is a N_S by N matrix whose rows contain the location, direction and scaling information linked to each output. A more compact notation, using an index to indicate which of the DOFs q is measured (i.e. $y = q_l$), is often used by other authors, but becomes cumbersome if sensor measurements are linear combinations of the response at different DOFs with arbitrary calibration coefficients (e.g. y in Volts for q in Inches).

A further motivation to use both input b and output c shape matrices is to explicitly show the duality of these two quantities (which is well known for control problems). In particular, if an actuator and a sensor are collocated and dual (e.g. force to collocated translation, moment to collocated rotation) their input and output shape matrices are transpose of each other ($c = b^T$) (provided that M, C, and K are mass, damping, and stiffness matrices of the system and that consistent calibration coefficients are used). This property, which clearly does not depend on a particular choice of coordinates q, will be used in the modal coordinate system to uniquely define scaled estimates of the system modal controllability and observability matrices.

In the model (2.1), the sensors/actuators are implicitly taken to have no dynamics and the system matrices are assumed to be symmetric positive definite. These two assumptions, motivated below, will be used throughout this work.

Time delays and other actuator/sensor dynamics should be characterized independently of the structural modeling process and appended to the model. Furthermore, the effect of such dynamics should be removed from the experimental data used as they are usually not considered to be part of the structural system described by (2.1). For control design however, it will generally be necessary to append those dynamics to the model.

Displacement or velocity actuators have dynamics (zeros) coming from the fact that the force input to the structure depends not only on the prescribed displacement, but also on the corresponding velocity and acceleration (see Ref. [gir1] for example). Furthermore, even the exact system equations (2.1) then depend on a particular actuator architecture, so that the use of a unique model for predictions in different configurations becomes a very difficult problem that will not be considered in the present work.

For most structural systems, symmetric equations of motion (M, C, and K symmetric) can be derived (e.g. [mei1]). Particular cases, such as aeroelasticity (where external aerodynamic forces lead to an asymmetric stiffness [bis1]) or rotating machinery with gyroscopic damping (antisymmetric damping matrix), will not be considered since this would only obscure the analysis.

Finally, the system matrices will be assumed to be positive definite because of the following physical properties: 1) all DOF have inertia, thus for non-zero motion the systems kinetic energy is strictly positive, so that the mass matrix must be positive definite, 2) for any forced harmonic motion the system does not create energy, so that the damping matrix C must be positive semi-definite, 3) as the kinetic energy, the strain energy is always positive, so that the stiffness matrix K must be positive semi-definite (it may be positive semi-definite if rigid body modes exist).

2.1.2. Complex Modes

For linear models, it is well known that the system response can be represented as a summation of uncoupled modal contributions (this is usually called a spectral decomposition). Without particular assumptions on the system damping matrix C, the modes of the system (2.1) are complex and can be found as follows. The set of equations (2.1) can be represented as a first order symmetric system

$$\begin{bmatrix} C & M \\ M & 0 \end{bmatrix}\begin{bmatrix} \dot{q} \\ \ddot{q} \end{bmatrix}+\begin{bmatrix} K & 0 \\ 0 & -M \end{bmatrix}\begin{bmatrix} q \\ \dot{q} \end{bmatrix}=\begin{bmatrix} b \\ 0 \end{bmatrix}u$$
$$y=\begin{bmatrix} c & 0 \end{bmatrix}\begin{bmatrix} q \\ \dot{q} \end{bmatrix} \tag{2.3}$$

To this representation of the system equations is associated the eigenvalue problem

$$\begin{bmatrix} C & M \\ M & 0 \end{bmatrix}\theta\Lambda+\begin{bmatrix} K & 0 \\ 0 & -M \end{bmatrix}\theta=0, \tag{2.4}$$

where θ is the $2N$ by $2N$ matrix of eigenvectors and Λ is the diagonal matrix of $2N$ eigenvalues (poles of the damped system). It can be easily shown that the eigenvectors θ have the specific form

$$[\theta]=\begin{bmatrix} \psi \\ \psi\Lambda \end{bmatrix} \text{ with } \Lambda=\begin{bmatrix} \lambda_1 & & \\ & \ddots & \\ & & \lambda_{2N} \end{bmatrix}. \tag{2.5}$$

where $2N$ complex modes ψ come in complex-conjugate pairs for the symmetric systems considered here (for the rest of this work it will thus be implicitly assumed that $\psi_{[N+1\cdots 2N]}=\overline{\psi}_{[1\cdots N]}$ and $\lambda_{[N+1\cdots 2N]}=\overline{\lambda}_{[1\cdots N]}$). Although it has not been proved in general that a full set of complex modes exist, this will be assumed here (except to treat cases with rigid body modes for which only the normal modes are defined).

The fact, that the complex modes are solution of the eigenvalue problem (2.4), implies two orthogonality conditions on the complex modeshapes

$$\theta^T\begin{bmatrix} C & M \\ M & 0 \end{bmatrix}\theta=\psi^T C\psi+\Lambda\psi^T M\psi+\psi^T M\psi\Lambda=\mu \tag{2.6}$$

$$\theta^T\begin{bmatrix} K & 0 \\ 0 & -M \end{bmatrix}\theta=\psi^T K\psi-\Lambda\psi^T M\psi\Lambda=-\mu\Lambda \tag{2.7}$$

where μ is a diagonal matrix of modal scaling coefficients which are non-physical quantities depending uniquely on the way the eigenvectors ψ are scaled.

Throughout the rest of this work it will be assumed that the modes are scaled so that $\mu=I$ *(identity) as this simplifies notations.* However, it should be noted that $\mu_j=\lambda_j-\overline{\lambda}_j=\pm i2\omega_j\sqrt{1-\zeta^2}$ is another traditional scaling for the complex modes, which tends to maximize the real part of the complex modes and, in the case of proportionally damped structures, leads to a particular matrix of complex modes $\psi=[\phi\ \ \phi]$, where the ϕ are the mass normalized normal modes (see section 2.1.3).

Finally, although the direction of a complex mode in the complex vector space is unchanged for different scaling conditions, the geometrical appearance of the real and imaginary parts of the complex mode depend on the phase implied by the scaling condition [ses1].

The complex modes lead to a spectral decomposition of the system equations: provided that the scaling condition (2.6) (with $\mu=I$) is verified, one can use complex mode states η defined by $q=\theta\eta$ to rewrite the system equations (2.3) in the frequency domain as

$$\begin{aligned} [I]s\eta-[\Lambda]\eta&=\begin{bmatrix}\psi^T & \Lambda\psi^T\end{bmatrix}\begin{bmatrix}b\\0\end{bmatrix}u \\ y&=[c\ \ 0]\begin{bmatrix}\psi\\ \psi\Lambda\end{bmatrix}\begin{bmatrix}\eta\\ s\eta\end{bmatrix}\end{aligned} \tag{2.8}$$

where the modal states η are uncoupled (Λ is diagonal), so that the transfer function matrix $H(s)$ from the input to a displacement output can be written as a simple sum over all the modes

$$H(s)=\sum_{j=1}^{2N}\frac{c\psi_j\psi_j^T b}{s-\lambda_j}\,. \tag{2.9}$$

In this representation, $c\psi_j$ is the j^{th} mode modal observability matrix, $\psi_j^T b$ is the j^{th} mode modal controllability matrix, and the contribution of each mode depends on their product (the residue matrix $R_j=c\psi_j\psi_j^T b$). For non-symmetric systems, left and right complex modes are defined. The modal observability is then $c\psi_j^R$ and the modal controllability $\psi_j^L b$, but the form of (2.9) is unchanged.

The scaling $\mu=I$ of the complex modes led to the expression (2.9) where the residue matrix for each of the modes is given by $R_j=c\psi_j\psi_j^T b$. Conversely for a measured residue matrix $\tilde{R}_j$ such that (2.9) can be used to generate the estimated transfer function, $c\psi_j\psi_j^T b=\tilde{R}_j$ is an estimate of the product of the modal observabilities and controllabilities corresponding to complex modes scaled by $\mu=I$. Thus, scaling the complex modes with the analytical condition (2.6) (with $\mu=I$) and the enforcement, for b and c known, of the formal equality $R_j=c\psi_j\psi_j^T b$ are equivalent. This property will lead to the possibility of scaling experimentally identified complex modes in section 3.2.3.

2.1.3. NORMAL MODES

Although this is not realizable in practice, one can consider the undamped system associated with (2.1) (i.e. set C to zero). As for the damped system which had complex modes, the dynamics of this hypothetical undamped second order system can be decomposed spectrally on a basis of *normal modes* defined by the eigenvalue problem

$$-M\phi\Omega + K\phi = 0. \tag{2.10}$$

where ϕ is the N by N matrix of normal modes, and Ω the diagonal matrix of N normal mode frequencies.

The fact that the normal modes are solution of the eigenvalue problem (2.10), implies that the normal modes verify two orthogonality conditions with respect to the mass and the stiffness

$$\phi^T M\phi = \mu \text{ and } \phi^T K\phi = \mu\Omega \tag{2.11}$$

where μ is a diagonal matrix of modal masses (which are non-physical quantities) depending uniquely on the way the eigenvectors ϕ are scaled. *Throughout this work it will be assumed that the modes are mass normalized so that μ=I.*

Using normal mode states p defined by $q=\phi p$ (where the normal modes ϕ are assumed mass normalized), the system equations (2.1) can be rewritten as

$$\begin{aligned} I\ddot{p} + \Gamma\dot{p} + \Omega p &= \phi^T b u \\ y &= c\phi p \end{aligned} \tag{2.12}$$

or, in the usual first order form,

$$\begin{aligned} \begin{bmatrix} \dot{p} \\ \ddot{p} \end{bmatrix} &= \begin{bmatrix} 0 & I \\ -\Omega & -\Gamma \end{bmatrix} \begin{bmatrix} p \\ \dot{p} \end{bmatrix} + \begin{bmatrix} 0 \\ \phi^T b \end{bmatrix} u \\ y &= \begin{bmatrix} c\phi & 0 \end{bmatrix} \begin{bmatrix} p \\ \dot{p} \end{bmatrix} \end{aligned} \tag{2.13}$$

where Ω is the diagonal matrix of squared undamped frequencies ($\Omega = \phi^T K\phi$) and Γ is the normal mode damping matrix projected on the mass normalized normal modes ϕ ($\Gamma = \phi^T C\phi$), $c\phi$ is the normal mode observability matrix and $\phi^T b$ the modal controllability matrix. Note that the identity matrix, Γ, and Ω are respectively the mass, damping, and stiffness matrices in the generalized coordinate system p (normal mode coordinates).

Proportional or modal damping is a usual assumption made for lightly damped structures (see section 2.2.3 for more details), which mathematically corresponds to

having a diagonal damping matrix Γ. Using the pole damping ratio ζ_j and natural frequency ω_j, one has for a proportionally damped system $\Omega_{jj} = \omega_j^2$ and $\Gamma_{jj} = 2\zeta_j\omega_j$. In this case, the system equations (2.12) are decoupled, leading to a spectral decomposition of the damped system response by pairs of poles

$$H(s) = \sum_{j=1}^{N} \frac{c\phi_j\phi_j^T b}{s^2 + 2\zeta\omega_j s + \omega_j^2} \tag{2.14}$$

where all the parameters except the damping ratios ζ_j only depend on the mass and stiffness distribution and can thus be predicted accurately with an undamped (FE) model.

Note that, as was the case for the complex modes, the use of the normal mode residue matrix $R_j = c\phi_j\phi_j^T b$ in (2.10) is a necessary and sufficient condition for the normal modes to be mass normalized ((2.11) verified with $\mu=I$).

In a number of cases the representation of damping by a diagonal Γ is not accurate, so that a non-proportional damping model must be used (Γ is then a full but positive definite matrix). However, even for a non-proportionally damped system, the normal mode frequencies Ω, modal controllability $\phi^T b$ and observability $c\phi$ matrices remain physical properties of the ideally undamped system and can thus be predicted by FE models.

A major problem for accurate predictions in cases with significant non-proportional damping is the determination of normal mode properties (Ω, Γ, $\phi^T b$ and $c\phi$) from a set of finite bandwidth experimental measurements. True normal and complex modes depend on the continuous infinite system, but the damping is measured experimentally for a restricted set of modes. The restriction of the damping model to a truncated set of normal modes will be discussed in section 2.2.3 and based on this assumption, a new method for the determination of normal modes from identified complex modes, leading to the first experimental characterization of non-proportional damping, will be introduced in Chapter III.

2.2. FINITE DIMENSIONAL MINIMAL MODELS OF CONTINUOUS STRUCTURES

Structures are non-linear, time-varying, and infinite dimensional systems. However, it will be assumed here (and it is usually true) that they are weakly non-linear, vary little and slowly with time. Under these assumptions, there theoretically exists an infinite linear time-invariant model of the form (2.1) representing the system very accurately.

For analytical models, all physical assumptions are valid for limited frequency ranges (or equivalently for long enough wavelengths). Thus the response can only be accurately

represented for finite bandwidths. Continuous infinite models are more likely to have large bandwidths, but systems such as real space structures are too complex to be represented in detail with continuous models, so that in practice the bandwidth limitations are very similar whatever the model used (discretized finite or continuous infinite).

Experimentally, the sensor/actuator architecture limits the number of points at which the modeshapes can be known. Furthermore, sensor and actuator dynamics (as well as the sampling frequency for digital systems) limit the frequency range were the measured response corresponds to the physical response being modeled. Overall, experimental models are generally less limited than analytical models in frequency, but more limited in spatial resolution. These properties motivated the introduction of hybrid experimental/ analytical models in Chapter V, which retain the accuracy of experimental models, but increase the spatial resolution by combining experimental and analytical modeshapes.

Thus only approximate models, valid over a finite bandwidth, can be obtained. The spectral decomposition into complex modes (2.9) or normal modes (2.12) allows to distinguish the frequency ranges of dynamic contributions as the largest fraction of the modal response is in a narrow (for lightly damped structures) frequency band near the modal resonance. The analysis presented below will focus on normal modes, as the case of complex modes is mostly useful for the identification of experimental models which is addressed in Chapter III. (Truncated complex mode models will be detailed in section 3.1.2).

As will be shown in Chapters IV and V, some of high frequency modes of a model, even if they are inaccurate, are useful for predictions of the response for multi-configuration systems. However, the meaning of these modes is linked to a particular modeling approach, their properties are not direct estimates of physical properties which should clearly be invariant, and an accurate use of these contributions can usually only be achieved for analytical models where their relation to the model is known.

It was seen in section 2.1.3 that normal mode coordinates were physical properties of the system, the objective of this section will thus be to describe the minimal set of physical parameters linked to the normal mode coordinates that characterize the response of the system in a finite bandwidth.

2.2.1. Truncated Normal Mode Models

To characterize the response of a single configuration system in a given model frequency range, one considers the spectral decomposition of the system dynamics into independent modal contributions assuming at first proportional damping as done in (2.14). The SISO frequency response of a generic lightly damped structural system is

plotted in Figure 2.1. It is clear that only the two modes with poles in the model frequency range have significant dynamic contributions (the truncated model which only keeps these two modes accurately captures the resonances in the model bandwidth). For other modes, only the asymptotic contributions (constant for high frequency modes and roll-off for low frequency modes) have a noticeable effect. When these asymptotic terms are added to correct the truncated model, the complete transfer function including zeros is well predicted in the model bandwidth.

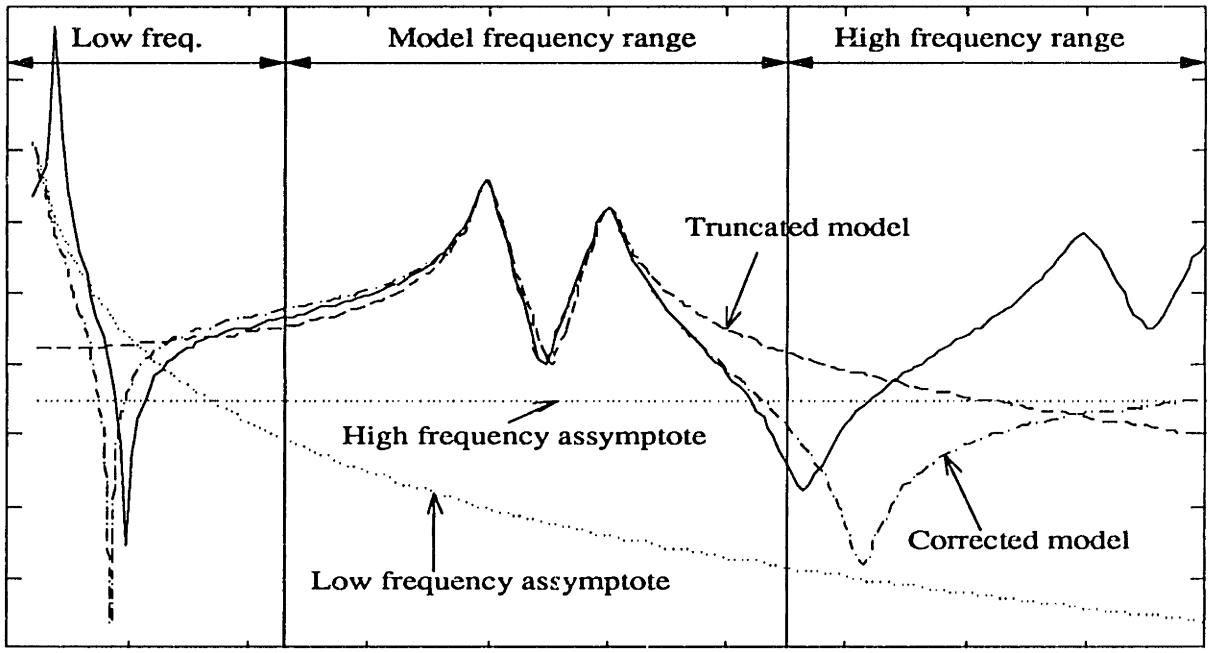

Figure 2.1: Finite bandwidth structural models: the physical parameters (important factors) are modes in the bandwidth and asymptotic contributions of modes in the low and high frequency ranges.

The generalization of this example leads to the creation of truncated modal models as follows. For a proportionally damped system, the contributions of the different modes are uncoupled as in (2.14). In the frequency range of the model, the physical characteristics of the system are the normal modes ϕ_T (whose frequencies are within the model frequency range), and the asymptotic stiffness E and mass F correction terms (which will be detailed in section 2.2.2). These properties are fully described by the truncated normal mode model

$$\begin{aligned} \left(s^2 I + s\Gamma_{TT} + \Omega_{TT}\right) p_T &= \phi_T^T b u \\ y &= c\phi_T p_T + E + \frac{F}{s^2} \end{aligned} \tag{2.15}$$

For a non-proportionally damped system the same truncation can clearly be applied, but it will only be accurate if the effects induced by off-diagonal terms in Γ (which couple the retained modes ϕ_T and the truncated modes) are negligible. For the interferometer testbed, it will be shown in section 3.3 that this is a good assumption even for a system with significant effects of non-proportional damping.

Truncated modal models of the form (2.15) are accurate representations of the Input/Output response of the system in a given configuration (where a unique set of modes is defined). Furthermore, all their terms have a significant influence on the modeled response in the considered frequency range, the model is thus *minimal* in the sense that any smaller model would not describe all the resonances in the response.

For a given sensor/actuator architecture, one could further reduce the model size, if some modes do not have a significant impact on the I/O response. Such reductions have been considered, in the low frequency range both for control design (e.g. [you1, gre1]) and for structural dynamics (e.g. [mor1]), and at higher frequencies using energy propagation arguments (e.g. [lyo1, nef1]). However, when using such methods it is important to assess the exact validity of the model for its final purpose. Considering a controlled structure application for example, a mode with a small open-loop contribution may lead to a closed-loop instability [ske1] so that stability must be checked with a model (such as those considered in this work) containing all the dynamics within the control bandwidth. (Note that such a check is not a full proof of stability as high frequency dynamics can also be destabilized).

Finally, the properties of the truncated modal model correspond to physical properties of the system. Ω_{TT}, Γ_{TT}, $\phi_T^T b$, and $c\phi_T$ are respectively estimates of the frequency, damping coupling coefficients, modal controllability, and modal observability of the corresponding true normal modes. E, and F are correction matrices allowing the model to have accurate static stiffness and mass properties respectively.

2.2.2. Asymptotic Corrections for Finite Bandwidth Models

A direct truncation of modes that are out of the model bandwidth neglects the effects of these modes in the bandwidth and results in a somewhat incorrect prediction of the system static stiffness (truncation of high frequency modes) and mass (truncation of low frequency modes). It is thus generally useful to add a stiffness and a mass correction to a truncated set of normal modes.

For a simpler presentation of the problem, it will at first be assumed that truncated high frequency modes are proportionally damped so that from (2.14) the displacement contribution of any of these modes takes the form

$$\frac{c\phi_j\phi_j^T b}{s^2+2\zeta\omega_j s+\omega_j^2}. \tag{2.16}$$

The dynamic contribution of high frequency modes in the model bandwidth tends to a constant (for $s\ll\omega_j$ one has $s^2+2\zeta\omega_j s+\omega_j^2\approx\omega_j^2$). This approximation can be used for all the high frequency modes in (2.14) leading to a model that is extremely accurate at low frequencies (in the model bandwidth), but does not have the dynamics of the truncated modes

$$H(s)=\sum_{j\in\left\{\begin{smallmatrix}\text{kept}\\ \text{dynamic}\end{smallmatrix}\right\}}\left\{\frac{c\phi_j\phi_j^T b}{s^2+2\zeta\omega_j s+\omega_j^2}\right\}+\sum_{j\in\left\{\begin{smallmatrix}\text{truncated}\\ \text{high freq.}\end{smallmatrix}\right\}}\left\{\frac{c\phi_j\phi_j^T b}{\omega_j^2}\right\} \tag{2.17}$$

The correction for high frequency modes is known in different forms to researchers using linear dynamic systems. For component mode synthesis problems (e.g. [cra3]), it is introduced as "static" modes used to complement the set of modes kept in the model. This leads to the physical interpretation of the asymptotic correction as modeling the exact static response. In fact, as shown in more detail in Ref. [bal5], the static correction can be expressed as a function of the true system stiffness as follows

$$\sum_{j\in\left\{\begin{smallmatrix}\text{truncated}\\ \text{high freq.}\end{smallmatrix}\right\}}\left\{\frac{c\phi_j\phi_j^T b}{\omega_j^2}\right\}=cK^{-1}b-\sum_{j\in\left\{\begin{smallmatrix}\text{retained}\\ \text{modes}\end{smallmatrix}\right\}}\left\{\frac{c\phi_j\phi_j^T b}{\omega_j^2}\right\} \tag{2.18}$$

where the correction for high frequency modes appears clearly as the true static response ($cK^{-1}b$) less the static contribution of retained (non-high frequency) modes. The right hand expression of the static correction in (2.18) should be used in practical FE applications where only the normal modes of the considered frequency band are known accurately but the static response can be computed through a solution of the static FE problem which is usually constructed to be very accurate.

For control applications, the static correction has been used for model reduction purposes. As high frequency dynamics are truncated from the model it was found that the asymptotic low frequency contribution of the truncated modes has a significant influence on the response (particularly on the location of zeros) so that a correction is needed. The so-called static correction is classically introduced as a constant feedthrough term (the constant in (2.18)), which leads to several problems:

- having a constant feedthrough term at all frequencies generates problems with many control synthesis methods which do not allow such a term
- the constant feedthrough does not verify the physical property that the response rolls-off at high frequencies (which is why control synthesis methods have problems)
- a constant feedthrough term has no correction for the velocity which introduces significant errors for controlled structures where velocity feedback is used [bal5].

An original solution [bal5] to these problems is to use a "correction" mode with critical damping and an arbitrary cut-off frequency ω_c (in practice cut-off frequencies a decade above the model bandwidth are appropriate). The dynamics of the correction mode are chosen so that one clearly has the same low frequency behavior for displacement

$$\sum_{j\in\left\{\begin{smallmatrix}\text{truncated}\\ \text{high freq.}\end{smallmatrix}\right\}} \left\{\frac{c\phi_j\phi_j^T b}{\omega_j^2}\right\} \approx \frac{\omega_c^2}{s^2+2\omega_c s+\omega_c^2} \sum_{j\in\left\{\begin{smallmatrix}\text{truncated}\\ \text{high freq.}\end{smallmatrix}\right\}} \left\{\frac{c\phi_j\phi_j^T b}{\omega_j^2}\right\}, \tag{2.19}$$

but a correction term for velocity measurements $y_{\text{vel.}}$ proportional to $\dot{u}$ is now naturally defined as shown in the following state-space model

$$\begin{bmatrix}\dot{p}\\ \ddot{p}\end{bmatrix} = \left[\begin{array}{cc|cc} 0 & & I & \\ & 0 & & I \\ \hline -\Omega & & -\Gamma & \\ & -\omega_c^2 & & -2\omega_c \end{array}\right] \begin{bmatrix} p \\ \dot{p}\end{bmatrix} + \begin{bmatrix} 0 \\ 0 \\ \phi^T\dot{o} \\ I \end{bmatrix} u$$

$$\begin{bmatrix} y_{\text{disp.}} \\ y_{\text{vel.}}\end{bmatrix} = \left[\begin{array}{c|c} c\phi\ \omega_c^2 c\left(K^{-1} - \sum_{j\in\{\text{dyn. mode}\}}\left\{\phi_j\phi_j^T/\omega_j^2\right\}\right)b & 0 \\ \hline 0 & c\phi\ \omega_c^2 c\left(K^{-1} - \sum_{j\in\{\text{dyn. mode}\}}\left\{\phi_j\phi_j^T/\omega_j^2\right\}\right)b \end{array}\right] \begin{bmatrix} p \\ \dot{p}\end{bmatrix} \tag{2.20}$$

The displacement correction is important for the normal mode properties (undamped system) and can be essential for good predictions in cases with large stiffness modifications. For the same reasons, the velocity correction becomes important when accurate damping models are sought and significant modifications of the local dissipation properties are considered (i.e. the addition of a local damper which in terms of modeling introduces a significant amount of rate feedback).

In MIMO cases, a different correction mode must be used for each input. Such an increase is perfectly acceptable for control purposes but may be too large when the

control input is used to represent a modification of the structure (see section 4.3.3 which describes the correction introduced using the FE perspective).

The analysis has been presented for modes with proportional damping. From (2.18) where the correction is seen as a corrected static response, it is clear that the asymptotic contribution of high frequency modes only depends on the system stiffness so that the results remain applicable even for a non-proportionally damped system. However non-proportional damping may induce a coupling of low and high frequency normal modes which will be addressed in section 2.2.3.

For prediction purposes it is also natural to consider the full shape of the correction mode as a mode appended to the set of kept normal modes. To each actuator can be related a correction modeshape

$$\phi_C = \left(K^{-1} - \sum_{j \in \left\{ \begin{matrix} \text{kept normal modes,} \\ \text{other static modes} \end{matrix} \right\}} \left\{ \phi_j \phi_j^T / \omega_j^2 \right\} \right) b, \tag{2.21}$$

which is defined as the static response to the actuator, less the contributions of retained normal modes. This shape is known at all the finite element DOFs q and using the FE shape functions at all the points linked to the underlying continuous model. For an augmented matrix of modes $\phi_T = \left[\phi_{\text{Kept Normal Modes}} \;\; \phi_{\text{Correction Modes}} \right]$ the equations for the truncated normal mode model (2.15) become

$$\begin{aligned} \left(s^2 \mu + s \Gamma_{TT} + \Omega_{TT} \right) p_T &= \phi_T^T b u \\ y &= c \phi_T p_T \end{aligned} \tag{2.22}$$

where the mass matrix μ is still diagonal as the correction modes are constructed in (2.21) to be mass-orthogonalized among themselves and mass-orthogonal to the retained normal modes, Ω_{TT} is a block diagonal matrix (one can easily show that correction modes as defined by (2.21) are also stiffness-orthogonal to the normal modes), the asymptotic term E present in (2.15) has been incorporated in the dynamic correction modes. The sub-bloc of Ω_{TT} corresponding to the static modes, can have arbitrary high frequency dynamics (e.g. a diagonal bloc with correction mode frequencies ω_c^2 as initially proposed in this section, or the projected stiffness matrix $\phi_C^T K \phi_C$ as used in component mode synthesis methods).

In some cases low frequency modes may also be truncated. The rigid mass properties of the system are then inaccurately modeled, so that a correction can be useful. In the model bandwidth, one has for these modes $s \gg \omega_j$ so that $s^2 + 2\zeta\omega_j s + \omega_j^2 \approx s^2$. The total contribution of the low frequency modes can thus be approximated by

$$\sum_{j\in\left\{\substack{\text{low freq.}\\ \text{truncated}}\right\}} \left\{ \frac{c\phi_j\phi_j^T b}{s^2 + 2\zeta\omega_j s + \omega_j^2} \right\} \approx \frac{1}{s^2} \sum_{j\in\left\{\substack{\text{low freq.}\\ \text{truncated}}\right\}} \left\{ c\phi_j\phi_j^T b \right\} \tag{2.23}$$

Using this approximation, the response of the different low frequency modes can be represented using a rigid body (frequency at zero) correction mode per actuator, leading to a corrected model which in the state-space takes the form

$$\begin{bmatrix} \dot{p} \\ \ddot{p} \end{bmatrix} = \left[\begin{array}{c|c} 0 & I \\ \hline -\Omega & -\Gamma \end{array}\right] \begin{bmatrix} p \\ \dot{p} \end{bmatrix} + \left[\begin{array}{c} 0 \\ \hline \phi^T b \end{array}\right] u$$

$$\begin{bmatrix} y_{\text{disp.}} \\ y_{\text{vel.}} \end{bmatrix} = \left[\begin{array}{c|c} c\phi & \sum_{j\in\left\{\substack{\text{low freq.}\\ \text{truncated}}\right\}} \left\{ c\phi_j\phi_j^T b \right\} \\ \hline 0 & c\phi \end{array}\right] \begin{bmatrix} p \\ \dot{p} \end{bmatrix} \tag{2.24}$$

For more details, including practical considerations on how to compute such corrections for cases where only some normal modes are estimated, see reference [bal5].

Except for component mode synthesis problems, such corrections are seldom useful for predictions using analytical models, since low frequency modes are usually known and retained in the truncated model. Their necessity, however, is clear for identification purposes, when tests of suspended structures do not include the low frequency range where the resonances of suspension modes are located.

2.2.3. Representation of Dissipation by the Viscous Damping Model

Dissipation in structures comes from several different sources (e.g. structural damping, friction, viscous damping) with different frequency and spatial characteristics. Dissipation and its frequency dependence has been well characterized for simple elements like bars of different materials (e.g. Ref. [ber5]), and it was even shown that the models obtained remain valid even for extremely low levels of vibration (e.g. Ref. [tin1]). But for complex systems like satellites, a number of uncharacterized phenomena (joint friction and free-play, bond dissipation, cable slackening, etc.) are generally the source of the system damping. Thus, an accurate local model of dissipation would use several types of representation for the different phenomena, would be non-linear, albeit weakly so, and could not in general be obtained for complex systems as most of the dissipation sources in such systems are not characterized.

The only practical solution is thus to represent the averaged contributions of all the dissipation mechanisms by a simplified and usually linear model. In the present work, the linear viscous damping model (rate dependent dissipation) used in the previous sections will be considered. As the viscous damping model is a simplified representation of more complex phenomena, it can only be validated by an assessment of how well the phenomena observed in the system tests are represented.

The viscous damping model is linear, it can thus only represent weakly non-linear dissipation mechanisms. Practically, this implies for experiments, that frequency response functions should not depend on the way they are tested. For example, if sine-sweep and broadband frequency response function estimation tests (see section 3.1.1.) give widely different results, the measured response is non-linear (provided the te s are correctly done) and the validity of the viscous damping model is dubious. The present work is restricted to cases such as the IT for which this property is verified.

It is convenient to consider the viscous damping matrix in normal mode coordinates (called Γ in this work), and a usual simplification of the damping representation is to assume that the matrix Γ is diagonal. This assumption called proportional or modal damping can be seen in many different ways.

An early description of proportional damping can be attributed to Lord Rayleigh [ray1], who showed that damping was proportional if the damping matrix was a linear combination of the mass and stiffness matrices. This description can be extended by describing C as a linear combination of the mass and stiffness matrices at different powers

$$C = \sum_{\alpha,\beta} \left(c_\alpha M^\alpha + c_\beta K^\beta \right). \tag{2.25}$$

A proof of the equivalence between (2.25) and the fact that Γ is diagonal can be found in [cau1]. Other mathematical descriptions linked to the commutation properties of the system matrices can also be used (see Ref. [lia1]).

The definition (2.25) leads to the physical interpretation of proportional damping as evenly distributed damping: if, at all points, dissipation is proportional to the local strain or kinetic energy, (2.25) will be true and a proportional damping model will be accurate. Conversely, (2.25) will not be true for a system with a few local dampers and a non-proportional damping model will be needed.

Although the proportional viscous damping model is very useful for many lightly damped structures, it is sometimes not accurate enough to represent test results well. It is then useful (and usually sufficient) to use a non-proportionally damped model with Γ being a full (but positive semi-definite) matrix.

The positive-definiteness of the damping matrix, expected physically and corresponding mathematically to the fact that the model will predict energy dissipation for any forced motion (as clearly expected from a passive system), limits the possible extent of the effects of non-proportional damping. In fact, as shown in the example treated in section 5.2.2 or in Ref. [par2], damping levels around 1% and modal densities with modal separation of less than 10% are needed to for the apparition of phenomena that cannot be well represented by a proportionally damped model.

A usual characterization of non-proportionally damped systems is that the residues of their complex modes are not in- or out-of-phase, a property which can be shown for the proportional damping case as follows.

As indicated in section 2.1.2, a particular set ψ of $2N$ vectors of dimension N is the set of complex eigenvectors of the system if it verifies the two orthogonality conditions (2.6) and (2.7). For a proportionally damped system, $\psi = [\phi \ \ \phi]$ (remember that there are $2N$ complex modes ψ and N normal modes ϕ (assumed mass normalized)) verifies

$$\begin{bmatrix} \psi^T & \Lambda\psi^T \end{bmatrix} \begin{bmatrix} C & M \\ M & 0 \end{bmatrix} \begin{bmatrix} \psi & \\ \psi\Lambda & \end{bmatrix} = \begin{bmatrix} \phi^T C\phi & \\ & \phi^T C\phi \end{bmatrix} + \Lambda \begin{bmatrix} \phi^T M\phi & \\ & \phi^T M\phi \end{bmatrix} + \begin{bmatrix} \phi^T M\phi & \\ & \phi^T M\phi \end{bmatrix} \Lambda$$

$$\begin{bmatrix} \Gamma & \\ & \Gamma \end{bmatrix} + \Lambda \begin{bmatrix} I & \\ & I \end{bmatrix} + \begin{bmatrix} I & \\ & I \end{bmatrix} \Lambda = \Lambda - \overline{\Lambda} = \begin{bmatrix} \ddots & & \\ & \pm i2\omega_j\sqrt{1-\zeta_j^2} & \\ & & \ddots \end{bmatrix} \qquad (2.26)$$

and

$$\begin{bmatrix} \psi^T & \Lambda\psi^T \end{bmatrix} \begin{bmatrix} K & 0 \\ 0 & -M \end{bmatrix} \begin{bmatrix} \psi & \\ \psi\Lambda & \end{bmatrix} = -\Lambda\left(\Lambda - \overline{\Lambda}\right) \qquad (2.27)$$

so that it is the matrix of the complex eigenvectors of the full order model. This eigenvector matrix however corresponds to the scaling coefficients $\mu = \Lambda - \overline{\Lambda}$ instead of $\mu = I$ (assumed throughout this work). This particular form of the complex mode matrix ψ, where the normal modes are repeated twice, allows (for proportionally damped systems only) to ignore the distinction between normal and complex modes.

Using the form $\psi = [\phi \ \ \phi]$ the complex modes are real, so that all the residues are in phase or out-off phase. When a system is tested the complex modal observability $c\psi$ is identified. From (2.26)-(2.27), the complex modes are, for proportionally damped

systems, equal to ϕ_j modulo a complex scaling coefficient. For any scaling, the complex modal observabilities are thus on a line and by a usual abuse of language they are called *real*. If the observabilities are not on a line (by the same abuse of language they are then called *complex*) and the system is non-proportionally damped. Different other difficulties linked to "complex" modes of non-proportionally damped systems must be addressed as will be done in section 3.3.

Another way to characterize proportional damping is to consider the transfer function expression linked to the complex residue. For the symmetric real problems considered here, the complex modes come in complex-conjugate pairs. Taking the modal transfer function description (2.9) and grouping the complex-conjugate terms leads to

$$H(s) = 2\sum \left\{ \frac{sA_j + \left(\zeta\omega_j A_j - \omega_j\sqrt{1-\zeta^2}B_j\right)}{s^2 + 2\zeta\omega_j s + \omega_j^2} \right\} \tag{2.28}$$

where $A_j = \mathrm{Re}\left(c\psi_j\psi_j^T b\right)$ and $B_j = \mathrm{Im}\left(c\psi_j\psi_j^T b\right)$.

Comparing this expression with the transfer function expression (2.14), one can characterize proportional damping as the fact that the terms A_j are *0* or, in other words, that the different modal velocities $\dot{p}_j$ roll-off independently as s tends to infinity (the system is described as a series of independent second order systems).

As the viscous damping model is a simplification of more complex phenomena, there is no reason to assume that it should be defined for all the model forms. In particular if the modal damping matrix Γ_{TT} of the truncated normal mode model (2.15) allows accurate predictions of system response, there is no need and in practice it is not possible to define the non-truncated matrix. Such a truncation is of course more restrictive than using a full matrix, so that there may exist cases where the model bandwidth needs to be extended to account for the actual phase distribution of the complex modal observabilities. But in practice, as shown in section 3.3, the use of a truncated non-proportional damping matrix is a very effective extension of the proportional damping assumption.

2.3. CONCLUSIONS

The assumptions used for this research, on the dynamics of the system and properties of the actuators and sensors, were reviewed. Analytical properties of complex and normal modes were detailed. Addressing the real case of models valid over a restricted

bandwidth, the validity of truncated normal mode models was discussed. The mass and stiffness corrections for low- and high-frequency truncated modes were detailed. Finally the use of a truncated non-proportional modal damping matrix was introduced as an efficient way to obtain an accurate linearized representation of the complex phenomena leading to the overall system damping.

Chapter III

Identification of Experimental Parametric Models

The most accurate models of the dynamic response are generally obtained through tests of the actual system. The estimation of parametric models (state-space models or other equivalent models detailed in section 3.1.2) from measured test data with no or little *a priori* knowledge of the system is a well studied problem usually called identification. Existing identification algorithms do not take full advantage of the specific properties of lightly damped structures and thus often do not achieve the high accuracy expected in this work. New solutions are proposed in this chapter, which have been successfully applied to analyze different experimental tests, including those from the Interferometer Testbed (IT), which will be used here as a supporting example.

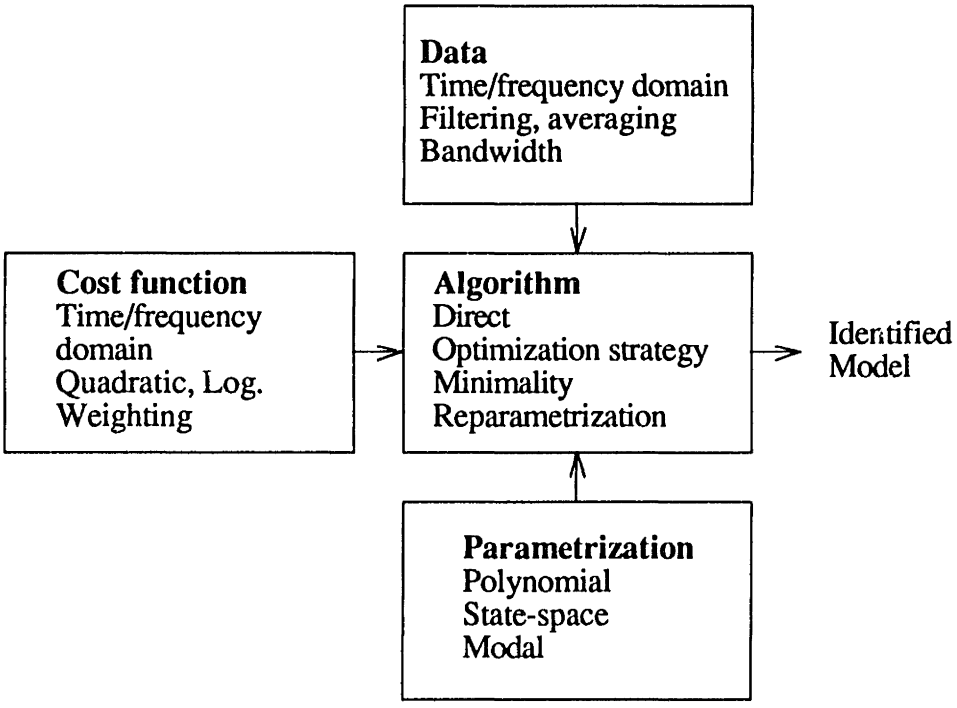

Figure 3.1: The general process of parametric model identification from test data.

As shown in Figure 3.1, identification methods can be seen as directed optimization algorithms, which are differentiated by the use of different treatments of data (applied to

minimize the effects of noise and high frequency dynamics), model parametrizations, cost functions (measuring the difference between the data and the corresponding model predictions), and optimization algorithm (leading to a set of parameters). In section 3.1, following the categories outlined in Figure 3.1, a complete review is done of the different options characterizing identification algorithms.

In section 3.2, a new identification algorithm based on the modal parametrization is detailed. This algorithm optimizes a initial guess of the pole structure determined through other identification algorithms and corrected by the user, so that results are often significantly more accurate than those of other methods. Implementation issues are discussed and the algorithm is shown to be very cost effective for the simultaneous treatment of multiple transfer functions. New solutions to treat problems of model minimality and determine scaled estimates of the complex modal observability and controllability matrices are introduced. In the case of the IT, the algorithm is shown to allow the accurate identification of all the dynamics in the 20-60 Hz frequency range, even though mode 9 is localized to one of the truss legs, modes 6 and 7 are extremely close in frequency, and the effects of non-proportional damping are significant.

Accurate identifications of non-proportionally damped systems imply the use of complex modes. However, only normal modes are predicted by FE analyses. Thus, for problems where a link with the FE predictions is wanted, it is necessary to define an efficient procedure to estimate normal modes from complex modes. However, existing methods (reviewed in section 3.3) have been of limited accuracy when applied to cases with significant contributions of non-proportional damping (most of today's mechanical systems). It is shown in section 3.3 that the complex modes of a non-proportionally damped truncated normal mode model verify a properness condition and that this condition is sufficient for the existence of an exact transformation between the complex and normal mode parametrizations. A new algorithm is then derived to determine, in both cases with as many and more sensors than modes, the set of proper complex modes closest to the measured modes. From these proper modes, the truncated normal mode model can then be determined with no further approximation. For the case of the IT, the overall procedure is shown to be very accurate and to only introduce small distortions from the identified complex mode model. The results presented mark the first successful experimental characterization of non-proportional damping (previous results only considered simple two-mode systems).

Finally, results of identification algorithms are sensitive to noise in the measured frequency response functions. In section 3.4, existing methods for the evaluation of this sensitivity are reviewed and extended to the new complex mode identification algorithm.

Applications to the IT case lead to the conclusion that identification errors obtained with the proposed identification algorithm are smaller than the experimental variations of the system between different tests.

3.1. A Classification of Identification Methods

Identification is the process of determining a parametric model matching the measured response of a system. Researchers in two fields, controls and structural dynamics, have devised a number of somewhat overlapping algorithms (see the reviews in Refs. [full, all1, ewi1, lju1, lev1] and the partial list in table 3.1). As was shown in Figure 3.1, four elements (data, parametrization, cost function, and algorithm) determine the identified models. Rather than describing the attributes of the different existing identification methods, the following sections will review the possible choices within these four categories.

Table 3.1: A *partial* list of usual identification algorithms in the Time (TD) and Frequency (FD) Domains.

Parametrization	Data / Cost fct.	Algorithm
Normal mode, pole	Maximize in-phase response	Force appropriation [ott1]
Complex mode, pole	FD Quadratic	Peak picking, MDOF residue fits [ewi1]
		Complex mode identification [bal3]
		Spanos [spa1]
	FD Log quadratic	Jacques [jac1]
State space model	TD quadratic	System realization [hob1]
		Ibrahim Time Domain [pap1]
		Eigensystem Realization Algorithm [jua1]
		Polyreference [cro1]
		Extended Kalman Filter (e.g. [kar1])
	FD quadratic	Polyreference [zan1]
Polynomial	TD quadratic	Polynomial (ARMAX, OE, etc.) [lju1]
	FD quadratic	Orthogonal polynomials [ric1]
Reduced system matrices	FD quadratic error	Direct system parameter identification [leu1, cra1]

3.1.1. EXPERIMENTAL DATA

Time-domain (TD) data are the only actually measured data. Limitations applicable to time domain data come from the resolution of sensors in space (all sensors have minimum and maximum measurable amplitudes) and frequency (sensors have bandlimited ranges where their output can be related to the quantity of interest). For digital systems the frequency band is also limited by aliasing, so that filtered bandlimited data must be used.

The major disadvantage of TD data is that an explicit treatment of noises is often necessary. Many traditional system identification methods (e.g. ARMAX [lju1], Extended Kalman Filters [kar1]) assume a filtered white noise model (or more recently a worst case deterministic noise) which is estimated at the same time as the system model. For structures in a clean environment, another usually quite efficient approach uses the assumption that noises are uncorrelated from the inputs used to excite the system. Although under this assumption some algorithms are asymptotically insensitive to the measurement noise, it is in general useful to do a non-parametric identification removing components that are uncorrelated to the inputs from the measured outputs. Such correlated measures of the response (pseudo-TD data) are fundamentally equivalent to the use of frequency domain (FD) data (they are related to frequency response functions through the Fourier transform).

For linear time-invariant systems, the response can be described in the frequency domain (FD) using frequency response functions (the FD equivalent of impulse response functions). Frequency response functions, which are estimated through a process of non-parametric identification, describe the response of the noise-free linear system to any type of excitation. In the FD, system and noise characteristics are thus readily separated into a set of frequency response functions and a noise spectrum (which is quite often also estimated [lju1]).

Sine-sweeps [ewi1, lju1] are probably the oldest non-parametric identification procedures. They consist of a measurement at different frequencies of the steady state response to sinusoidal excitation. If the system is linear and the noise is not correlated with the input, they allow unbiased estimates of points of the frequency response functions. For non-linear systems, they allow a determination of the amplitude dependence of the frequency response (valid frequency domain information for non-linear structures is usually obtained using sine-sweeps). Although very popular for structural dynamic testing and considered more accurate (particularly for the measurement of damping properties), sine-sweeps have the main drawback of implying extremely long acquisition times if many frequency points are to be tested.

For other inputs with a larger spectrum (e.g. impact, pseudo-random), many frequency response function estimators have been developed (see Refs. [ewi1, lju1, cob1, all2]),

which allow the measurement of frequency response functions with extremely low bias and variance. Averaging and windowing are often successfully used to reduce the estimate variance, at the cost of an increase in its bias, which should be well understood for a proper test. Tests with simultaneous multiple inputs are possible and lead to more consistent sets of data, which linearize and average the structural response in a sense that should be further investigated.

The validity of non-parametric identification depends of the statistical assumption that inputs and noises are uncorrelated (which, as shown in Ref. [lju1], allows the unbiased estimation of frequency response functions for open-loop systems). This statistical assumption, which is usually met for the systems of interest here, is clearly much less restrictive than parametric noise models usually limited to small dimensions, so that the use of FD (or pseudo-TD derived from FD) data seems much more appropriate for the structural dynamic applications considered here.

A last advantage of FD data for the application at hand is that it allows an accurate truncation of high frequency dynamics. Contributions of poles can, for lightly damped structures, be very well approximated by asymptotes even at frequencies close to the pole resonance. The use of FD frequency response function estimates in restricted frequency bands thus allows the identification of all the modes of interest, while approximating the contributions of other modes by simple asymptotes. (Note that the same effect can be obtained in the TD when using pseudo TD data generated by the inverse Fourier transform).

For the present work it will be assumed, as is generally done for structural dynamic applications, that estimates of the continuous time frequency response functions can be derived from test data at a finite number of frequencies ω. If the data acquisition is done digitally, discrete frequency response functions (based on the z-transform rather than the Laplace transform) may be available, but can be transformed to estimates in the Laplace domain as discussed in Ref. [fra1].

3.1.2. PARAMETRIZATIONS

Several categories of models are considered for parametric identification, and have led to techniques that can usually be developed in both the time and the frequency domain.

Polynomial or rational fraction models where among the first used for system identification. They have been applied both in the time domain (leading to the well known ARMAX, OE, etc. models detailed in Ref. [lju1]), and in the frequency domain (e.g. the Rational Fraction Polynomial method [ric1, shi1] which uses polynomial orthogonalization

techniques to obtain better numerical conditioning). A general form of these models is for SISO discrete TD systems [lju1]

$$A(z)y(t) = \frac{B(z)}{F(z)}u(t) + \frac{C(z)}{D(z)}e(t) \tag{3.1}$$

where the input is u, the output y, the white noise disturbance e (to be used for TD identification), and five possible polynomials are considered: A, B, F (corresponding to the system response) and C, D (shaping the noise input). For MIMO problems, matrix polynomials can be used (Ref. [ric2], etc.), but it may then be difficult to guarantee the minimality of the model.

Polynomials tend to be badly numerically conditioned if many poles are used and if the frequency range of poles or zeros is very large (the case of interest here). It is thus sometimes more appropriate to use a pole/zero decomposition (products of 1st order polynomials)

$$y(s) = G\frac{(s-z_1)\ldots(s-z_j)}{(s-\lambda_1)\ldots(s-\lambda_{N_T})}u(s) \tag{3.2}$$

where the overall gain is given by G, the zeros by the z_j and the poles by the λ_i.

The use of the polynomial parametrization implies a choice of polynomial orders. This choice introduces problems of definition for the identified parameters. For example, some the model poles correspond to estimates of the system poles, but others (called computational poles) allow a better agreement with the measured data (the meaning of the modes associated with such poles is unclear and these modes probably deteriorate the accuracy of estimates of true modes).

The polynomial parametrizations (3.1)-(3.2) are not very appropriate for MIMO problems since the uniqueness conditions on poles, modal controllabilities and observabilities are difficult to relate to conditions on the polynomials linked to each SISO transfer function. All these difficulties are however easily treated when using MIMO state-space models of the form

$$\begin{aligned} \dot{x} &= Ax + Bu \\ y &= Cx + Du \end{aligned} \tag{3.3}$$

General state-space models are used in the system realization theory, first introduced by Ho and Kalman [hob1]. Based on similar considerations, the Ibrahim Time Domain (ITD) method [pap1, pap2], the Polyreference method [cro2, cro1], the Eigensystem Realization Algorithm (ERA) [jua1] and several other variants were developed and are still actively used and refined.

In an effort to identify the normal mode models, a restriction of the general state space form (3.3) was introduced and led to reduced system matrix approaches (see Refs. [cop1, leu1, cra1, lee1, cra2]) which assume a second order parametrization of the model

$$\begin{aligned} xs^2 &= -C_T xs - K_T x + bu \\ y &= cx \end{aligned} \tag{3.4}$$

for the identification. These methods assume a knowledge of the input u and of the state response (acceleration, rate and displacement) so they have been generally applied in the frequency domain (where the state response is given by xs^2, xs and x) and restricted to cases with more sensors than modes, where c and x can be easily defined from measured frequency response functions. As will be seen for the interferometer in section 3.3.4, these methods tend to have difficulties in identifying damping contributions. The use of FD data in these approaches allows truncating high frequency resonances, but asymptotic terms are difficult to introduce.

Free parameters for these methods are choices of sensors or generalized sensors and input frequency weightings. The results can give satisfactory estimates of frequencies and modeshapes but are often quite inaccurate for the damping representation.

The general polynomial and state-space forms do not easily allow the specification of further knowledge of the system and thus iterative refinements of the models. Frequency weightings or shaped TD inputs (the only tools generally available to improve results judged unsatisfactory) do not give a direct mechanism for eliminating computational modes or specifying true modes that are not initially identified (e.g. local modes). These limitations are however alleviated if a physical parametrization (pole/complex mode or pole/zero) is used, since different parameters can then be improved independently.

In the polynomial form (3.2), one can clearly remove or specify a pole or a zero. But, as mentioned above, the polynomial form is not appropriate to deal with MIMO problems, so the pole/complex mode parametrization has been studied in more detail for the present work.

The complex mode parametrization is a particular representation (without restriction) of the state-space models (3.3), corresponding to choosing modal states for x (which leads to a diagonal A matrix). For structures, this parametrization corresponds to the complex mode model introduced in section 2.1.2, whose response in the FD can be written as

$$H(s) = \sum_{j=1}^{2N} \frac{c\psi_j \psi_j^T b}{s - \lambda_j} \ . \tag{3.5}$$

Because real structures have an infinity of modes, the only possible objective is to create a model keeping the terms having significant contributions in the test bandwidth (the frequency range where the estimated frequency response functions are used). For lightly damped structures, only the modes in the test bandwidth (indices between n_1 and n_2) have significant dynamic contributions. The contribution of other modes can be extremely well represented by asymptotic terms (introduced in section 2.2.2): constants for poles above the measured bandwidth (since $s\text{-}\lambda_j \approx \lambda_j$ for those poles) and terms in $1/s$ for modes below (since $s\text{-}\lambda_j \approx s$ for those poles). This simple analysis leads to a first complex mode model parametrization

$$H_1(s) = \sum_{j=n_1}^{n_2} \frac{R_j}{s-\lambda_j} + E + \frac{F}{s} \ , \tag{3.6}$$

where R_j is the complex residue matrix associated with a given pole (it is the experimental equivalent of the analytical $c\psi_j\psi_j^T b$) and the complex terms E and F are respectively correct for the asymptotic behavior of high frequency and low frequency poles (including negative imaginary poles).

Since the terms of this model are the only ones having a significant influence on the frequency response, they are the only ones that can be identified accurately. However, for the real systems considered here, the residue matrices of complex-conjugate poles are complex-conjugate matrices. Thus, even though the test only contains positive frequencies, one can introduce a symmetric pole pattern which is physically known to exist. This consideration leads to a second complex mode model parametrization

$$H_1(s) = \sum_{j=1}^{n_2} \left\{ \frac{R_j}{s-\lambda_j} + \frac{R_j^*}{s-\lambda_j^*} \right\} + E + \frac{F_1}{s} + \frac{F_2}{s^2} \ , \tag{3.7}$$

that describes the contributions of complex-conjugate pairs of poles, corrects for the high frequency modes with the real static correction matrix E, and for the low frequency modes with two contributions described by the real matrices F_1 and F_2 (see motivation below).

Regrouping the contributions of the complex-conjugate poles as in (3.7), one can express the model in terms of real valued quantities

$$H_1(s) = \sum_j \left\{ 2\frac{T_j' s + T_j}{s^2 + 2\zeta\omega_j + \omega_j^2} \right\} \ . \tag{3.8}$$

where $T_j' = \mathrm{Re}(R_j)$ and $T_j = -\mathrm{Re}(R_j)\zeta\omega_j + \mathrm{Im}(R_j)\sqrt{1-\zeta^2}\,\omega_j$. Note that the direct link between the residue matrices and the complex modes is lost in this form (used among

others by Spanos [spa1] and Gilpin [gil1]), which is thus less appropriate for the analysis of physical properties of the system.

From (3.8) it appears that the asymptotic high-frequency contribution linked to T'_j is in $1/s$ and the contribution linked to T_j is in $1/s^2$. This motivated the two correction matrices F_1 and F_2 used in the modal parametrization (3.7). Note also that a correction of the form Es could be introduced to account for effects of the T'_j matrices of high frequency modes.

For structural dynamic applications, the assumption of proportional damping is very useful since complex and normal modes are then exactly proportional. In the form (3.8), the proportional damping assumption corresponds to $T'_j = 0$ (see section 2.2.3), which leads to a real mode parametrization

$$H_1(s) = \sum_{j=n_1}^{n_2} \left\{ \frac{T_j}{s^2 + 2\zeta\omega_j + \omega_j^2} \right\} + E + \frac{F}{s^2} , \tag{3.9}$$

This parametrization corresponds to a (normal mode)/(pair of complex-conjugate poles) parametrization (since theoretically $T_j = c\phi_j\phi_j^T b$, see section 2.1.3). However, the enforcement of this parametrization, consistent with the assumption of proportional damping, does not exactly estimate the normal modes for non-proportionally damped systems (see the example in section 3.3.4).

Finally, the modal parametrization is also the underlying basis of the force appropriation method, which should be mentioned as one of the oldest identification methods for structures. This method, which tunes relative amplitudes and phases of multiple sinusoidal inputs to excite the resonance of a single mode, was first introduced in Ref. [lew1] and has since been widely developed (e.g. Refs. [bre1, nie1, wil1]). It is still widely used in industry through highly automated testing packages. Modal damping must often be assumed, because the appropriation of phase differences other than 0° or 180° at different excitation locations can be extremely long.

3.1.3. COST FUNCTIONS

Cost functions are measures of the difference between the model prediction and the data. Identification algorithms have the objective of minimizing the prediction error as measured by the cost function which thus plays a key role in the result of any method.

In the time domain, most algorithms use cost functions on the prediction error, such as

$$\|y_M - y_1\| = \sum_{\substack{j \in \{\text{measured sensor location}\} \\ k \in \{\text{measured actuator location}\} \\ t \in \{\text{measured time point}\}}} \left| \left(y_{Mjk}(t) - y_{1jk}(t) \right) \right|^{\zeta} , \tag{3.10}$$

or norms on the Hankel matrix (which for some problems is equivalent to the use of (3.10)). For more details on time domain cost functions, see Ref. [lju1] for example.

In the frequency domain, experimental frequency response functions are estimated at a discrete number of frequency points (e.g. the test frequencies of a sine-sweep or the frequencies associated with a finite length matrix of time domain measurements (see Ref. [lju1])). Because the comparisons between experimental and modeled frequency responses can only be made for a finite number of points, any norm could be used (and they are all equivalent in the limit of perfect data). In practice however, two factors determine the choice of a given norm: the easiness of use, and the sensitivity to the measurement noise and to variations of the estimated parameters.

Because of its useful mathematical properties (it leads to least-squares problems), the quadratic cost function

$$J_{\text{quadratic}} = \sum_{\substack{j\in\{\text{measured sensor location}\} \\ k\in\{\text{measured actuator location}\} \\ l\in\{\text{measured frequency point}\}}} \left|\left(H_{Mjk}(\omega_l) - H_{ljk}(\omega_l)\right)\right|^2 \tag{3.11}$$

is often used as a measure of the difference between the estimated and predicted frequency response functions. (In the limit, as the frequency response is known at all points, this cost function corresponds to the square of the H_2 norm).

Least-squares problems derived from the use of the quadratic cost function allow fast computations, but better mathematical properties can be obtained using other norms. In particular, the logarithm (the complex log or, with less accuracy, the log magnitude) of the frequency response function can be used in a Log Least Squares (logLS) cost function

$$J_{\text{Log Least Squares}} = \sum_{\substack{j\in\{\text{measured sensor location}\} \\ k\in\{\text{measured actuator location}\} \\ l\in\{\text{measured frequency point}\}}} \left|\left(\text{Log}\,H_{Mjk}(\omega_l) - \text{Log}\,H_{ljk}(\omega_l)\right)\right|^2 \tag{3.12}$$

To highlight the properties of the logLS cost function, a one DOF example is considered

$$H(s) = \frac{R}{s^2 + 2\zeta\omega s + \omega^2} \tag{3.13}$$

with nominally the non-dimensional parameters R=1, ω=1, ζ=0.01.

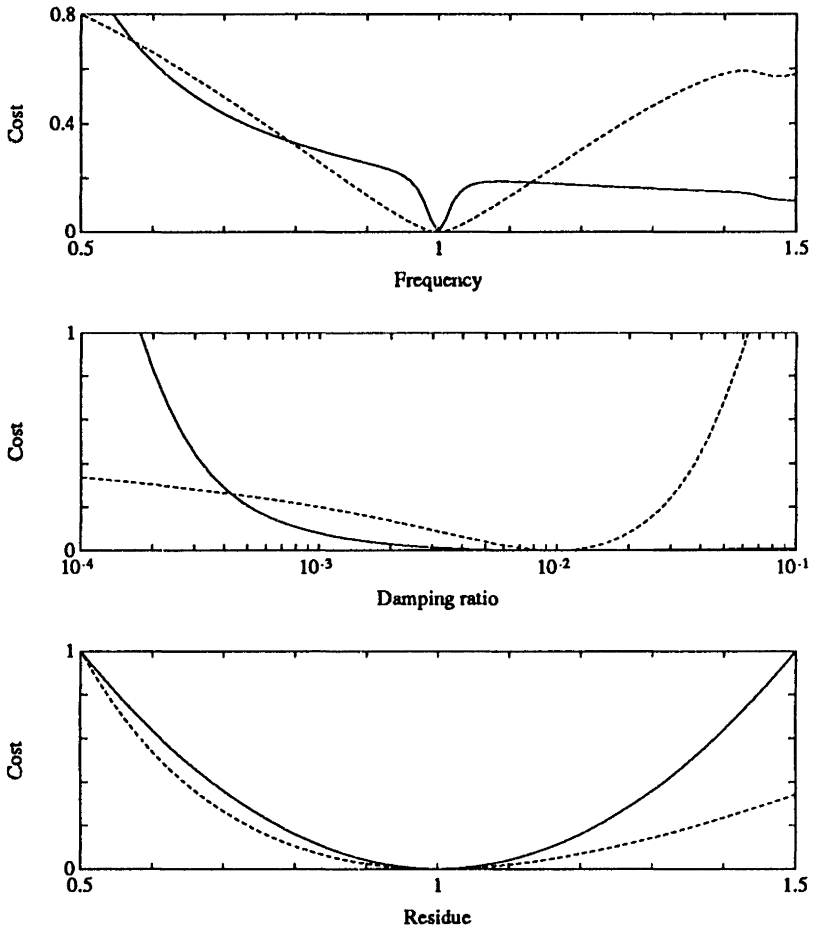

Figure 3.2: Artificially normalized (—) quadratic (3.11) and (---) logLS (3.12) costs for varying estimated a) normalized frequency, b) damping ratio, c) normalized residue, the other parameters being nominal.

Figure 3.2 shows the quadratic (3.11) and logLS costs (3.12) corresponding to errors on the three parameters (pole frequency, damping and residue) for a frequency response function estimate with 1000 experimental frequencies linearly spaced between 0 and 2. It can be seen that both the quadratic and logLS cost functions have local minimums at the nominal values. However, the quadratic cost decreases for an estimated frequency above 1.07, so for a large initial error on the pole frequency the minimization would probably not converge. For identification such errors are unrealistic, so the quadratic cost is sufficient (and will be used for the new identification algorithm proposed in this chapter), but initial FE modal frequency errors are often quite large, therefore the logLS cost (3.12) is indicated for FE update procedures (it will be used in Chapter IV).

Both cost functions are locally convex with respect to all the parameters near the minimum, but for inaccurate frequencies, the quadratic cost is convex in a region of approximately ±2% (around the nominal frequency), versus ±15% for the logLS cost.

Practically, this means that minimization algorithms will converge much more easily using the logLS cost.

From this analysis and that of further test cases with more modes, the logLS cost can be shown to have better properties than the quadratic cost on several points:

- It is a strictly decreasing function of the inaccurate parameters in much larger regions around the minimum.
- It is locally convex in much larger regions which will help minimization algorithms.
- It is inherently more sensitive to zeros (anti-resonances) and thus to mode shape errors. This property might be a major motivation for the use of the logLS cost to identify models for control design purposes.
- As observed in Ref. [arr1], problems of local minimums for insufficient frequency spacing are solved.

For a given cost function and identification algorithm, the input content can often be tailored, thus giving a powerful but of difficult use tool to improve results. In the TD this possibility is implicit in the fact that the cost functions measure the discrepancy between measured and predicted outputs, for an input that can be designed by the user (e.g. Ref. [hun1]). In the FD, changing the input corresponds to multiplying the frequency response functions by a frequency weighting corresponding to the input spectrum. For example, a weighted quadratic cost function will take the form

$$J_{\text{Wheighted Least Squares}} = \sum_{\substack{j\in\{\text{measured sensor location}\}\\ k\in\{\text{measured actuator location}\}\\ l\in\{\text{measured frequency point}\}}} \left|W(\theta,\omega_l)\left(H_{Mjk}(\omega_l)-H_{ljk}(\omega_l)\right)\right|^2, \qquad (3.14)$$

where the weighting W may depend on both frequency and the identified model parameters θ. Such weightings are essential to some algorithms, such as those based on the ARX model structure [lju1], but are usually not necessary for the new algorithm presented in section 3.2.

3.1.4. Resolution Algorithms

Resolution algorithms (see a partial list in Table 3.1) are usually constrained by the ability to obtain a useful solution to the minimization problem in a reasonable time.

A number of identification algorithms use particular formulations of the minimization problem allowing direct or fast resolutions of the problem. This is the case in particular of algorithms based on the polynomial parametrization (3.1) (ARMAX, OE, orthogonal polynomials, etc.) and the quadratic cost functions in the TD or FD.

System realization algorithms (ITD, ERA, Polyreference, etc.), based on the general state-space parametrization, use operator norms on the Hankel matrix and find a direct, but sub-optimal, solution to the minimization problem.

These algorithms are usually called "black-box" identification algorithms since their solution is only based on mathematical properties of the stated problem. In the present case, two essential properties can be assumed, thus leading to more appropriate algorithms:

- The type and length of inputs used in experiments are not limited, and levels of noise present are small compared to the achieved levels of response, so estimates of frequency response functions can be obtained with high levels of accuracy (meaning low bias and variance of the estimate). In other words, noise is not a problem.
- Structures are inherently stable systems with, in general, imaginary dynamics (poles with less than 10% percent damping), so a good model truncation can be achieved by using frequency response functions in a limited frequency range.

From the second property, the modal parametrization detailed in section 3.1.2 allows minimal descriptions of the actual system dynamics and thus the identification of the physical properties of the system (the poles, complex mode observabilities and controllabilities).

The most easily obtained information on the system response is the location of the poles whose frequencies can generally be graphically picked with high accuracy using one or several measured frequency response functions or mode indicator functions combining the response of several frequency response functions (e.g. Ref. [wil2]). Such visual comparisons of measured and estimated frequency response functions usually allow the user to determine a number of errors in identified models. Using the traditional "black-box" algorithm, these errors are corrected on an *ad-hoc* basis (by using sub-frequency ranges to improve results for particular modes, by introducing frequency weightings, by removing computational poles, etc.), but the results obtained have no guarantee of accuracy.

To properly use this easily available knowledge of the system pole structure, the identification algorithm must be iterative and use an initial model where the pole frequencies appear explicitly. Such an algorithm is introduced in the next section and shown to give accurate models for structures with high modal densities, local modes, and significant effects of non-proportional damping.

3.2. A NEW IDENTIFICATION ALGORITHM BASED ON THE COMPLEX MODE PARAMETRIZATION

This section addresses in more detail the implementation of the algorithm developed as part of this work. (Like all the results of the present work, this algorithm is implemented in a Toolbox for Matlab [bal2]). The main characteristics of the algorithm are:

- frequency domain data, which allow the treatment of measurement noises through non-parametric identification and the identification of all the modes of a particular bandwidth as well as the truncation of other modes through the use of the estimated frequency response function in that band.
- the complex mode parametrization (3.6), which is consistent with the objective of identifying **all** the modes of the considered bandwidth. (The parametrizations (3.7) and (3.9) are also implemented in [bal2]).
- an iterative update of an initial guess of the pole structure (while simultaneously estimating the corresponding residues), which allows the use and in general the improvement of the results of other ID algorithms.
- the quadratic cost function (3.11) without weighting, which allows a cost-efficient and yet extremely accurate algorithm.

Implementation details of the basic algorithm are discussed in section 3.2.1. The solutions of the basic algorithm are not minimal MIMO models, so new methods to determine the modal multiplicity, as well as scaled estimates of the complex mode controllabilities and observabilities, are introduced in sections 3.2.2 and 3.2.3. The efficiency of the overall procedure is demonstrated in section 3.2.4, using experimental data taken on the IT. Finally for reference, the problem of reparametrization into a real parameter state space model is addressed in section 3.2.5.

3.2.1. IMPLEMENTATION OF THE COMPLEX MODE IDENTIFICATION ALGORITHM

For any of the modal parametrizations (3.6)-(3.9), the transfer function depends linearly on the residues and asymptotic correction terms (matrix R_j for each of the complex modes of the model, and matrices E and F for the correction terms). For the rest of this section, the elements of these matrices will be stored in the matrix $R = \left[R_j, E, F\right]^T$ of dimensions N_T+2 *by* $N_S * N_A$. For a system with N_T poles, the first N_T rows of R contain the residue matrix associated with the N_T poles. The last two rows contain the correction matrices. For MIMO systems, an arbitrary storage scheme such as storing the columns

sequentially (i.e. $[R_{11},R_{21},\cdots,R_{12},R_{22},\cdots]$) is used to make the link between the row storage in R and the N_S by N_A matrix form defined in the parametrizations (3.6)-(3.9).

A pole contribution matrix $\Phi(\lambda_j)$ is defined as follows. The first N_T columns of $\Phi(\lambda_j)$ are equal to $1/(s-\lambda_j)$ evaluated at the measured frequency points $s=\{j\omega_i\}$ for each of the N_T poles λ_j. The last two columns correspond to the asymptotic contributions: a column of ones for the stiffness correction E and a column equal to $\{1/j\omega_i\}$ for the mass correction F. (See Ref. [bal2] for more details if necessary).

The frequency response functions predicted by a model of the form (3.6) (a similar expression would hold for (3.7) and (3.9)) are the product of the matrices Φ and R defined above

$$[H_I]_{\{j\omega_i\}}=\left[\sum_{j=n_1}^{n_2}\frac{R_j}{s-\lambda_j}+E+\frac{F}{s}\right]_{s=\{j\omega_i\}}=\left[\frac{1}{s-\lambda_j},1,\frac{1}{s^2}\right]_{s=\{j\omega_i\}}[R_j,E,F]^T=\Phi(\lambda_j)R \quad (3.15)$$

The identified model is the model which minimizes, near an initial model, the chosen cost function (here the quadratic cost function (3.11)). Even with a good initial model, a simultaneous minimization on the poles and residues is difficult, computationally intensive, and unreliable. Therefore, doing the minimization in two steps is proposed here.

Using the expression (3.15) of the predicted frequency responses, the minimization of quadratic cost function (3.11) leads to the following linear least-squares problem for the matrix R

$$R=\arg\min\left\{\text{trace}\left((H_M-\Phi R)^*(H_M-\Phi R)\right)\right\} \quad (3.16)$$

which, for a given set of poles, is solved as the first step of the proposed method (for the identification/optimization, the residues are solutions of (3.16) and not free parameters).

The use of the least-squares problem (3.16) to determine residues for a given set of poles has been proposed independently by several authors (the interpretation using a maximum likelihood error criterion in [jeo1] is worth noting). However, such evaluations are only accurate if the poles are accurate.

To improve the results obtained with the initial set of poles, the method proposed here considers the poles as free parameters and searches (second step) for the minimum of the cost function (3.11) for sets of poles near the initial guess. During the search the residues are defined as solutions of the least-squares problem (3.16).

The least squares problem (3.16) has, for any given set of poles λ_j, a closed form solution

$$R = \left(\Phi^T \Phi\right)^{-1} \Phi^T H_M(s) \tag{3.17}$$

which can be used directly, although better numerical conditioning can be obtained with different algorithms designed to solve least-squares problems (see Ref. [law1]). From (3.16) and (3.17), the cost J can be rewritten as

$$J = \text{trace}\left(\left(H_I - H_M\right)^T \left(H_I - H_M\right)\right) = \text{trace}\left(H_M^T \left(I - \Phi\left(\Phi^T \Phi\right)^{-1} \Phi^T \right)^2 H_M \right) \tag{3.18}$$

From (3.18), a closed-form expression of the gradient of the cost J with respect to free parameters θ (here the free parameters are the frequency and damping ratio of each of the estimated poles) can be obtained as follows. Using $\varepsilon = H_I - H_M$, the partial derivative of J with respect to θ is

$$\begin{gathered} \frac{\partial J}{\partial \theta} = \varepsilon^T \frac{\partial \varepsilon}{\partial \theta} + \frac{\partial \varepsilon^T}{\partial \theta} \varepsilon = 2\varepsilon^T \frac{\partial \varepsilon}{\partial \theta} = 2H_M^T \left(I - \Phi\left(\Phi^T \Phi\right)^{-1} \Phi^T \right) \left(-\frac{\partial \Phi}{\partial \theta} R - \Phi \frac{\partial R}{\partial \theta} \right) = \\ \frac{\partial J}{\partial \theta} = 2\left(H_I - H_M\right)^T \frac{\partial \Phi}{\partial \theta} R \end{gathered} \tag{3.19}$$

To update the poles, any optimization algorithm would be appropriate, but it appears in practice that the sign of the cost function gradient for a given pole frequency ($\partial J/\partial \omega$) or damping ratio ($\partial J/\partial \zeta$) does not depend on the error made on other parameters (the damping ratio or the frequency of the same pole and the parameters of other poles). Therefore, from the sign of the gradient one can determine whether or not each of the parameters is over- or under-estimated. By using a limited initial step size for each parameter, and decreasing the step of each parameter every time it passes over its optimum, one obtains a very efficient path to a local optimum, which was found to be satisfactory in almost all the cases treated. (For more details see [bal2]).

This approach, which takes advantage of specific decoupled properties of the problem, has proven to be extremely effective on several actual data sets (reducing computation times by orders of magnitude when compared to other optimization strategies). However, it does not come with any mathematical guarantee of convergence, so that in some cases more traditional optimization algorithms might be more appropriate. Traditional optimization methods would however be much more computationally expensive and may not converge because the cost function used is only convex for very small errors (see section 3.1.3).

The user freedom in this algorithm is related to the choice of the initial guess for the model poles. This choice restrains the optimization by only allowing solutions near the guess. This property allows the identification of all the modes in the bandwidth where the

frequency response functions are estimated and, if another identification method is used to provide the initial guess, the elimination of all computational modes.

The simplest (and usually sufficient) way to provide an initial guess of the poles is to graphically pick pole frequencies (which correspond to resonances (peaks) for the lightly damped systems considered here) and to use a realistic but non-measured damping ratio (e.g. 1%). After a few iterations, it is usually possible to remove poles that do not converge since they do not correspond to actual poles of the system, and to add poles that may have been overlooked in the initial guess (such as poles of local modes with only a significant contribution in a few frequency response functions, or very close poles of structures with high modal densities).

Finally, accurate results were obtained using the present method without frequency weightings (used in many traditional methods to enhance the sensitivity of the cost function to parts of the frequency response which are of interest). However, in particular cases, such as a structure with a rapid roll-off of the measured frequency response functions, the method might not obtain accurate results if used without frequency weightings.

3.2.2. Problems of Minimality for MIMO Tests

The residue matrix of a single mode is a dyad (product of the modal observabilities $c\psi$ and controllabilities $\psi^T b$). Therefore the pole multiplicity in a model is equal to the rank of the residue matrix. For MIMO tests, the models identified through the approach introduced in section 3.2.1 are not minimal (in the sense that they use poles with multiplicities higher than 1 even if the pole is isolated). Ways to enforce it minimality as a post-treatment of the identified model will be detailed in this section.

Using the formal analytical description of the response in terms of complex modes (detailed in section 2.1.2), the modal observability takes the form $c\psi_j$ (a column vector with an element for each sensor) and the controllability takes the form $\psi_j^T b$ (a row vector with an element for each actuator). For example, the residue matrix of a single mode in a system with 2 actuators and 3 sensors will have the form

$$R_j = \begin{bmatrix} R_{j11} & R_{j12} \\ R_{j21} & R_{j22} \\ R_{j31} & R_{j32} \end{bmatrix} = \begin{bmatrix} c_1\psi_j \\ c_2\psi_j \\ c_3\psi_j \end{bmatrix} \begin{bmatrix} \psi_j^T b_1 & \psi_j^T b_2 \end{bmatrix}. \tag{3.20}$$

Note that ψ_j and ψ_j^T use the same vector because structures are symmetric systems. In the general case, these vectors would be the distinct right and left eigenvectors of the system equations.

The residue matrix R_j in (3.20) is clearly of rank 1 since it is the product of a column vector by a row vector (in mathematics, such a matrix is called a dyad). Furthermore, from (3.20) it is clear that the contribution of a single complex mode is always a dyadic residue matrix (unless the mode is uncontrollable or unobservable in which case the residue matrix is equal to zero).

For truly multiple poles, the denominators $(s-\lambda_j)$ of the modal contributions in the spectral decomposition (3.5) are equal. The dyads associated with each pole can thus be summed to form a single residue matrix

$$R_j = c\psi_{j_1}\psi_{j_1}^T b + c\psi_{j_2}\psi_{j_2}^T b + \ldots \tag{3.21}$$

This residue matrix has the same rank as the modal multiplicity if:

- the residue matrices corresponding to the different modes sharing the same pole location are not proportional to each other and
- the number of sensors and actuators is larger than the modal multiplicity (a residue matrix has N_A columns and N_S rows, so that its maximum rank is the minimum of N_A and N_S).

The results of identification algorithms give an estimate of the residue matrix R_j. However, many algorithms (including the one proposed here) do not constrain the rank of the residue matrices, so that in MIMO problems the identified residue matrices are of rank higher than 1. (Obviously, in SISO, MISO, or SIMO problems the residue matrix has one dimension equal to 1 so that it is necessarily of rank 1).

As seen in (3.21), residue matrices of a rank higher than 1 correspond to the existence of multiple modes having identical poles. To obtain **minimal** models (models which do not use more modes than there actually exist) one must determine whether there are effectively multiple modes and, if not, use dyadic residue matrices. The singular value decomposition of the residue matrix gives a decomposition into dyads of decreasing magnitude

$$R_j = U_1\sigma_1 V_1^T + U_2\sigma_2 V_2^T + \ldots \tag{3.22}$$

If a mode is not multiple, identification errors will often result in a full rank residue matrix. However for small identification errors, the contribution of the true mode dyad $c\psi_j\psi_j^T b$ will be most important, and other terms will be small. By definition, the first dyad of the singular value decomposition is such that the matrix norm of other dyads is minimal. In the case of a single mode, the dyadic residue matrix

$$\tilde{R}_j = U_1\sigma_1 V_1^T \tag{3.23}$$

is a thus the best possible dyadic (therefore leading to a minimal model) estimate of the true residue matrix $c\psi_j\psi_j^T b$ (where "best" means that the matrix norm of the residual $\tilde{R}_j - R_j$, which is given by the second singular value σ_2, is minimal). The ratio of the first two singular values σ_2/σ_1 is equal to the ratio matrix norms $\|\tilde{R}_j - R_j\|/\|R_j\|$, which gives a measure of how close to a minimal MIMO model the initial estimate of the residue matrix was (see the application to the IT in section 3.2.4).

True modal multiplicity is an extremely rare phenomenon, which happens for perfectly symmetric or uncoupled structures, and even then the multiplicity is rarely larger than 2 (see Ref. [bal5]). However, it was shown in Ref. [bal6], that for damping levels such that the mode half-power bandwidths ($\zeta_j\omega_j$) are significantly larger than the frequency separation between two modes (ω_1-ω_2), it may not be possible to distinguish poles that are not truly multiple. Therefore, almost perfectly symmetric structures may have poles so close to each other that the identification algorithm will not be able to distinguish them. In such cases, as many dyads as the modal multiplicity should be kept (e.g. for a double mode $\tilde{R}_j = U_1\sigma_1 V_1^T + U_2\sigma_2 V_2^T$).

In a well devised test, the modal subspace (see Ref. [bal6]) should span the spatial input and output subspaces, so that all the singular values of the true residue matrix are relatively large. Under this condition, usually achieved with a regular distribution of actuators and sensors, the matrix norm of the residual $\tilde{R}_j - R_j$ (given by the first singular value not kept in the minimal residue matrix $\tilde{R}_j$, σ_3 for a double mode) should be small compared to the singular values kept in $\tilde{R}_j$. This condition can be used to determine the effective modal multiplicity from experimental results, although a clear drop in the singular values is needed for good confidence in the analysis.

Note that the results, applied here accurately on the residue matrix, can also be seen using the singular value decomposition of the frequency response matrix (called the Multivariate Complex Mode Indicator Function [wil2] in the structures community). Near an isolated modal resonance, the frequency response functions are nearly proportional to the residue matrix. The ratio of the singular values at the peak therefore corresponds to the ratio of the singular values of the residue matrix, so the same conclusions as to the multiplicity of the mode can be made. However, if several closely spaced modes contribute to the peak, the test on frequency response function singular values may be misleading.

Theoretically, it is possible for a multiple pole to not correspond to multiple modeshapes (non-diagonal Jordan form). The system equations of proportionally damped systems can always be diagonalized (as the system matrices are symmetric and the mass matrix is positive-definite) and there is no reason to think that the introduction of non-proportional damping could lead to a non-diagonal Jordan form for the first order system

equations. Rigid-body modes are the only exception (known to the author) where the complex residue matrices introduced in the parametrizations (3-5)-(3.7) cannot be used. And even in that case where the contributions of these modes take the form F/s^2, the present analysis can be applied on the real-valued F matrix rather than on the usual complex residue matrix R_j (assuming that the rigid-body motion can be accurately measured).

3.2.3. Determination of Scaled Complex Modal Observability and Controllability Matrices

To estimate normal modes and for other prediction purposes, it is necessary to determine estimates of the modal controllability and observability scaled in a way that is independent from a particular test, thus independently defining the influence of actuators and sensors. These scaled quantities are obtained using the residues of collocated transfer functions, as will be detailed in this section.

A useful property of dyads is that both the directions of input and output are known. Thus, for a single mode j, the singular vectors U_1 and V_1^T (defined in the decomposition (3.23) of the minimal residue matrix in the previous section) are respectively unscaled estimates of the modal observability $c\psi_j$ and controllability $\psi_j^T b$ (which respectively characterize the way the complex mode ψ_j is seen at the sensor and actuator locations).

The relative information for sensors or actuators (i.e. $c_1\psi_j/c_2\psi_j$ or $\psi_j^T b_1/\psi_j^T b_2$) is invariant for any scaling and can thus be used directly, but one is interested in uniquely defining the scaled complex modal observability $c\psi_j$ and controllability $\psi_j^T b$. Since the relative information is invariant, the problem is to find one scaled component of the observability and controllability. The properly scaled components for other sensors or actuators will then derived from the identified relative quantities (i.e. $c_1\psi_j/c_2\psi_j$ or $\psi_j^T b_1/\psi_j^T b_2$).

For a collocated transfer function (i.e. such that $c=b^T$, for example: a transfer function from force input to displacement at the same point and in the same direction) the modal controllability and observability are by definition equal. Imposing $c_l\psi_j = \psi_j^T b_l$ at the considered collocated location l defines a scaling coefficient for each mode j

$$\alpha_j = \sqrt{\left(\tilde{R}_j\right)_{ll}} = \sqrt{U_{ll}\sigma_1 V_{ll}} = c_l\psi_j = \psi_j^T b_l \tag{3.24}$$

leading to scaled estimates of the modal observabilities $\left(c\psi_j\right)_l$ and controllabilities $\left(\psi_j^T b\right)_l$

$$\left(c\psi_j\right)_l = \frac{\alpha_j}{U_{ll}} U_1 \quad \text{and} \quad \left(\psi_j^T b\right)_l = \frac{\alpha_j}{V_{ll}} V_1^T \tag{3.25}$$

An important fact introduced in section 2.1.2 was that the application of this scaling condition is strictly equivalent to the analytical scaling condition (2.6) with $\mu=I$ and, ideally, is independent of which collocated transfer function is used for the scaling.

Many tests are done with more than one collocated transfer function. In such cases the problem is over-constrained (since the scaling implied by different collocated transfer functions may be inconsistent). A way to resolve the additional constraints must be found, such as choosing a particular collocated transfer function to do the scaling, or using an algorithm, yet to be defined, to find an averaged scaling compatible with all the collocation constraints.

For multiple modes, modeshapes are not uniquely defined. The directions are now subspace directions (U_1 and U_2 span the same subspace as $c\psi_{j_1}$ and $c\psi_{j_2}$; for more details see Ref. [bal6]). But, outside the fact that it is more difficult to compare multidimensional subspaces, results are the same as for the single mode case.

Finally, these results, developed for complex modes, can be easily extended to normal modes if the normal mode residue matrix $T_j = c\phi_j\phi_j^T b$ is identified. (For example, when the structure is proportionally damped so that the parametrization (3.9) can be used accurately for the identification).

3.2.4. Results of Application to the Interferometer Testbed Modal Test Data

To demonstrate the efficiency of the methods proposed in this section, the results of the modal test of the IT (see the testbed description in section 7.1) are used. All the theoretical results of this work are implemented numerically in a Toolbox for Matlab [bal2], with which the results presented here were obtained.

The first identification step is to determine a complex mode model. Considering the 20-60 Hz range for the IT, initial estimated pole frequencies were determined by graphically indicating the peaks of the measured frequency response functions, and assuming 1% pole damping. The 28 measured frequency response functions were used to identify the complex mode model corresponding to each of the 6 tested shaker locations (see the description of the modal test in section 7.2). After some iterations, the results obtained were extremely satisfactory, and showed that the algorithm is particularly well suited to treat multiple measurements simultaneously.

Most of the frequency response functions are extremely well identified, so only problems will be noted. Figure 3.3 shows an example of a **bad** fit (the worst fit of the 28 frequency response functions treated simultaneously for the shaker on leg I). The only minor problem in this frequency response function is that the non-minimum phase zero at

47 Hz is predicted to be too lightly damped and minimum-phase (when the true zero is more damped and non-minimum phase). Note that at these frequencies the frequency response function is 40 dB lower than the response peaks for the modes at 36 Hz, so in terms of predictions this error is extremely small. Furthermore, if such errors had a significant effect (e.g. for a particular closed loop system), one could easily modify the zero location for this transfer function using the parametrization (3.2) with poles and zeros.

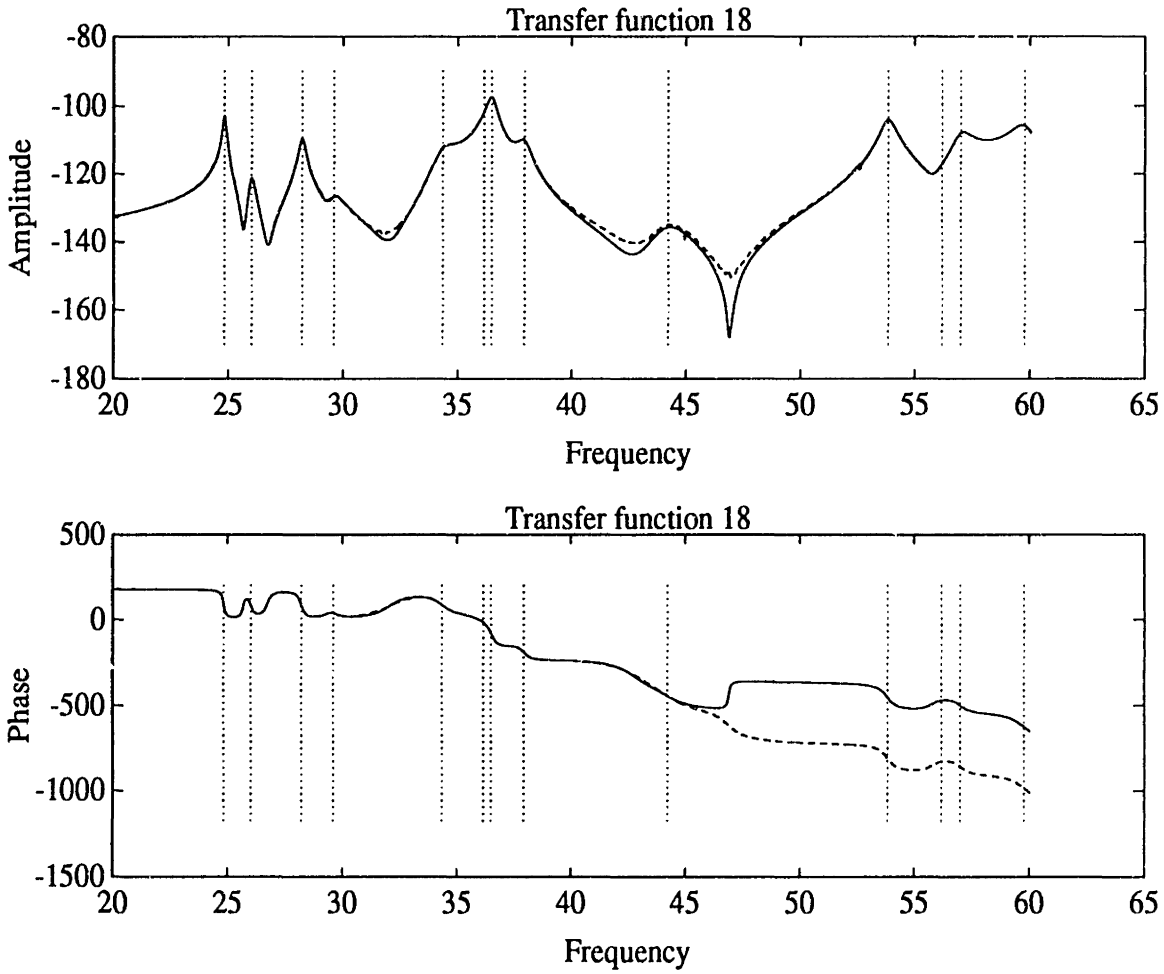

Figure 3.3: **Bad** fit of a frequency response function for the modal test of the IT. (---) measurement, (—) fit (complex mode model, with symmetric pole pattern, low and high frequency asymptotic correction terms)

Major difficulties in the 20-60 Hz frequency range, which could not be accurately identified with traditional identification algorithms, but were correctly resolved using the proposed method are:

- the mode at 45 Hz, which is a mode mostly localized to leg IV (see Figure 7.3 for the leg numbering scheme) and thus tends to have very low levels of response (as in the frequency response function shown in Figure 3.3)
- the suspension modes at 45.1 Hz and 53 Hz (only appearing as small magnitude excursions in Figure 3.3) which make the identification more difficult
- the two modes at 36.1 Hz (2.6 % damping) and 36.5 Hz (0.7 % damping), which are very close and heavily coupled by non-proportional damping.

The motivation for the independent identification of each physical test (shaker location) was that coupling with the shaker might modify the dynamics significantly. Table 3.2 gives the averaged pole estimates for the six independent identifications and the corresponding sample standard deviations on both frequencies and damping ratios (as percent deviations of the nominal value). The small variations from test to test clearly indicate both that the test was surprisingly well done and that the identification algorithm is very efficient.

Table 3.2: Mean pole locations and standard deviations for the 6 identified models (6 shaker locations).

Mean frequency in Hz $\overline{\omega} = \frac{1}{6}\sum \omega_i$	Frequency standard deviation in % of $\overline{\omega}$ $\sigma_\omega = \sqrt{\frac{1}{5}\sum(\omega_i - \overline{\omega})^2}$	Mean damping ratio $\overline{\zeta} = \frac{1}{6}\sum \zeta_i$	Damping ratio std. deviation in % of $\overline{\zeta}$ $\sigma_\zeta = \sqrt{\frac{1}{5}\sum(\zeta_i - \overline{\zeta})^2}$
24.816	0.05	0.0031	16.9
26.005	0.04	0.0054	6.5
28.199	0.06	0.0051	10.5
29.645	0.20	0.0113	7.4
34.331	0.15	0.0144	7.0
36.126	0.19	0.0281	11.6
36.490	0.07	0.0059	7.8
37.912	0.04	0.0089	5.8
44.187	0.08	0.0219	8.0
53.845	0.05	0.0064	5.0

The next step was to verify that the identified complex modes were consistent from test to test, thus improving confidence in both the identification procedure and the quality of the test that led to the identified data. For this, the collocated residues of each test were used to scale the complex modal observabilities and controllabilities as shown in section 3.2.3. For six different tests (shaker located on legs I to VI), the 28 terms of the identified scaled observabilities of the 7th complex mode are shown in Figure 3.4. Clearly, for this mode, the complete identification was very efficient since the variations from test to test of these

complex modeshape estimates are small (the corresponding terms linked by dotted lines are clustered).

For other modes, the agreement of one of the six models is sometimes less clear. However, it can be verified that the variations seen are mostly related to the scaling condition. This points to the obvious fact that modeshape scaling is very sensitive to identification errors on the collocated residues and to experimental errors linked to an imperfect measurement of the force input and its collocated displacement (which lead to the frequency response function estimate).

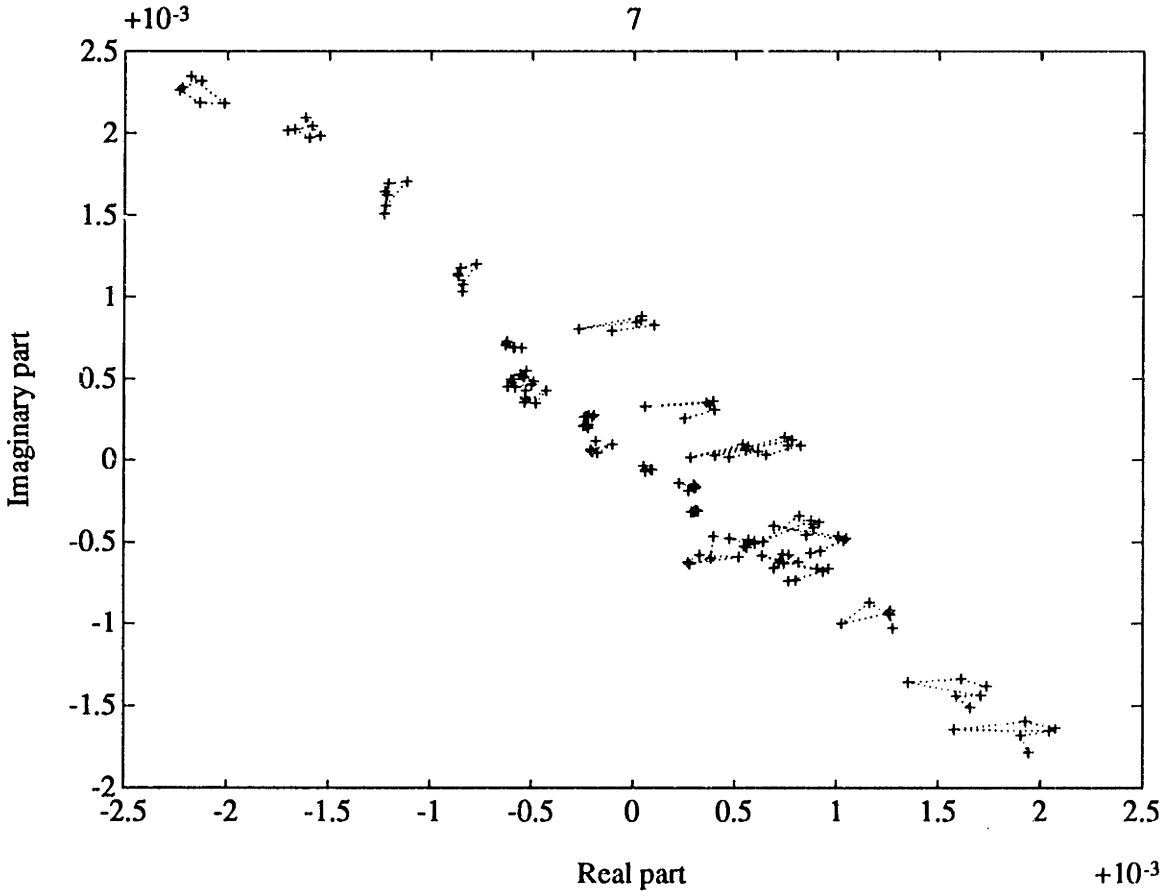

Figure 3.4: Comparison of identified scaled complex modal observabilities $c\psi_7$ of the 7^{th} mode for the six tests (dotted lines link corresponding estimates for the different tests).

Since such inconsistencies between the results of different SIMO tests of the same structure are very likely, multiple SIMO tests, like those done for the IT are very useful. Multiple SIMO tests provide redundant information on the complex mode observabilities, which can help to define a better overall model of the true system through the creation of a MIMO model (using the approach described in section 3.2.2 for example).

Such a determination, of a unique modal observability matrix from those identified in the 6 different tests, was done for the IT. The ability to scale the results properly was however lost as the modal test did not maintain a sensor at all six shaker locations for the different tests (only the current shaker location was instrumented). Table 3.3 shows the ratios to the first singular value for the MIMO interferometer testbed model (6 shakers, 27 sensors; the collocated accelerometer measurement is not included for the reason mentioned above). Even if the agreements for the scaled residues are not all as good as those shown for mode 7 in Figure 3.4, it clearly appears in this table that the identified complex modes obtained for the different tests are fairly consistent. All the ratios σ_2/σ_1 are smaller than 0.1, which means that the matrix norm of the difference between the minimal residue matrix $\tilde{R}_j$ (with only one modeshape) and the full residue matrix R_j (with 6 modeshapes) is less than a tenth of the matrix norm of R_j. Furthermore, the other ratios of singular values (σ_3/σ_1, etc.) do not drop very fast, as expected in a case where the modes are not multiple and the errors have no physical meaning.

Table 3.3: Combination of the 6 SIMO identification tests. Mean pole locations and ratios to the first singular value.

Mode frequency	Mode damping	σ_2/σ_1	σ_3/σ_1	σ_4/σ_1	σ_5/σ_1	σ_6/σ_1
24.814	0.0027	0.0250	0.0139	0.0047	0.0032	0.0018
26.010	0.0051	0.0209	0.0120	0.0070	0.0045	0.0038
28.190	0.0055	0.0184	0.0074	0.0044	0.0041	0.0015
29.672	0.0123	0.0918	0.0414	0.0249	0.0113	0.0050
34.258	0.0152	0.0894	0.0247	0.0175	0.0079	0.0043
36.185	0.0312	0.0922	0.0470	0.0212	0.0156	0.0092
36.496	0.0062	0.0521	0.0175	0.0081	0.0045	0.0022
37.915	0.0095	0.0256	0.0136	0.0089	0.0066	0.0036
44.174	0.0240	0.0632	0.0262	0.0189	0.0100	0.0060

Finally, the only remaining problem with the IT test is to determine the origin of the small inconsistencies seen between different tests. They could be linked to both system variations during the experiments and identification errors for the different tests. A further analysis will be made in section 3.4 to show that most of the discrepancies are probably of experimental origin (as the shaker was moved from test to test, the coupling of the structure with the shaker mass and stiffness introduced some variations of the system response between the different tests, which probably account for most of the observed discrepancies between different estimated modal observabilities).

3.2.5. TRANSFORMATION TO THE REAL PARAMETER STATE-SPACE FORM

For control design purposes on the tested system configuration, the complex mode model is generally sufficient (there is no need to refer to the underlying second order properties of the system as will be done in section 3.3). One is however interested in a parametrization with real parameters which will be detailed here.

As shown in section 3.2.2, the residue matrix can be decomposed into a dyad formed of a column vector $(c\psi_j)_I$ (the modal observability), and a row vector $(\psi_j^T b)_I$ (the modal controllability). From these two matrices can be derived the B and C matrices of a real parameter state-space description of the system with a bloc diagonal A matrix

$$\begin{bmatrix}\dot{x}\\ \ddot{x}\end{bmatrix}=\begin{bmatrix}0 & I\\ -\Omega^2 & -2Z\Omega\end{bmatrix}\begin{bmatrix}x\\ \dot{x}\end{bmatrix}+\begin{bmatrix}B_1\\ B_2\end{bmatrix}u$$
$$y=\begin{bmatrix}C_1 & C_2\end{bmatrix}\begin{bmatrix}x\\ \dot{x}\end{bmatrix} \tag{3.26}$$

where Ω is the diagonal matrix with the pole magnitudes (not the imaginary parts) and $-Z\Omega$ is the diagonal matrix with the real parts of the poles.

To obtain a general expression of the matrices B_1, B_2, C_1, and C_2, let us consider the transfer function linked to a single pole. The system matrix linked to this pole is

$$\begin{bmatrix}0 & 1\\ -\omega^2 & -2\zeta\omega\end{bmatrix} \tag{3.27}$$

whose left and right eigenvectors (not scaled) associated with the eigenvalue $-\zeta\omega+i\omega\sqrt{1-\zeta^2}=\lambda$ are respectively

$$\begin{bmatrix}-\bar{\lambda} & 1\end{bmatrix} \text{ and } \begin{bmatrix}1\\ \lambda\end{bmatrix}, \tag{3.28}$$

with the norm

$$\begin{bmatrix}-\bar{\lambda} & 1\end{bmatrix}\begin{bmatrix}1\\ \lambda\end{bmatrix}=\lambda-\bar{\lambda}=2i\omega\sqrt{1-\zeta^2}. \tag{3.29}$$

From these vectors one can easily prove that the complex dyadic residue matrix $R_j=c\psi_j\psi_j^T b$ (see section 3.2.2) associated with the single mode system

$$\frac{y}{u}=\begin{bmatrix}C_1 & C_2\end{bmatrix}\begin{bmatrix}s & -1\\ \omega^2 & s+2\zeta\omega\end{bmatrix}^{-1}\begin{bmatrix}B_1\\ B_2\end{bmatrix} \tag{3.30}$$

verifies the following matrix equation

$$\left(\lambda-\bar{\lambda}\right)\, c\psi_i\psi_i^T b=\left(C_1+\lambda C_2\right)\left(-\bar{\lambda}B_1+B_2\right). \tag{3.31}$$

Clearly, this equation does not uniquely define C_1, C_2, B_1, and B_2. Without any other constraint (such as the collocation constraint introduced in section 3.2.3), one can only say that for an arbitrary constant a the solution verifies

$$\begin{aligned} ac\psi_i &= \left(C_1+\lambda C_2\right) \\ a^{-1}\left(\lambda-\bar{\lambda}\right)\, \psi_i^T b &= \left(-\bar{\lambda}B_1+B_2\right) \end{aligned} \tag{3.32}$$

A sensible, but arbitrary choice is to use $a=1$, which leads to the following transformation between the modal observabilities and controllabilities, and the real valued matrices C_1, C_2, B_1, and B_2

$$\begin{aligned} \begin{bmatrix} C_1 \\ C_2 \end{bmatrix} &= \begin{bmatrix} 1 & -\zeta\omega \\ 0 & \omega\sqrt{1-\zeta^2} \end{bmatrix}^{-1} \begin{bmatrix} \mathrm{Re}(c\psi_i) \\ \mathrm{Im}(c\psi_i) \end{bmatrix} = \frac{1}{\omega\sqrt{1-\zeta^2}} \begin{bmatrix} \omega\sqrt{1-\zeta^2} & \zeta\omega \\ 0 & 1 \end{bmatrix} \begin{bmatrix} \mathrm{Re}(c\psi_i) \\ \mathrm{Im}(c\psi_i) \end{bmatrix} \\ \begin{bmatrix} B_1 \\ B_2 \end{bmatrix} &= 2 \begin{bmatrix} 1 & 0 \\ -\zeta\omega & -\omega\sqrt{1-\zeta^2} \end{bmatrix} \begin{bmatrix} \mathrm{Re}\left(\psi_i^T B\right) \\ \mathrm{Im}\left(\psi_i^T B\right) \end{bmatrix} \end{aligned} \tag{3.33}$$

From this transformation, it clearly appears that in a MIMO case both a B_1 and a C_2 term exist (unless a particular choice of a allows making one of them zero, an option which always exists for SIMO problems using $a=\left(\lambda-\bar{\lambda}\right)\, \psi_i^T b$ for example). In the modal contribution, the terms are thus mixed as follows

$$\frac{y}{u}=\frac{C_v s+C_p}{s^2+2\zeta\omega s+\omega^2}=\frac{\left(C_1B_1+C_2B_2\right)s+\left(2\zeta\omega C_1B_1-\omega^2C_2B_1+C_1B_2\right)}{s^2+2\zeta\omega s+\omega^2} \tag{3.34}$$

The matrices C_v and C_p (used in different Refs. [kal1, gil1, spa1]) describe the combined effects of the complex-conjugate pair of modes. The relation between the rank of these two matrices and the modal multiplicity is unclear, and should be investigated for a proper use of such a parametrization. (The parametrization proposed in this chapter describes each mode separately, so that the mode multiplicity can be deduced from the dyadic decomposition of the residue matrix as described in section 3.2.2).

3.3. Identification of Normal Modes from Complex Modes

Because most finite element models are undamped, comparisons between the finite element predictions and experimental modes can only be done using "experimental" normal modes. Since normal modes are the modes of the ideal undamped system which cannot be tested, true modes are always complex and normal modes are idealizations whose

determination involves more assumptions on the system response. However, since this parametrization is essential for the use of undamped structural models, numerous methods have been created to estimate normal modes from identified complex modes, using different assumptions that have proven to be too constraining for many real structures (see the review in Ref. [ses1]).

After a review of existing results in section 3.3.1, a new approach will be detailed. The weak assumption is made that the non-proportional damping only couples the identified modes (as first done in section 2.2.1) or, in other words, that the dissipation of the low frequency normal modes depends on the states of other low frequency normal modes, but not on the states of higher frequency modes. In section 3.3.2, it is shown that the verification of a properness condition by the complex modes is sufficient for the existence of an exact transformation (detailed in the section) between the complex and normal mode parametrizations. Recognizing that identified poles are generally much more accurate than identified modeshapes, a new algorithm is derived in section 3.3.2 to determine, in both cases with as many and more sensors than modes, the set of proper complex modes closest to the measured modes. From these proper modes, the truncated normal mode model can then be determined with no further approximation. Finally in section 3.3.4, results from the IT modal test are analyzed, showing the method to be very accurate and marking the first successful experimental characterization of non-proportional damping (previous results only considered simple two-mode systems).

3.3.1. Review of Existing Work

For the estimation of normal modes from identified complex modes, early approaches considered the norm of the complex modal observability, and adjusted its sign to optimize the resulting modeshape

$$c\phi_j = \pm\left|c\psi_j\right|. \tag{3.35}$$

As seen in section 2.1.2, this approach is exact for a proportionally damped system, but it gives poor results for systems with even relatively small effects of non-proportional damping (see Ref. [ibr1] for example). An extension of this approach uses a projection of the identified complex modes into a subspace of real modes

$$c\psi = (c\phi)_{ID} T \tag{3.36}$$

where $(c\phi_j)_{ID}$ is the matrix of identified normal modes, and T is a complex valued transformation matrix. References [ses1, zha1, imr1] detail different ways of determining the transformation matrix T, but none of the methods have been sufficiently accurate for

systems with even low effects of non-proportional damping (when the phase dispersion ("complexity") of the identified modeshapes is non-negligible). The new approach presented here gives a particular transformation T and estimated normal mode observability $\left(c\phi_j\right)_{ID}$, which is shown to be exact because proper complex modes are used (see section 3.3.2).

Several Direct System Parameter Identification (DSPI) techniques have used a reduced second order system parametrization $\left[M^{-1}C\ M^{-1}K\right]$ (which can be transformed to the normal mode form) and data obtained, experimentally [leu1, cra1] or analytically with the experimental complex mode model [wei2] (sometimes augmented with high frequency analytical modes [ibr1, ibr2]). Although such approaches are tempting, successful identifications of non-proportional damping have only been reported for extremely simple structures. The identified pole locations are often inaccurate (e.g. unstable poles at inexact frequencies). Furthermore, it is difficult to enforce the identification of mostly local modes and to remove computational poles from the estimation process. Also, the contributions of modes outside the bandwidth are not accounted for.

Finally, the work of Natke [nat1] is often mentioned (although not as being more efficient than other traditional methods) and the ongoing work by Alvin and Park [alv1, alv2, par1] seems to contain the elements for an efficient solution. However, the identification results used by these authors do not have the accuracy obtained with the method proposed in section 3.2, so the validity of their method could not be demonstrated for experimental results.

3.3.2. The Properness Condition and The Exact Transformation Between Complex and Normal Modes

As normal modes are idealizations, their determination is necessarily linked to assumptions. Here it will be assumed that non-proportional damping does not couple low and high frequency normal modes. As seen in section 2.2.1, the response of the system can thus be accurately described by a truncated normal mode model of the form

$$\begin{aligned} \left(s^2 I + s\Gamma_{TT} + \Omega_{TT}\right)p_T &= \phi_T^T bu \\ y &= c\phi_T p_T + E \end{aligned} \tag{3.37}$$

To this model are associated complex modes ψ_{Tj} which are uncoupled from the effects of out-off band modes (whose effects are approximated by the E term; see section 2.2.2 for more details) and which can be used to describe, as in section 2.1.2, the transfer function from a force input u to a velocity measurement y_{vel}

$$y_{vel} = \sum_{j=1}^{2N_T} s \frac{c\psi_{Tj}\psi_{Tj}^T b}{s-\lambda_j} u + E \ . \tag{3.38}$$

It is well known that for a structural system, force commands acceleration and not velocity. The velocity roll-off at high frequencies is thus a **properness** condition that is clearly verified by the normal mode states p_j in (3.37) and must thus also be verified by the transfer function using the complex mode description in (3.38), which implies that

$$\lim_{s\to\infty} \sum_{j=1}^{2N_T} \frac{s\left(c\psi_{Tj}\psi_{Tj}^T b\right)}{s-\lambda_j} = \sum_{j=1}^{2N_T} \left(c\psi_{Tj}\psi_{Tj}^T b\right) = 0. \tag{3.39}$$

Note that the E term is omitted in (3.39). This is where the assumption of uncoupling with higher frequency normal modes appears.

Equation (3.39) must be verified for all b and c, so that

$$\sum_{j=1}^{2N_T} \psi_{Tj}\psi_{Tj}^T = \psi_T \psi_T^T = 0 \ . \tag{3.40}$$

As seen in section 2.1.2, ψ has dimensions N by $2N$, so that the matrix equation (3.40) has many other solutions than the trivial $\psi = 0$. The matrix equation (3.40) is a set of constraints on all the complex modes of the truncated model (the index j is summed over all these modes) applicable independently at any degree of freedom (in (3.39) the matrices b and c are arbitrary).

The novelty of the proposed approach is to recognize that the properness condition (3.40) is sufficient for the existence of an exact transformation, between complex and normal modes, which will be detailed now.

In a non-modal coordinate system, the second order dynamics of the truncated modal model (3.37) are described by "truncated" mass M_T, damping C_T, and damping K_T matrices. It was seen in section 2.1.2, that the corresponding complex modeshapes ψ_T, if scaled using collocation constraints (see section 3.2.3), verified two orthogonality conditions

$$\theta_T^T \begin{bmatrix} C_T & M_T \\ M_T & 0 \end{bmatrix} \theta_T = I \text{ and } \theta_T^T \begin{bmatrix} K_T & 0 \\ 0 & -M_T \end{bmatrix} \theta_T = -\Lambda_T \text{ where } [\theta_T] = \begin{bmatrix} \psi_T \\ \psi_T \Lambda_T \end{bmatrix}. \tag{3.41}$$

Simple algebraic manipulations of the two orthogonality conditions in (3.41) lead to two inverse orthogonality conditions

$$\begin{bmatrix} C_T & M_T \\ M_T & 0 \end{bmatrix}^{-1} = \begin{bmatrix} 0 & M_T^{-1} \\ M_T^{-1} & -M_T^{-1} C_T M_T^{-1} \end{bmatrix} = \theta_T \theta_T^T = \begin{bmatrix} \psi_T \psi_T^T & \psi_T \Lambda_T \psi_T^T \\ \psi_T \Lambda_T \psi_T^T & \psi_T \Lambda_T^2 \psi_T^T \end{bmatrix} \tag{3.42}$$

$$\begin{bmatrix} K_T & 0 \\ 0 & -M_T \end{bmatrix}^{-1} = \begin{bmatrix} K_T^{-1} & 0 \\ 0 & -M_T^{-1} \end{bmatrix} = -\theta_T \Lambda_T^{-1} \theta_T^T = -\begin{bmatrix} \psi_T \Lambda_T^{-1} \psi_T^T & \psi_T \psi_T^T \\ \psi_T \psi_T^T & \psi_T \Lambda_T \psi_T^T \end{bmatrix} \tag{3.43}$$

where it can be easily verified that the properness condition (3.40) is indeed a necessary and sufficient condition for the system to be second order (the sub-blocs, that are zero in the two algebraic left hand expressions of (3.42)-(3.43), are effectively equal zero in the two experimental right hand expressions if and only if $\psi_T \psi_T^T = 0$).

From equations (3.42) and (3.43), one obtains the following simple expressions for M_T, C_T, and K_T

$$M_T = \left(\psi_T \Lambda_T \psi_T^T\right)^{-1},\ C_T = -M_T \psi_T \Lambda_T^2 \psi_T^T M_T,\ \text{and}\ K_T = -\left(\psi_T \Lambda_T^{-1} \psi_T^T\right)^{-1} \tag{3.44}$$

which can be easily transformed to the normal mode coordinates p_T of (3.37), by solving the undamped reduced eigenvalue problem $-M_T \phi_T \Omega_T + K_T \phi_T = 0$ as was done for the full system considered in section 2.1.3.

This last transformation may however lead to some problems if the identified matrices do not verify the expected conditions of positive definiteness. It is known from physical principles that the mass, damping and stiffness matrices of structural systems are positive definite (see section 2.1.1). Therefore, the truncated matrices as well as their inverses should be positive definite. Based on the inverse orthogonality conditions (3.42)-(3.43), the positive definiteness of the truncated system matrices is clearly equivalent to the three conditions

$$\psi_T \Lambda_T \psi_T^T > 0, \quad \psi_T \Lambda_T^2 \psi_T^T < 0, \quad \text{and}\ \psi_T \Lambda_T^{-1} \psi_T^T < 0 \tag{3.45}$$

corresponding respectively to the positive definiteness of the identified mass, damping, and stiffness matrices (the stiffness and damping matrices can only be semi-definite for systems with rigid body modes, to which this transformation does not apply).

If the identified mass and stiffness are positive definite, normal modes can be determined with, in general, a good accuracy. If not, any of several problems may have occurred: the complex modes may not have been well identified, they may have been improperly scaled, the complex modes used may not be proper (see section 3.3.3) or, even though it was never found to be the case, the assumption of normal mode decoupling from higher frequency modes may not be good enough (so that the proper complex modes determined by the method proposed in section 3.3.3 are not good approximations of the identified complex modes).

The positive definiteness of the damping matrix is less of a problem, since for the lightly damped structures considered here, extremely small errors may make the damping matrix non-positive-definite and yet result only in minor differences in the predicted

response. For the case of the IT, this can be seen as the fact that the identified damping matrices for the 6 different tests lead to damping matrices which are in good agreement for the important terms (diagonal and significant non-proportional damping coupling terms) but have larger differences for other small off-diagonal terms (see section 5.2.3).

Finally, an important property that must be verified is the invariance of the transformation through a change of coordinates. For a new set of eigenvectors $\psi_N = T\psi_0$ it is easy to verify that all the system matrices are multiplied on the left by T^{-T} and on the right by T^{-1} so that the overall input-output properties are unchanged. In practice however, the properness condition must be enforced as will be shown in section 3.3.3, so that a coordinate transformation T may influence different transfer functions in a selective way.

3.3.3. Optimal Approximation of the Identified Complex modes by Proper Complex Modes.

The scaled estimates of the modal observabilities $\left(c\psi_j\right)_I$ and controllabilities $\left(\psi_j^T b\right)_I$ allow the definition of a complex mode at the degrees of freedom of the chosen sensors and actuators. If the degrees of freedom measured by the sensors c_1 to c_{Ns} are arbitrarily chosen to be the model "physical degrees of freedom" q_T, one thus has a scaled estimate of the complex modeshape $\psi_{Tj} = \left(c\psi_j\right)_I$ (note that the finite element degrees of freedom are usually not such that this is true, which initially motivated the introduction of the input shape matrix c in section 2.1.1).

As a first step, it will be assumed that there are as many sensors as modes (so that $\psi_T = \left(c\psi\right)_I$ is a N_T by $2N_T$ matrix). The transformation (3.44) between complex and normal modes is only exact if the properness condition (3.40) is verified. Since such is usually not the case, an algorithm will be derived to determine a good but proper approximation of the identified modes ψ_T.

The objective of this algorithm is to find the smallest correction $\Delta\psi$ to the measured eigenvector ψ_T, that will lead to a set of proper modes verifying (3.40). For this, $\sum_{i,j} \Delta\psi_{ij}^* \Delta\psi_{ij}$, which is a quadratic norm of $\Delta\psi$, will be minimized under the constraint that $\tilde{\psi}_T = \psi_T + \Delta\psi$ must meet the properness condition $\tilde{\psi}_T \tilde{\psi}_T^T = 0$.

This constrained minimization problem can be solved using a matrix of complex Lagrange multipliers $\delta = \delta^R + i\delta^I$. Following the standard mathematical procedure, the Lagrangian cost function H is derived

$$H = \left\{ \sum_{i,j} \Delta\psi_{ij}^* \Delta\psi_{ij} + \sum_{i,j,l} \delta_{ij}^R \left(\psi_{il}^R \psi_{jl}^R - \psi_{il}^I \psi_{jl}^I \right) + \sum_{i,j,l} \delta_{ij}^I \left(\psi_{il}^R \psi_{jl}^I + \psi_{il}^I \psi_{jl}^R \right) \right\} \qquad (3.48)$$

and one seeks $\Delta\psi = \arg\min(H)$. At the minimum, the derivatives of H with respect to the components of $\Delta\psi$ must be zero

$$\begin{aligned}\frac{\partial H}{\partial \Delta\psi_{ij}^R} &= \Delta\psi_{ij}^R + \sum_l \left(\delta_{il}^R + \delta_{li}^R\right)\psi_{lj}^R + \sum_l \left(\delta_{il}^I + \delta_{li}^I\right)\psi_{lj}^I = 0 \\ \frac{\partial H}{\partial \Delta\psi_{ij}^I} &= \Delta\psi_{ij}^I - \sum_l \left(\delta_{il}^R + \delta_{li}^R\right)\psi_{lj}^I + \sum_l \left(\delta_{il}^I + \delta_{li}^I\right)\psi_{lj}^R = 0\end{aligned} \tag{3.49}$$

This necessary condition of optimum with respect to $\Delta\psi$ can be rewritten in a more compact matrix form as

$$\Delta\psi + \delta\left(\overline{\psi}_T + \Delta\overline{\psi}_T\right) = 0, \tag{3.50}$$

where $\delta = \delta^R + i\delta^I$. Combining (3.50) with its complex-conjugate one obtains

$$\Delta\psi = \left(I - \delta\overline{\delta}\right)^{-1}\left(\delta\overline{\delta}\psi_T - \delta\overline{\psi}_T\right) \quad \text{or} \quad \tilde{\psi}_T = \psi_T + \Delta\psi = \left(I - \delta\overline{\delta}\right)^{-1}\left(\psi_T - \delta\overline{\psi}\right) \tag{3.51}$$

Using the expression of $\tilde{\psi}_T$ in (3.51) to rewrite the properness condition leads to

$$\tilde{\psi}_T\tilde{\psi}_T^T = \left(I - \delta\overline{\delta}\right)^{-1}\left(\psi_T - \delta\overline{\psi}\right)\left(\psi_T - \delta\overline{\psi}\right)^T\left(I - \delta\overline{\delta}\right)^{-T} = 0. \tag{3.51a}$$

Multiplying equation (3.51) by $\left(I - \delta\overline{\delta}\right)$on the left and its transpose on the right leads to the following algebraic Riccati equation

$$\psi_T\psi_T^T - \delta\overline{\psi}_T\psi_T^T - \psi_T\overline{\psi}_T^T\delta + \delta\overline{\psi}_T\overline{\psi}_T^T\delta = 0 \tag{3.52}$$

Riccati equations have multiple solutions, so it is difficult to ascertain that a particular choice is the best "global" minimum. Here it will be shown that the real-valued positive-definite solution δ, chosen in control theory as the steady-state solution of an optimal regulation problem for a linear time-invariant system (see Ref. [mac1]), is appropriate.

A necessary and sufficient condition for the solution to be a minimum is that the matrix of second order derivatives of H be positive definite. The second order derivatives of H (Hessian) are the following

$$\frac{\partial^2 H}{\partial\Delta\psi_{uv}^R\partial\Delta\psi_{kl}^R} = e_{vl}\left(e_{uk} + \delta_{uk}^R\right), \quad \frac{\partial^2 H}{\partial\Delta\psi_{uv}^I\partial\Delta\psi_{kl}^I} = e_{vl}\left(e_{uk} - \delta_{uk}^R\right), \text{ and } \frac{\partial^2 H}{\partial\Delta\psi_{uv}^R\partial\Delta\psi_{kl}^I} = e_{vl}\left(\delta_{uk}^I\right) \tag{3.53}$$

where e_{vl} is the delta operator (equal to 1 if $v=l$ and equal to 0 otherwise). Thus, in matrix form, the condition of positive definiteness of the second order derivatives is

$$\begin{bmatrix} I + \delta^R & \delta^I \\ \delta^I & I - \delta^R \end{bmatrix} > 0 \tag{3.54}$$

If the optimal control solution for δ (the real-valued positive-definite solution) is used when solving the Riccati equation (3.52), δ is real, so that the condition (3.54) is the equivalent to $I+\delta>0$ and $I-\delta>0$. The first condition is clearly verified for a positive definite δ. The second implies that eigenvalues of δ must be of norm less than 1. No proof that this is necessarily true was found, but all the cases treated verified this condition.

A good but proper approximation of the identified complex modes ψ_T is thus defined by (3.51), where δ is taken to be the real-valued positive-definite solution of the Riccati equation (3.52). This solution has proven to be efficient in all the cases treated, but it might still be interesting to study

- the effect of coordinate system choice in cases with both as many sensors as modes and more sensors than modes: the properness could be enforced on ψ_T such that $(c\psi)_I = c_T \psi_T$ for any possible coordinate transformation matrix c_T. Different choices for c_T might lead to somewhat different results.
- the interest of other (non-positive-definite and/or non-real) solutions of the Riccati equation.
- cases with less sensors than modes (see the work of Alvin and Park on this subject [alv1]).

In many practical applications, the number N_T of identified modes is often smaller than the number N_S of sensors (in the normal mode form (3.37), the size of u the input or y the output vectors are not limited). In such cases, the sensor/actuator degree of freedom coordinate system q_T has more degrees of freedom than modes in the system to be identified, which implies that these degrees of freedom are not independent. (Using the comparison to a finite element model with N DOFs, it is possible to define any number of sensors (N_S can be larger than N) defined as constant linear combinations of the FE DOFs ($y=cq$)).

For the identification problem in cases where there are more sensors than modes, one must thus define a reduced set of N_T generalized "physical" coordinates q_T, with known input and output shape matrices (c_T and b_T) to pass from the measurement coordinates to the generalized coordinates q_T. These generalized coordinates should be such that the product of the input shape matrix c_T and complex modeshape matrix ψ_T is a good approximation (retaining most of both the magnitude and phase information) of the identified complex mode observability matrix

$$c_T \psi_T \approx (c\psi)_I \tag{3.46}$$

A method, found to be efficient for all the cases treated in this research, is to choose c_T so as to obtain the best possible approximation of M^{-1}. For this, the expression of the reduced mass (3.44) is used as follows

$$(c\psi)_l \Lambda (c\psi)_l^T = c_T \psi_T \Lambda \psi_T^T c_T^T = c_T M^{-1} c_T^T \tag{3.47}$$

In (3.47), M^{-1} is of rank N_T. Using for c_T the first N_T eigenvectors of the eigenvalue decomposition of $(c\psi)_l \Lambda (c\psi)_l^T$ thus results in a good approximation of M^{-1}. It is useful to note that since the matrix $(c\psi)_l \Lambda (c\psi)_l^T$ is symmetric, the singular values of this matrix are the absolute values of the eigenvalues. Using the eigenvalues rather than the singular values allows one to verify that the main contribution (the terms that are kept) are indeed positive definite, and such that a positive definite mass matrix will be obtained in the transformation (3.44).

Having determined c_T, the best set of N_T complex eigenvectors ψ_T can be found by a least-squares fit derived from (3.46). Finally, using a proper approximation of ψ_T, the transformation can be done as for the case with $N_s = N_T$. For all the cases considered on the IT, these choices for c_T and ψ_T were appropriate since they led to normal mode models that accurately matched the measured frequency response functions.

One might be tempted to use the approximation of M^{-1} in (3.47) and similar expressions for K^{-1} and C rather than find a proper approximation of the complex modes first, this is however usually gives poor results, since such approximations do not conserve poles which are very well known and should thus not be modified. In fact, the principal advantage of the proposed method may be that it does not modify the location of the identified poles.

3.3.4. Applications to the Interferometer Testbed Modal Test

The first 9 modes of the IT are relatively well separated from higher frequencies (mode 9 is at 44.2 Hz and mode 10 at 53.8 Hz). Furthermore, these modes are well correlated with the finite element results so that comparisons can be easily made. It was therefore decided, for the examples of this section, to identify the normal modes corresponding to the first 9 flexible modes of the IT.

A first problem is to evaluate the differences between the identified complex modes and their proper approximations introduced in section 3.3.3. Using the modal test of leg V with 28 sensors, proper complex modeshapes $\tilde{\psi}_T$ were computed, and Figure 3.5 compares the identified complex modal observabilities $c\psi_6$ for mode 6, the proper complex modal observabilities $c\tilde{\psi}_6$, and for reference the complex modal observabilities $c\hat{\psi}_6$ that would exist for a proportionally damped structure.

Clearly, the proper approximation of the complex mode maintains the strong phase information present in the modal observabilities (the phase dispersion is higher than 30° for mode 6). In comparison, the complex mode of the proportionally damped model is a bad approximation, because all its observabilities are forced to be either in-phase or out-of-phase (on the -45° line here, because of the scaling condition used).

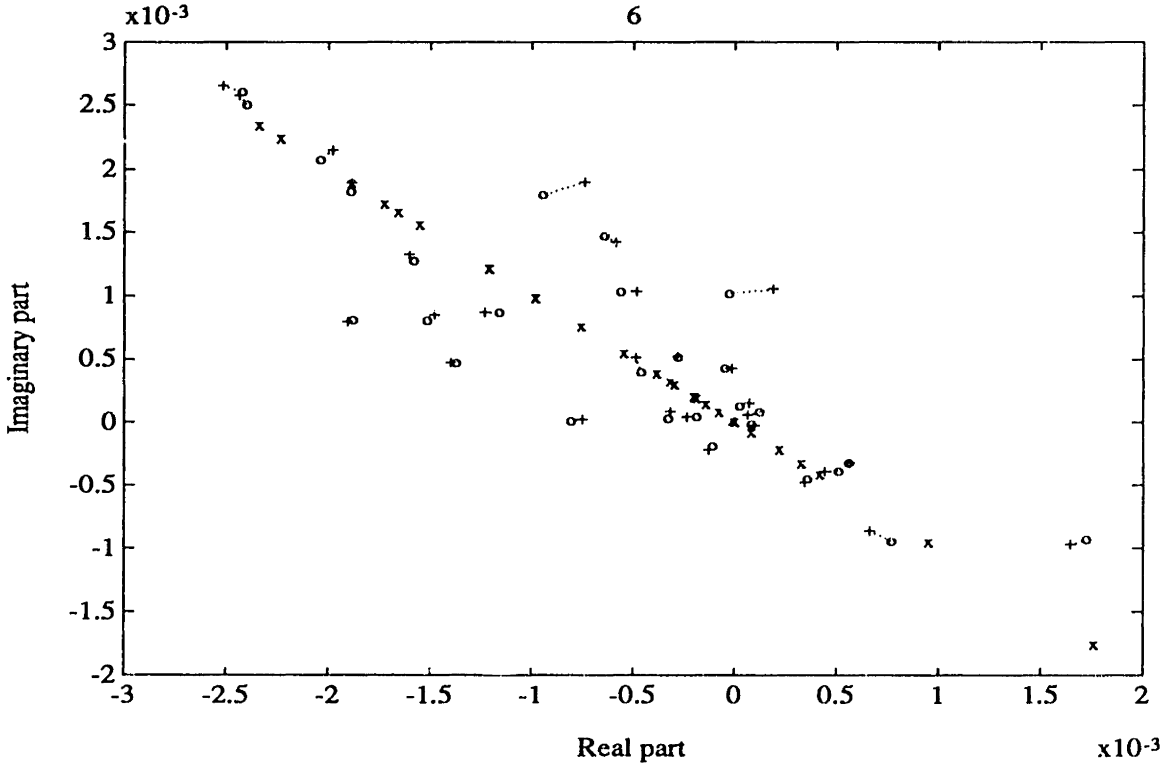

Figure 3.5: Comparison of complex residues $c\psi_6$ for the 6th mode: (+) non-proper complex mode, (o) non-proportionally damped normal mode model, (x) normal mode model constrained to be proportionally damped. Dotted lines link corresponding proper and non-proper complex residues.

The influence of proportional damping is particularly important for mode 6 because it is strongly coupled with mode 7, which is very close in frequency (see more details in section 5.2.3). For other modes, which are less coupled by damping, the residues tend to be much closer to the line of the proportionally damped model (phase dispersion between 4° for mode 2 and 25° for mode 9, versus 33° for mode 6) so that the error linked to the use of a proportional damping assumption is smaller.

Frequency response functions provide another usual way to visualize the model accuracy. Figure 3.6 compares in a small frequency range the measured frequency response function (leg IV, sensor 1) with the predictions of three different models.

The non-proportionally damped normal mode model identified using the new methods introduced in sections 3.2 and 3.3 matches the measurement both in phase and magnitude.

The Direct System Parameter Identification model (method proposed by Craig [cra1]) is clearly not accurate, even though a significant effort was made to find the frequency weighting giving the best results. As shown in the frequency response function, this model does not properly capture the two modes at 36.1 Hz and 36.5 Hz and, in the parametric model, it has a clearly inexact representation of damping (some poles of the DSPI model are unstable).

Finally, the proportionally damped model obtained by setting to zero the off-diagonal terms of the identified Γ makes significant errors both in magnitude (close to 10 dB) and phase (close to 30°).

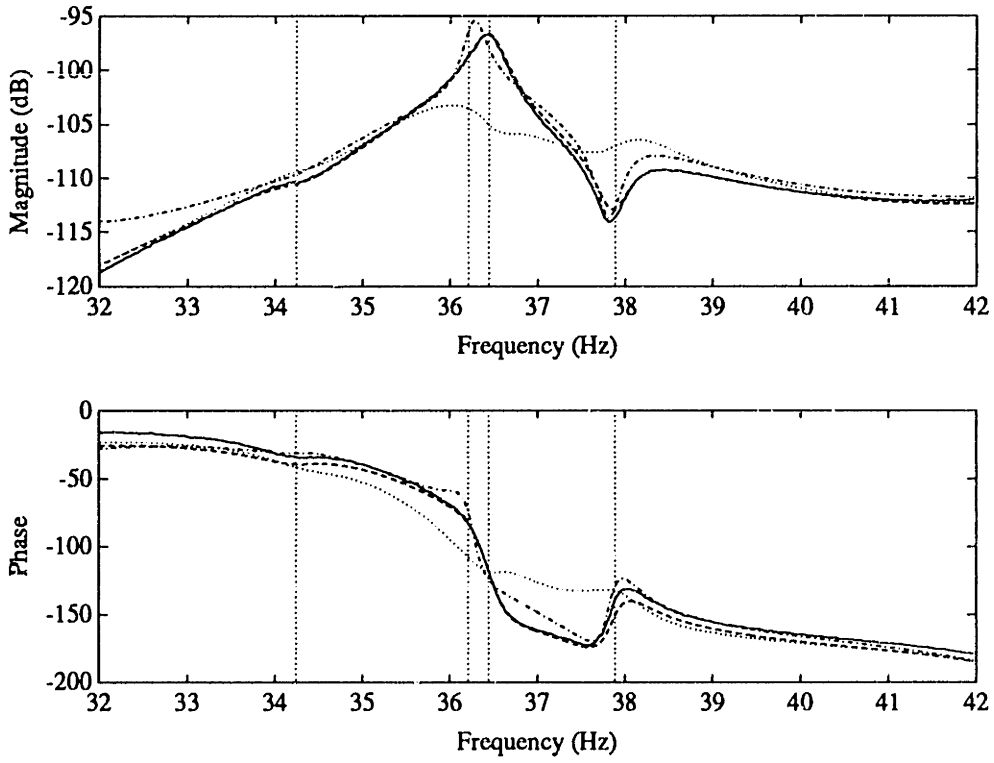

Figure 3.6: Frequency response function predictions: (—) measurement, (---) normal mode model, (·—·) direct system parameter identification (best estimate found), (·····) normal mode model constrained to be proportionally damped.

The frequency band shown, with the very close and coupled modes 6 and 7, is particularly difficult to identify, and only the new normal mode identification method gave appropriate results. In many other cases, traditional approaches are efficient, but their

results can generally be improved by using an optimization similar to that considered in section 3.2.

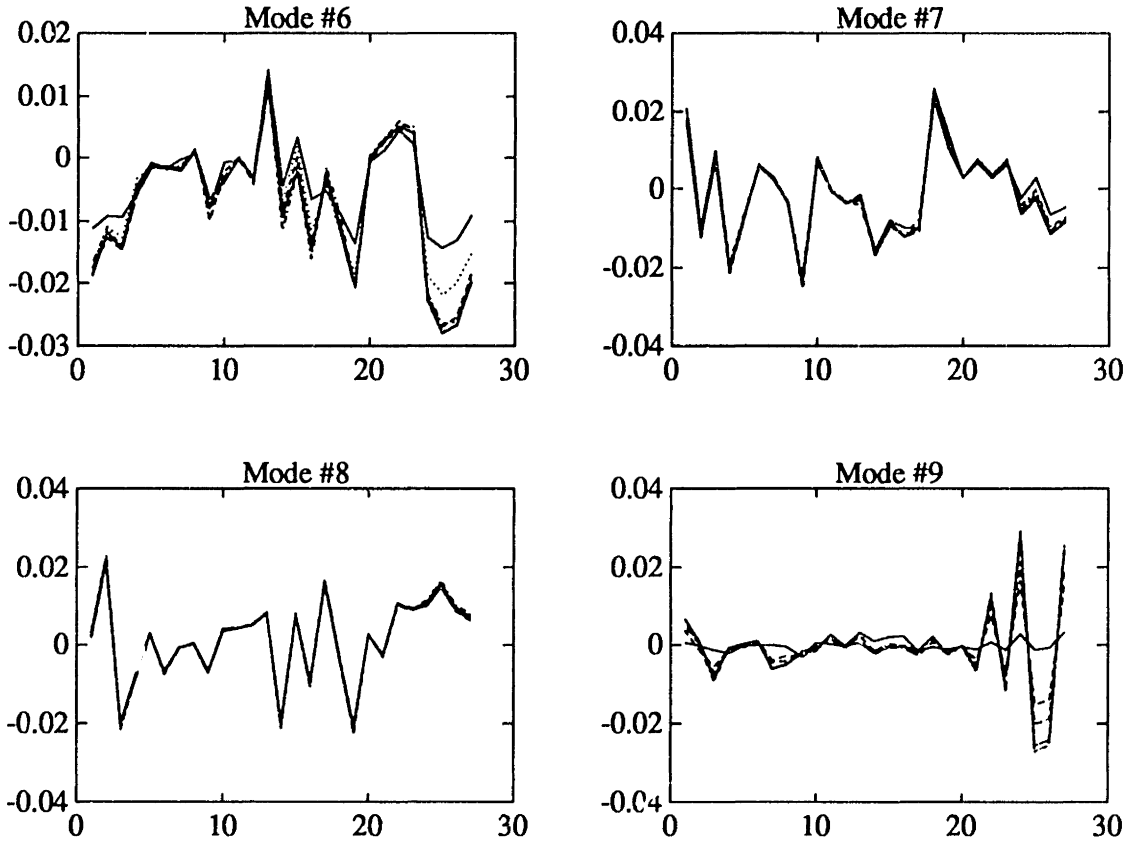

Figure 3.7: Comparison of the 27 scaled normal mode observabilities $c\phi_j$ of modes 6 through 9 as identified from the 6 different tests.

Another useful evaluation of the identification accuracy is to compare normal modeshapes. The scaled normal mode modal observabilities $c\phi_j$ at the 27 non-collocated sensors (for the 6 tests) are compared in Figure 3.7 for modes 6 through 9. The overall agreement between the different tests is clear, but some difficulties are worth mentioning. The estimated modeshapes of modes 6 and 9 for leg I (solid lines in the figure) depart significantly from the other estimates. This can be related to the fact that the test on leg I does not excite these two modes very well, so their identification can be expected to be less accurate, particularly for the scaling (the collocated residues for these two modes are very small, so errors that would otherwise be insignificant can have a large impact). Note also that many of the residues of mode 9 are small which can be seen as due to the fact that this mode is mostly localized to leg IV.

Finally, the parametrization (3.9) allowing the direct identification of real modes was introduced in section 3.1. The identification algorithm derived from this parametrization implicitly assumes proportional damping, but has the advantage, over the approach introduced in section 3.3, of being a direct normal mode identification method. In Figure 3.8, the normal mode residues $c\phi_j\phi_j^T b$ obtained for leg II through this identification method are compared with those obtained through the non-proportionally damped identification method. Clearly, except for mode 9, the agreement is relatively good (even though not as good as the consistency of the non-proportionally damped models obtained using the 6 tests). This was expected since the proportional damping assumption is, in most cases, a good assumption.

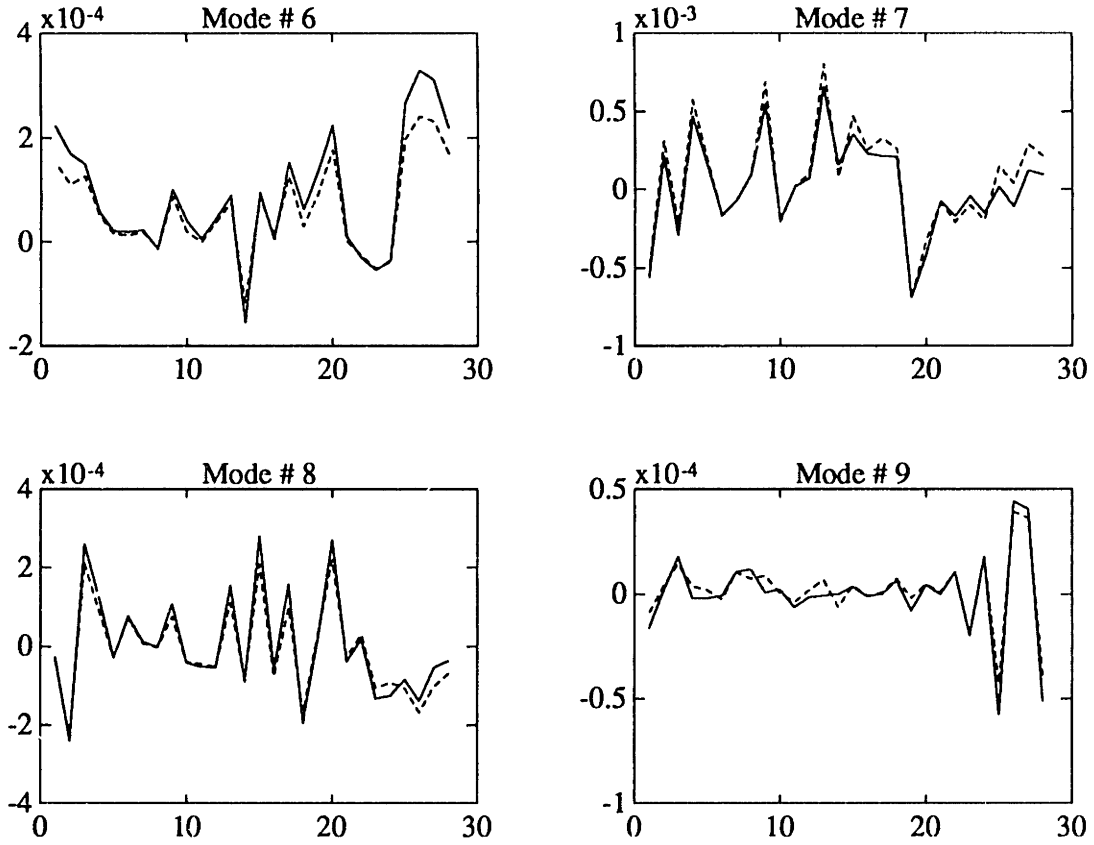

Figure 3.8: Comparison of normal modes residues $c\phi_j\phi_j^T b$ for the identified non-proportionally damped normal mode model, and for the "real" mode identified model.

This model is, however, not accurate enough to define scaled estimates of the normal modeshapes. The parametrization (3.9) does not guarantee and does not always yield positive collocated normal mode residues (since for a collocated transfer function $c_i\phi_j$ and

$\phi_j^T b_l$ are equal, the residue $c_l \phi_j \phi_j^T b_l$ should be positive). When a collocated residue is negative, the corresponding mode cannot be scaled so that another test is necessary. This hard limitation on the use of the real mode parametrization probably comes from the constraints implied by the use of a proportionally damped model, but might also indicate that the transfer function thought to be collocated is actually not exactly collocated.

3.4. Evaluation of the Identification Error

A last point of interest for the validation of the proposed identification method is an evaluation of how much error in the estimated parameters can result from the identification process. Under the assumption that the structure is linear and that there exists an accurate truncated linear model of one of the parametric forms detailed in this chapter for the considered frequency range, which ensures the validity of the identification approach, this section evaluates the sensitivity of identified parameters to errors in the measured frequency response functions.

A partial review of existing work on this subject is done in section 3.4.1. Since the proposed complex mode identification algorithm gives optimal results, a sensitivity of the identified results with respect to error in the measured frequency response functions can be obtained as detailed in section 3.4.2. However, the practical evaluation of the sensitivities is quite complicated, so that, in practice, only partial information is available. An example drawn from the IT case is detailed in section 3.4.3, allowing some conclusions on the IT models and the applicability of sensitivity approaches.

3.4.1. Partial Assessment of Existing Work

In references [jua2, lon1], Juang gives a good analysis of the limitations of the ERA algorithm, which could be generalized to other "black-box" identification algorithms.

These algorithms identify major dynamic contributions in the measured input/output response. If, as done in Ref. [jua2], a measure can be obtained for the identification criterion of the level of contribution linked to noise in the measured response (after non-parametric identification in general), one can expect that all identified dynamics with a smaller impact on the response will be excessively dependent on the measurement error. This argument may, however, be invalid if the measurement error and the identified quantity contribute to the system response in very distinct ways. For example, the response of a local mode may be small, but, if the mode resonance is in a frequency region with low noise levels, it can be accurately estimated. This argument gives another reason to prefer,

as proposed in this chapter, an identification through a directed optimization, which allows use of this type of physical knowledge that is available for lightly damped structures.

A second argument, developed in Ref. [jua2] and used in industrial applications [lms1], is linked to the fact that many algorithms use "computational" modes that do not represent physical properties of the true system but help creating a model. The properties of the true modes (which do represent the physical system characteristics) should clearly be independent from the number of computational modes. The consistency of the estimated properties for different numbers of computational modes can thus be used as a good indication of their accuracy. The present work applies to the large class of structures, such as the IT, for which a model of the same rank as the underlying physical system can be determined (which thus has no computational modes). It was shown that efficient model identification is possible under these conditions.

A third argument developed in Ref. [lon1] uses the direct mathematical expression of the ERA identified model as a function of the measured data. Assuming that this expression is differentiable and can thus be linearized around the nominal solution, statistics on the measurement data can be related to statistics on the predicted parameters using Bayes theorem. The linearization corresponds to the traditional engineering method of sensitivity analysis and the estimated statistical properties of the measured data define a characteristic perturbation, which will allow the determination of a characteristic error.

This type of approach can be applied to most identification methods and will be developed for the complex mode identification algorithm in the next section. It should be noted, however, that such analyses only give a measure of the error within the identification procedure, and not of the actual prediction error for the true physical parameters.

3.4.2. Variance of the Estimated Parameters in the Complex Mode Identification Method.

The exact dependence of identified parameters with respect to the data is obviously extremely non-linear, so statistics on the measurements cannot be exactly translated into statistics on the identified parameters. However, an approximation can be made using a linearization of the relation (measurement data)↔(identified parameters). Assuming that the linearization is valid, estimated bias and variance of the measurement points can then be propagated into bias and variance estimates for the identified parameters.

In the case of the method proposed in section 3.2, the identified parameters are the solution of an unconstrained minimization problem (the user-given constraints on the pole structure force convergence to an appropriate local minimum, but are never met at the

chosen local minimum). For parameters solution of a minimization problem, the linearization of the relation (measurement data)↔(identified parameters) can be done as follows. For a cost function J, parameters p and a data vector x, the parameters locally minimize the cost function, so that

$$\frac{\partial J(p(x),x)}{\partial p} = 0. \tag{3.55}$$

Furthermore, the parameters depend on the data vector x in such way that (3.55) remains true for any variation of x. Therefore, the derivative of (3.55) with respect to x is also equal to 0

$$\frac{d}{dx}\frac{\partial J(p(x),x)}{\partial p} = \frac{\partial^2 J(p(x),x)}{\partial x \partial p} + \frac{\partial^2 J(p(x),x)}{\partial p^2}\frac{\partial p}{\partial x} = 0. \tag{3.56}$$

This relation provides the expected local linear relationship between p and x in the general case of identified parameters solution of an unconstrained minimization. For each specific identification algorithm, the problem is now to find a practical algorithm to determine (3.56).

Using the complex mode identification algorithm proposed here, the relationship for the residues is easily obtained. Considering a SISO case (clearly MIMO cases are for this problem independent SISO problems), one has from (3.15)-(3.17):

$$\left(\frac{1}{2}\right)\frac{d}{dx}\frac{\partial J}{\partial R} = \frac{d}{dx}\left\{\Phi^T\left(-H_M + \Phi R\right)\right\} =$$
$$= \left\{\Phi^T\Phi\frac{\partial R}{\partial x} - \Phi^T\frac{\partial H_M}{\partial x} + \Phi^T\frac{\partial \Phi}{\partial x}R + \frac{\partial \Phi^T}{\partial x}\left(\Phi R - H_M\right)\right\} = 0 \tag{3.57}$$

which leads to

$$\frac{\partial R}{\partial x} = \left(\Phi^T\Phi\right)^{-1}\left\{\left(\Phi^T\frac{\partial H_M}{\partial x}\right) - \left(\Phi^T\frac{\partial \Phi}{\partial x}R + \frac{\partial \Phi^T}{\partial x}\left(\Phi R - H_M\right)\right)\right\}. \tag{3.58}$$

where two parts can be distinguished. As expected (since R is the solution of a quadratic minimization problem), the first part is a direct dependence on the error in the measured data ($\partial H_M/\partial x$) which takes the same form as the dependence (3.17) of the estimated residues on the data H_M. However, the second part appears because the error made on the estimated poles introduce variations in Φ (shown here as $\partial\Phi/\partial x$) which indirectly introduce errors in the estimated residues.

If an unbiased frequency response function estimator is used, the variance of the measured frequency response function points is usually estimated in the form of a coherence spectrum $\kappa(\omega_l)$ (defined in Ref. [lju1] Chapter 6 for example), which is used to define an approximate diagonal covariance matrix Σ_M for the elements of H_M. For each measured frequency point, the corresponding diagonal element of Σ_M is given by

$$\sigma_{H(\omega_l)} = H(\omega_l)^2\left(1-\kappa(\omega_l)\right) \tag{3.59}$$

Using the frequency response covariance matrix Σ_M, the variance of the residues R linked to the direct dependence on the measured frequency response function H_M is simply

$$\Sigma_R = \left(\Phi^T\Phi\right)^{-1}\Phi^T\Sigma_M\Phi\left(\Phi^T\Phi\right)^{-1}. \tag{3.60}$$

However, the overall estimation error also depends on the second part of (3.58). This indirect dependence is linked to the fact that errors in H_M induce errors in the pole estimation, so the computed base responses Φ used to solve the linear least-squares problem are inaccurate, which in turn leads to indirect errors on the residues.

Using (3.56) to determine the exact dependence of the pole estimates on errors in H_M does not seem feasible for non-trivially simple problems. One must thus somewhat arbitrarily decide what realistic bounds on these errors are. With such estimates, the accuracy evaluation can be completed by estimating the effect of pole location error on the identified residues. Since this last step can only be done on a case by case basis, such an analysis will be done for the IT case in the next section.

3.4.3. Application to the Interferometer Testbed Case.

The first difficulty is determining a bound on the pole variations that might be linked to noise in the measured data. Using the proposed identification method, iterations on the pole frequencies are never stopped before the relative step sizes are below 0.005 %, and iterations on damping ratios for relative step sizes are below 1%. In the case of the IT, where the measured data has very little noise, these numbers are probably good bounds for the actual error made on the estimated poles.

On the other hand, the results of different tests of the structure led to sample standard deviations as large as 0.2 % for the frequencies and 10 % (of the nominal value) for the damping ratios (see Table 3.2). With the accuracy achieved in the identification, there are good reasons to think that these variations are not linked to identification error but to small changes in the system (coupling with the shaker which was located in a different position for each test might easily explain variations of that order, particularly for the frequencies).

However, to be more conservative in the evaluation of the uncertainty on residues, these unrealistically large values will be used initially.

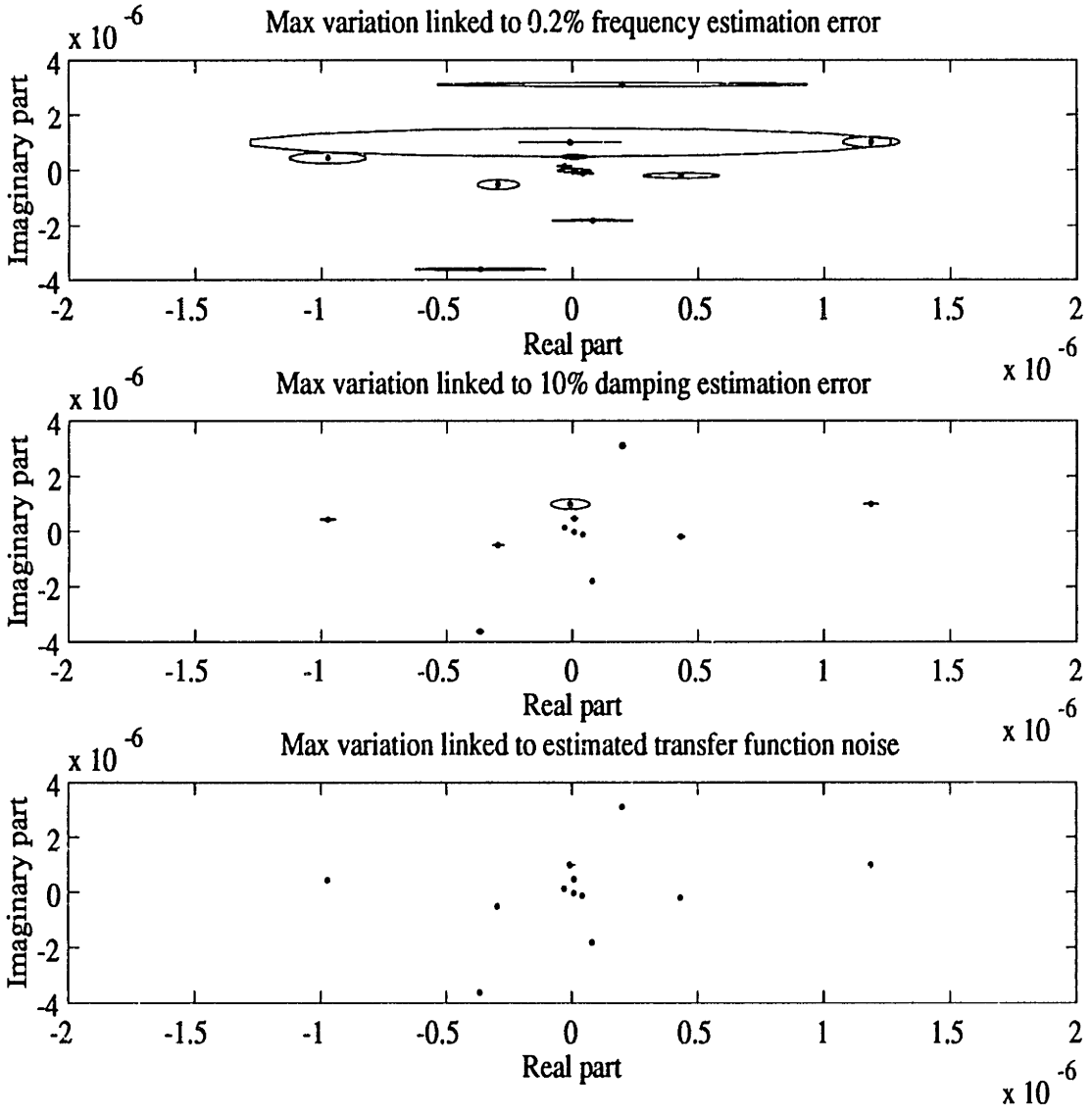

Figure 3.9: Estimated residues and corresponding uncertainty bound for
a) an uncertainty of 0.2% in the estimated frequencies
b) an uncertainty of 10% in the estimated damping ratios
c) the estimated variance of the measured frequency response function

Allowing variations of 0.2% and 10% on the pole frequency and damping ratios, the possible variations on the residues were computed using (3.58) (the validity of (3.58) was also verified for a few cases). In these results, an error on all the residues is linked to each of the pole variations, which rapidly leads to an untractable number of uncertainties. As a practical solution for this difficulty, a quadratic norm of the different contributions was used to determine a conservative over-bound of the error.

Figure 3.9 shows the application of this procedure on the estimated residues of the transfer function from shaker I to sensor 1. Both the contributions linked to noise in the frequency response function and uncertainty in the estimated pole damping ratio are clearly negligible. Even for ten times higher levels of noise, the direct error on the measured parameters would be small compared to the indirect contribution linked to pole estimation error. The facts that the contributions linked to the damping estimation errors are small and that damping is difficult to measure are strongly related. Errors in measured damping that may seem significant in terms of parameters, do not imply large variations in the prediction (much smaller than those linked to mass and stiffness contributions), and thus do not induce large indirect errors on the residues.

In Figure 3.9, the contributions of errors in the estimated pole frequencies is quite large. However, the levels of uncertainty assumed (0.2 % from best estimated frequency) are based on the variations of these frequencies between different tests, and are quite unrealistic bounds for the actual error made for any given test (0.01 % would be more appropriate). For any given test, the uncertainty ranges on the residues should thus be about ten times smaller than shown in Figure 3.9, which would then be negligible (except for modes 6 and 9). It was seen in Figure 3.7 that, for the test on leg 1 considered here, the modes 6 and 9 are not well identified. The present sensitivity analysis thus confirms the conclusion made previously, that the test with the shaker on leg I does not allow a very accurate identification of these two modes.

The analysis of the five other tests leads to the conclusion that the identification error for the complex residues is very small for a case such as the IT, where the noise levels are very small. This however only means that the complex residue identification algorithm is insensitive to the considered noise levels.

As seen in previous sections, the results show larger variations from test to test, indicating that the system invariance should be questioned. Furthermore, several non-optimal steps lead to the final MIMO normal mode model. For each SIMO test, the estimation of scaled complex modal observabilities $c\psi_j$ is very sensitive to even small errors on the residues of the collocated transfer function. The transformation to the normal mode model relies on the enforcement of the properness condition which introduces some errors. Therefore, although the complex residues are extremely well identified, the MIMO normal mode model may not be as accurate. (A further discussion of this point is made in Chapter V, where hybrid analytical/experimental models are introduced).

3.5. CONCLUSIONS

A classification of identification methods has been proposed and the existing approaches relative to the categories of this classification have been reviewed. The use of bandlimited frequency domain data was motivated for the identification of structural dynamic models. Different forms of the truncated normal mode model parametrization have been discussed and were used. The properties of the quadratic and log-least-squares cost functions have been discussed and led to the conclusion that the quadratic cost was appropriate for identification and the log-least-squares cost for FE model updates.

New solutions were proposed to obtain accurate scaled estimates of complex mode modal observabilities and controllabilities. A new algorithm for the identification of poles and complex mode residues was introduced. This algorithm identifies the residues while iteratively updating an estimate of the pole structure, which allows using and generally improving significantly the results of other algorithms. A procedure to determine minimal models from full-rank non-minimal residue matrices was discussed. Finally, using the minimal model description, the scaling of the modal observabilities and controllabilities based on collocation constraints was discussed. The accuracy of the proposed approach was demonstrated for the interferometer testbed.

It was shown that the complex modes of truncated normal mode models are proper, and that this property is sufficient for the existence of an exact transformation between complex and normal modes (which was detailed). A new algorithm was proposed to find proper approximations of identified complex modes, thus allowing an accurate identification of the normal modes and of the non-proportional modal damping matrix. The application of this new methodology to the case of the interferometer testbed, led to the first experimental characterization of non-proportional damping, thus demonstrating the breakthrough made with the introduction of the proposed algorithm.

Finally the effects of errors in the measured frequency responses on the identification results were discussed and shown to be extremely small, thus giving another confirmation of validity of the proposed methodology.

Chapter IV

Finite Element Model Update

Finite element models allow predictions that cannot be done with experimental models (see the applications in Chapter V). However, for these predictions to be accurate, it is necessary to obtain FE models with relatively minor errors. Initial FE models usually differ significantly from the actual system so that they must be improved, as will be detailed in this chapter.

As shown in Chapter I, finite element models are created using the measured properties of system components. In many cases the properties of some components are not well known or are arbitrarily simplified in the modeling process. Such simplifications lead to two types of errors:

- Analytical limitations inherent in the elements may lead to a model that could not accurately represent the system behavior (the model is not physically significant). For example, if a component has local dynamics at low frequencies (e.g. the science plates of the Interferometer Testbed (IT) have strong local bending motion above 60 Hz), the model must include enough DOFs on that component to accurately represent the local dynamics.
- Design parameter errors linked to faulty measurements of component properties or to incorrect modeling assumptions may lead to inaccurate predictions, even if the model allows a correct representation of the low frequency dynamics (i.e. the model is physically significant). For example, struts in truss structures are usually represented by connected beam elements. In reality joints make the connection, and the stiffness properties of these joints must be incorporated as a correction to the properties (design parameters) of the element representing the strut.

Analytical limitations only have a significant impact if the incorrectly represented component has a large influence on the response in the frequency range of interest. It is a prerequisite for a meaningful model update to determine and correct all the analytical limitations that may influence the response in the frequency range of interest.

As most FE convergence studies have been done for particular (and usually simple) systems, few systematic tools exist to demonstrate the analytical validity of most models. However, as shown in Ref. [bal5], analytical limitations are often linked to the inability of

a given element to represent wavelengths characteristic of the system motion in the model frequency range. Thus, a comparison of characteristic wavelengths with the element lengths at the highest frequency of interest [bal5] or, similarly, a comparison of the first internal element resonance with the highest frequency of interest (as done in Ref. [bou1] to validate a Guyan condensation), might give starting points for the development of such analysis tools which will not be addressed here.

Under the necessary (for the validation of any parametric update) assumption that the model elements do not impose analytical limitations on the predictions, algorithms to estimate (update) with high accuracy the values of certain design parameters (E, A, ρ, etc. of different elements) will be analyzed in this Chapter. Well devised component tests allow both verification of the analytic validity of the component model and accurate updating of specific design parameters, so *whenever possible* such tests should be used first.

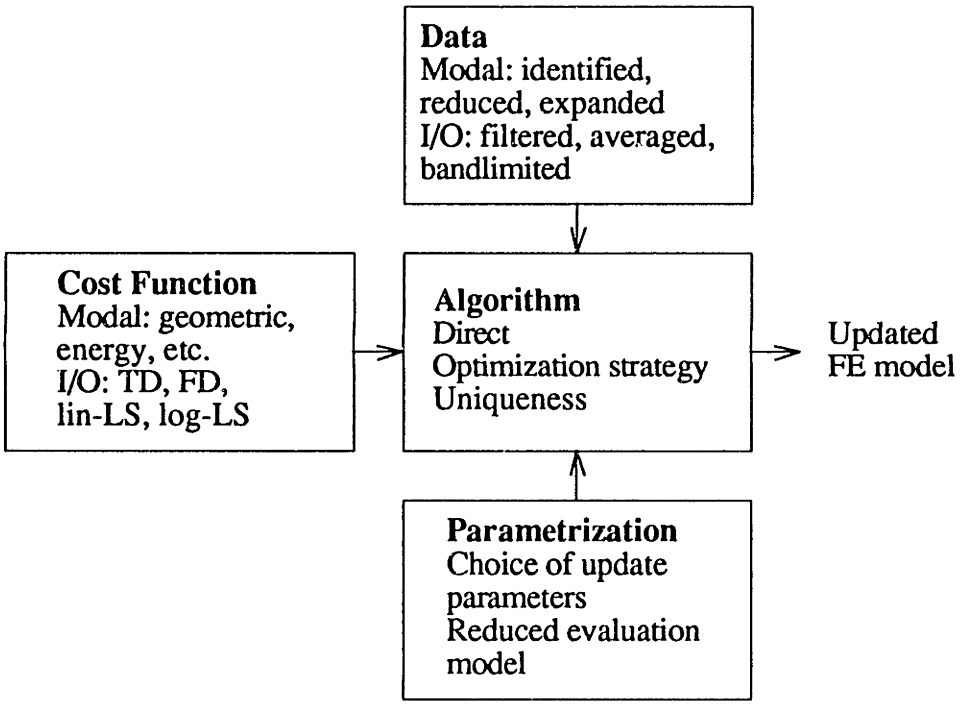

Figure 4.1: A general characterization of parameter updating procedures.

When all possible efforts have been made to ascertain the validity of the component models and to estimate their design parameters (as when integrated into the system), global system tests provide a way to evaluate the model accuracy, and thus to update some of its parameters. As for all parameter estimation procedures, four main components (shown in Figure 4.1) characterize different algorithms:

- the measured data (and the process used to obtain it)
- the cost function used to compare predictions and measurements

- the choice of parameters to be updated and the reduced model used for predictions
- the algorithm used to determine the parameters values which will optimize the model prediction.

Most choices within this matrix have been already investigated, so that any new work can only lead to incremental improvements. Rather than doing a linear survey of existing algorithms which would only repeat the work of others (e.g. refs. [cae1, roy1, lin1, ber1, lev1]), this chapter addresses the different points of the proposed classification, reviewing existing as well as innovative solutions and using the IT case as an example.

For evaluations of the model accuracy, both identified normal mode data (see section 3.3) and I/O response data (see section 3.1.1) can be used, as will be detailed in the review section 4.1. Local element design parameter values cannot always be identified from a global system test, so that a sensitivity analysis (introduced in section 4.2) is necessary prior to any FE model update. Computer limitations do not allow the repeated use of full FE models during an iterative update procedure, so reduced order predictive models (introduced and analyzed in section 4.3) are used, allowing orders of magnitude decreases in computation time. A particular FE update algorithm, differentiated from existing work by the use of the logLS cost function and of reduced predictive models (introduced in section 4.3), was developed as part of this research (see Ref. [bal4]). The history of the IT finite element update and this update algorithm are used in section 4.4 to highlight fundamental limitations of FE update algorithms based on the comparison of global system properties.

4.1. Data and Cost Functions for FE Update Procedures

For procedures linked to undamped FE models, two main types of data can be used.

Analytical normal modes are easily accessible from the FE model, but experimental normal modes are only indirectly identified from measured data (as shown in Chapter III). Furthermore, experimental measurements of the normal modes are only partial (the modal observabilities and controllabilities are measured) so that further analysis tools (reduction or expansion; reviewed in section 4.1.1) are needed to obtain "compatible" experimental and analytical modes. For compatible modeshape estimates, many criteria have been defined (see the review in section 4.1.2) using geometric and energy considerations.

Input/Output data are easily available from experiments (usually in the form of frequency response functions) with a higher degree of accuracy than modal data. Furthermore, many measures of model agreement have been defined for this type of data (see section 3.1.3) and can be readily used. In fact, the only significant difficulty

(addressed in section 4.1.3) is now linked to the analytical model, which must contain a representation of damping (that was not needed for criteria based on normal modes).

4.1.1. Compatibility of Identified and FE Normal Mode Information

The first obvious problem in using experimental modal data is that the identification results provide estimates of normal modes at sensor and actuator locations (the modal observability matrix $(c\phi)_I$ and the modal controllability matrix $(\phi^T b)_I$), and the FE model estimates of modeshapes ϕ at all the FE DOFs q. For many applications it is necessary to have an estimate of the experimental modeshape at all the FE DOFs, so that different methods to attain this objective have been devised and will be reviewed here.

To retain the natural decomposition of components into elements (and thus the link (physical component parameter)↔(element design parameter)), the initial FE model generally must be defined using more DOFs than available sensors. Historically, the first approach has been to reduce the active FE DOFs to the available sensors (in order to obtain a model where $c\phi = \phi$). In the structures community such approaches are known as condensation methods, but in a control-oriented approach this would be seen as a model reduction procedure with an imposed choice of states.

The principle underlying the different condensation methods is to partition the full order model into active DOFs q_A corresponding to sensors and dependent DOFs q_D that will not be measured, and to assume that a constant linear relationship exists between the dynamic states of the dependent DOFs and the states of the active DOFs

$$q = \begin{bmatrix} q_A \\ q_D \end{bmatrix} = \begin{bmatrix} I \\ T \end{bmatrix} q_A \tag{4.1}$$

Assuming that the motion of the dependent DOFs verifies (4.1), the system equations can be rewritten as

$$\begin{aligned} \left\{ s^2 \left(M_{AA} + M_{AD}T + T^T M_{DA} + T^T M_{DD} T \right) + \left(K_{AA} + K_{AD}T + T^T K_{DA} + T^T K_{DD} T \right) \right\} q_A &= \left(b_A + T^T b_D \right) u \\ y &= \left(c_A + c_D T \right) q_A \end{aligned} \tag{4.2}$$

where the dynamics of the full order model are fully described using the active DOFs q_A. It is then usually assumed that external forces are only applied on active DOFs and that sensors are only placed on the same DOFs. Thus dependent DOFs have no influence on the input ($b_D = 0$ so that $b_A + T^T b_D = b_A$) or the output ($c_D = 0$ so that $y = q_A$).

The first, and probably the most robust, condensation method is the Guyan reduction (or static condensation) which assumes that the dependent DOFs behave quasistatically (i.e. $\ddot{q}_D = 0$ and $\dot{q}_D = 0$). This assumption can easily be shown to correspond to the following linear relationship between the active and dependent DOFs

$$q_D = Tq_A = -K_{DD}^{-1}K_{DA}q_A \tag{4.3}$$

Several variations of this initial solution have been introduced (see Refs. [oca1, fre1, oca2, paz1, oca3]), which give better results than the Guyan reduction in a number of cases, but in a way that is difficult to characterize.

Overall, condensation methods are extremely useful for model reduction purposes but they have major limitations:

- They tend to be sensitive to model error and to lose the spatial information linked to errors [hej1].
- They are fundamentally limited in frequency by the first mode of the dependent DOF set. The assumption (4.1) of linear dependence of the dependent DOFs becomes very inaccurate above the frequency of the first fixed-interface mode (mode of the dependent DOFs with fixed active DOFs, see Refs. [gor1, bou1]). (Note that it is possible to define condensations for other "non-low" frequency bands [ard1], but this is not of interest for the present research).
- Unlike the truncation approach (introduced in Chapter II), which acknowledges the existence of low frequency asymptotic contributions of high frequency modes (and can thus use the exact low frequency modes), condensation methods use a proper second order model (thus implying that the modes of the model are somewhat inexact in order to incorporate the effects of high frequency modes).

The second approach introduced to reconcile measurements with the finite element model is to combine experimental and analytical predictions to define modeshapes at all the DOFs of the full order FE model.

To obtain this expansion, some methods (e.g. refs. [hej1, ber2]) assume that a constant linear relationship (described by the N by N_T matrix T) exists between the known modal observability matrix $(c\phi)_I$ and the modeshape expanded to the full set of DOFs

$$\phi_{Ex} = [T](c\phi)_I \tag{4.4}$$

The assumptions used for condensation are then used to define the matrix T. For example, assuming that the unmeasured DOFs behave quasistatically (as done for the Guyan reduction) leads to the so-called "static expansion"

$$\phi_{Ex} = [T]\phi_A = \begin{bmatrix} I \\ -K_{DD}^{-1}K_{DA} \end{bmatrix}\phi_A. \tag{4.5}$$

Because they use the same assumptions, these approaches have the same fundamental frequency limitations as condensation methods.

The other expansion methods are essentially geometric. A basic result of perturbation theory is that small variations in the system can only introduce large recombinations of modes that are close to each other in frequency [bal6]. Therefore, assuming that the identified system can be represented by a small perturbation to the initial FE model, the true modeshapes at the FE DOFs are, with a small approximation, a linear combination of the modeshapes of the initial FE model $\phi_{True} \approx \phi_{FE0}A$.

(In the usual case, all actuators have a collocated sensor, so that all the information is contained in the modal observabilities. To simplify notations, this will be assumed in the rest of this work.)

The basic objective of the geometric expansion methods is to obtain expanded modes $\phi_{Ex} = \phi_{FE0}A$ which match the measurements (the identified modal observability $(c\phi)_I$ matrix) as closely as possible, or in other words, to minimize a norm of

$$\left(c\phi_{Ex} - (c\phi)_I\right) = \left(c\phi_{FE0}A - (c\phi)_I\right). \tag{4.6}$$

The simplest solution is to define A as the solution of the least squares problem associated to the minimization of (4.6)

$$A = \arg\min\left\{\text{trace}\left(\left(c\phi_{FE0}A - (c\phi)_I\right)^T\left(c\phi_{FE0}A - (c\phi)_I\right)\right)\right\} \tag{4.7}$$

which corresponds to the use a pseudo inverse of the FE modal observability matrix $(A = (c\phi_{FE0})^+(c\phi)_I)$.

For cases with as many sensors as modes, the minimization problem (4.7) leads to the use of the true inverse $(c\phi_{FE0})^{-1}$ and the modal observabilities of the expanded modes match the measured modal observabilities $(c\phi)_I$ exactly. This, however, may not be appropriate since there are identification errors in $(c\phi)_I$. In fact, for an accurate initial model where pairing of modes has been achieved, the j^{th} expanded mode should be relatively close to the corresponding prediction of the modeshape ($\phi_{Exj} \approx \phi_{FE0j}$). Therefore, the transformation matrix A should introduce a "smoothing" of the measured modeshape so that the expanded modeshape is closer to the analytical prediction. This trade-off between matching the identified modal observability and introducing "smoothing" (to account for the inaccuracy of identification and the relative accuracy of the FE prediction) has been formalized in Ref. [roy2], but reintroduces the need to "pair" analytical and experimental

modes. Finally, other possible choices for the transformation matrix A have been introduced (e.g. refs. [oca2, kam1, smi2]) allowing the addition of further constraints (on the mass orthogonality of expanded modes in particular).

It should be noted that modeshape expansion does not change the scaling of the measured modal observabilities. Therefore, for the true mass and stiffness matrices, the expanded modeshapes will be mass orthonormal and stiffness orthogonal (the equivalence between the equality of collocated modal observabilities and controllabilities and the mass and stiffness orthogonality conditions was discussed in section 2.1.3).

In the present work, the limitations of condensation methods are considered to be too stringent, so that these methods are not used. The geometric expansion to the full FE DOF size, using the least squares solution (4.7) for the matrix A, with more sensors than modes (so that A is a pseudo-inverse which introduces some smoothing of the measured modeshapes), will be used in Chapter V to create hybrid analytical/experimental predictive models.

4.1.2. Comparison Criteria Using Normal Modes

Several criteria, which will be reviewed here, have been developed to evaluate the agreement between identified and analytical normal modes. The use of these criteria implies that the experimental and analytical modeshapes are known at the same points ($(c\phi)_l$ and $c_{FE}\phi_{FE}$ should be known) and in some cases that all the DOFs are measured ($y=q$ so that $c\phi=\phi$, which can be obtained using the methods proposed in section 4.1.1).

The first and obvious comparison can be made on the modal frequencies, using, for example, a quadratic norm

$$\text{error} = \sum_{\text{identified modal frequencies}} \left|\omega_{ID} - \omega_{FE}\right|^2. \tag{4.8}$$

The main difficulty with such criteria is that they imply the possibility of "pairing" measured and predicted modes, a process which may be quite difficult for models with large errors and systems with high modal densities (which tend to become the usual case).

In a second step, analytical and experimental predictions of normal modeshapes are compared. The Modal Assurance Criterion (MAC) [ewi1] is probably the most used (mainly because of its simplicity) criterion on modeshapes. For the identified modal observabilities $(c\phi)_{lj}$ of the j^{th} mode at the sensors l, and the analytical observabilities $c_l\phi_k$ (product of the output shape functions c_l corresponding to the sensors l by the k^{th} analytical modeshape ϕ_k) the MAC is defined as

$$\mathrm{MAC}_{jk} = \frac{\sum_l \left((c\phi)_{lj} c_l \phi_k\right)}{\sqrt{\sum_l (c_l \phi_k)^2 \sum_l \left((c\phi)_{lj}\right)^2}} \tag{4.9}$$

which gives a measure of how the j^{th} experimental and k^{th} analytical modal observabilities are correlated. If the modeshapes (and thus the modal observabilities) are equal, the diagonal terms ($j=k$) are equal to *1* (perfect correlation). Furthermore, off-diagonal terms will be close to zero for a well-designed modal test (it would clearly be bad practice to have two modes with the same or very correlated modal observability matrices).

The MAC measures the shape correlation without any reference to scaling (because of the denominator in (4.9)); this makes the MAC easy to use but also limits its applicability (since the modeshape scaling governs the influence of a given mode on the overall system response, a proper scaling is necessary when comparing the relative influence of different modes). In other terms, the MAC is not a norm (two vectors can be perfectly correlated and yet different), so care must be taken in interpreting results.

When a proper scaling is defined, it is useful to evaluate at each sensor location how well the different identified and predicted modeshapes are correlated. This can be done using the COordinate Modal Assurance Criterion (COMAC) defined in Ref. [lie2].

When possible, it is more accurate to directly compare the scaled modal observabilities at the points where they are measured, using, for example, a quadratic norm

$$\text{error} = \sum_{l,j} \left| (c\phi)_{lj} - c_l \phi_j \right|^2 . \tag{4.10}$$

The problem in such an error measure is that it implies a proper scaling of the identified modes and the pairing of identified and predicted modes (as did the criterion (4.8) on the frequencies). Solutions to alleviate the need to pair modes have been proposed, but they come at the cost of more complex procedures which will not be considered here.

Cost functions combining norms on the modal frequencies and scaled observabilities (e.g. a weighted sum of the criteria (4.8) and (4.10)) give a complete characterization of accuracy with which the undamped I/O characteristics of the system are modeled. If the errors in both (4.8) and (4.10) are equal to zero, the normal modes (both frequency and scaled shape) are predicted exactly. Assuming that the damping is properly modeled, discrepancies between I/O measurements and predictions are thus limited to unmodeled dynamics and noises. Criteria which do not consider modeshape scaling (such as the MAC) give no guarantee on the agreement of the overall system response.

Conversely, direct comparisons of predicted and measured transfer functions (addressed in section 4.1.3) are criteria measuring both the error on modal frequencies and scaled modeshapes. Their use implies a proper model of damping and often neglects effects of noises and unmodeled dynamics, but alleviates the difficulties linked to the identification of experimental modes and to the pairing of modes.

A second category of criteria assume that the full modeshapes are measured (this either implies that the system matrices have been reduced or that the modeshapes have been expanded) and are based on the orthogonality conditions introduced in Chapter II

$$\phi^T M \phi = I \quad \text{and} \quad \phi^T K \phi = \Omega. \tag{4.11}$$

A measure of the model quality can be obtained by using mixed experimental and analytical modeshapes and seeing how well the equalities (4.11) are verified. For example, one should have

$$\phi_{FE}^T M_{FE} \phi_{ID} \approx I \quad \text{and} \quad \phi_{FE}^T K_{FE} \phi_{ID} \approx \Omega. \tag{4.12}$$

These measures or variants of them have been used to define update algorithms. Although modeshape scaling is implicitly considered, some problems should be noted:

- The two conditions must be verified simultaneously to prove the equality of the measured and predicted modeshapes (the mass orthogonality, often used by itself, has little more value than the MAC, and is much more difficult to use).
- In real systems, all the modes are not identified. Since the reduction is often not accurate enough, there is a clear problem of model truncation. The partial orthogonality conditions that can be computed only guarantee the agreement of frequency response measurements and predictions if the validity of the expanded modeshapes can be proved.

A useful interpretation of the orthogonality conditions relates to the so-called modal energies [roy3]. In the modal coordinate system of identified normal modes, the identified modal mass and stiffness are diagonal. (Assuming that the modes have been scaled using a collocation constraint; the modal mass matrix is the identity and the stiffness is the diagonal matrix of frequencies squared. See section 2.2.3). The FE modal mass and stiffness matrices can also be expressed in the coordinate system associated with the expanded modeshapes ϕ_{Ex}

$$\mu_S = \phi_{Ex}^T M \phi_{Ex} \text{ and } \Omega_S = \phi_{Ex}^T K \phi_{Ex}, \tag{4.13}$$

and the terms of the mass μ_S and stiffness Ω_S can be seen as kinetic and strain energies associated to the FE model modes in the true normal mode coordinate system. If the FE

modes are accurate estimates of the true modes, μ_S is close to the identity matrix and Ω_S to the diagonal matrix of squared normal mode frequencies. An updated model should thus match this condition better than the initial model.

4.1.3. Use of Criteria Based on Input/Output Response

All the difficulties linked to the use of modes (identification, mode pairing, etc.) can be circumvented by directly comparing the measured and predicted I/O response (usually but not necessarily under the form of transfer functions). However, when using direct comparisons with measurement data (time or frequency domain), damping must be represented since it has a significant impact on the predicted response. Three main approaches have been considered:

- A proportional damping representation with measured damping ratios (if mode pairing is possible and experimental values for the pole damping ratios are available) or a uniform estimated damping ratio (i.e. 1% for all poles).
- As proposed by Ref. [ibr3], a damping proportional to element mass or stiffness matrices of elements

$$C = \sum_{s \in \{\text{structural element}\}} (\gamma_{1s} M_s + \gamma_{2s} K_s) \tag{4.14}$$

  which has the inconvenience of using many parameters γ_{is} that are hard to identify (as the influence of any such parameters on the response is extremely small, one cannot expect to find a unique mapping between measurements and the parameters γ_{is}).
- A non-proportional modal damping model. This would be the truncated non-proportionally damped normal mode model introduced in section 2.2.3, identified in section 3.3, and used in the hybrid models of Chapter 5. The reader should refer to these sections for more details on this damping representation. (The present research introduces the first successful experimental identification of a non-diagonal modal damping matrix, this type of model was thus never used previously).

With a damped model defined, the I/O response can be predicted and compared with the measurement data using different criteria reviewed in sections 3.1.1 and 3.1.3.

4.2. Choice of Parameters to be Updated

The final objective of this research is to use test results in a given system configuration to create models which allow accurate predictions of the system response for another I/O

architecture or for a modified system. This objective is achieved in part by obtaining an accurate description of local component mass and stiffness properties, which can then be used to predict the effects of local changes.

A perfect match of a restricted set of measured I/O responses does not necessarily imply that the local element properties are well described. Therefore, to correctly identify or update (which is the same thing, except that one calls update cases where an initial estimate is available) a given parameter, one must be able to: first differentiate its influence from the expected residual model error, and second ensure that the correction is not needed because of the inaccuracy of another parameter (see example in section 4.4).

Section 4.2.1 briefly reviews three areas (component tests, check of analytical validity, check of "identifiability") which must be addressed to obtain correct update of local model properties. In section 4.2.2, these different points are detailed for the IT case.

4.2.1. Definition of the Parametric Error Structure

Design parameters of the FE model represent the properties of physical components described by different elements. They can be direct physical parameters (i.e. properties of a beam modeled as a beam element), but often are the result of a condensation of several physical parameters (properties of a beam + joint assembly represented as a beam element without joint).

When carefully done, component tests are very useful in determining design parameters (especially when they differ from physical parameters). For example, for a beam/joint component represented as a single beam element, a test of the component will give a measure of the overall stiffness which should be used as the element stiffness. The validity of such tests clearly depends on a proper relation between the design parameters (properties of the element or model of subsystem tested) and the parameters measured in the test (boundary conditions are extremely important). However for a valid test, the update is extremely reliable and the investment in testing is usually worthwhile if accurate and physically significant models of the structure are to be created. (Uses of such component or subsystem tests are documented in refs. [bal5, bal4] for the MIT/SERC interferometer testbed, and refs. [car1, red1] for the JPL Micro-Precision Interferometer Testbed).

Parameter updates based on the comparison of global system test results can only be validated if all the errors that may exist in the FE model have been characterized. These errors can be linked to inaccurate parameters (the element is appropriate but does not use the right parameters) but also to insufficient model refinement (the type or the frequency

range of the element does not allow an accurate representation of the structural dynamics [bal5] so the model should be refined).

A prerequisite, for a meaningful update of the element design parameters, is the correction of all non-parametric model errors (i.e. analytical model limitations and user input errors related to the system geometry, the mass distribution, the stiffness distribution, etc.). This requirement can only be achieved if the analyst and the test engineer work in close cooperation to determine whether the assumptions made in the model are indeed valid for the considered system (or set of systems) and to eliminate discrepancies between the actual system and its description in the model (geometry, etc.).

When the model is constructed with a good knowledge of the actual system properties (for many reasons this knowledge is not always available), the precision with which different design parameters are known should be evaluated to allow a proper use of the system test data. To obtain good results with an update methodology, most parameters should be well known and a few should need to be updated.

The second step to validate a model update is to demonstrate the ability to uniquely determine the incorrect parameters. In practice, residual model errors are significant, so the only parameters that can be updated are those that have an influence on the tested response larger than the residual error. The sensitivity of the update cost function to a nominal parameter change (defined trough an assessment of the uncertainty on the parameter) gives a measure of the parameter influence on the response, and thus an idea of which parameters can be estimated with accuracy.

To update parameters with low impact on a given test, other tests must be performed, in a different frequency range, using different sensors, or using a subcomponent. For example, the first modes of the IT are thousands of time less sensitive to the mass of a plate attachments than to their stiffness, therefore extremely small changes in the stiffness have more influence on the response than large changes in the mass. Therefore, one cannot known the stiffness well enough to distinguish the effect of a mass change from a stiffness change in a global system response.

However, since the residual error is obviously unknown, it is difficult to prove which parameters can actually be estimated. Indicative measures of the "identifiability" (such as sensitivities of the update cost function) must thus be used instead.

The geometric energy distribution for different modes is also a useful indicator of the model sensitivity to parameter changes. The influence of a stiffness change on a given mode is roughly proportional to the ratio of the strain energy in the mismodeled element to the total strain energy. High strain regions in the model frequency range are thus the

regions where stiffness errors will have a significant influence. Similarly, mass errors will only have a significant influence in regions of high density of kinetic energy. (However, masses can be well measured, so that effects of residual errors on the mass are usually smaller than that of errors on the stiffness).

Finally, a number of papers (e.g. refs. [lin2, ber3, ber1, lie3]) address the problem of identifying the geometric location of a modification made to a known structure; clearly, the work of these authors should be used for the problem at hand.

4.2.2. Application to the Interferometer Testbed Case

This section describes the application to the IT of the three steps outlined in the previous section (component test, check of analytical validity, check of "identifiability").

To allow the creation of better models, the axial stiffness of struts and joints used to build the IT truss were first characterized using a component tester. There were difficulties in devising a test to measure the design parameter used in the model, which in the present case is the axial stiffness of the component (ball joint, connection screws, tube strut) represented as a single beam element. However, once this design parameter was accurately measured by testing the full component (11.2 N/μm for the short struts and 7.77 N/μm for the long struts), the agreement between the system test of the naked truss and the model prediction was extremely good up to around 140 Hz [bal4] (the number of suspension modes above that frequency does not allow a good analysis of the data). As is well documented for the JPL Micro-precision Interferometer testbed [car1], such a good agreement can in fact be expected for most truss structures up to the range of local strut bending modes (above 200 Hz for the IT).

For the model update of the completed IT, it was thus known that the only significant errors would be located on the new added components (i.e. science plates, see section 7.1). As schematically shown in Figure 4.2, the model for each of the science plates is constituted of 25 plate elements used to represent the large support plate, 4 beam elements used to represent the U-shaped connectors linking the plate with the truss, and 4 beam elements to represent the support of the cat-eye mirror which itself is represented as a concentrated mass/inertia. The geometry and the different masses were carefully measured and used in the model (with an error for the overall plate mass which was later updated, see section 4.4 which shows that this was a case where two parameters could not be updated simultaneously).

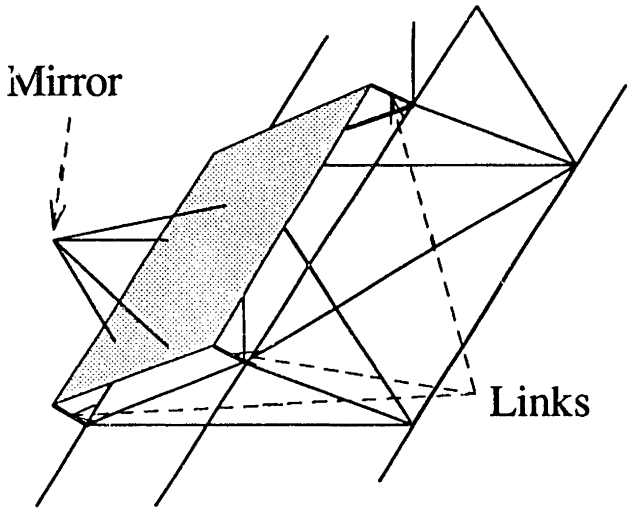

Figure 4.2: Sketch of the FE representation of the science plates. (See a picture of a science plate in section 7.1).

As a first step, meant to eliminate analytical limitations, the mesh size for the plate models was refined until a further refinement did not produce significant modification of the component modes below 100 Hz. For pinned boundary conditions (free rotations but fixed translations) at the attachment points to the truss, the first plate modes were found at 50.5 Hz. From the initial model, three refinements of the plate model were necessary to obtain an apparent convergence of the component model.

For the cat-eye model using beams and a concentrated mass, a more detailed model with plate elements and a more accurate mass distribution did produce significant changes, so that the 4-beam model was considered a physically significant representation of the actual system.

These tests do not provide a complete characterization of the plate assemblies, which might have included a better validation of the cat-eye assembly model, and/or a dynamic component test allowing a better characterization of the individual plates. However, for purposes of the present work, the overall model physical significance was considered sufficient to allow a meaningful parametric model update.

A number of parameters in the model could not be measured with high accuracy and were considered for the different updates. However, to simplify the presentation, only five of the most important will be presented here as possible model errors

- three stiffness errors for the plate/truss links: the longitudinal (along the leg) bending, the transverse bending and axial stiffness.
- two mass errors: the concentrated mass of the mirror assembly and a distributed mass error for the main plate.

The three link stiffness coefficients were known to be inaccurate since there was no simple way to evaluate good values for the design parameters (any value between 5.0 10^{-12} and 10^{-10} m^4 for the beam element bending section inertia, and between 10^{-6} and 10^{-4} m^2 for the element section area seemed realistic). The two mass coefficients were introduced when it became apparent that the residual discrepancy after update of the link stiffness could not be related to a stiffness error, thus casting a doubt on the mass model (which is easier to measure and is thus usually more accurate). Such an error could not be rigorously bounded even though a mass decrease or a total testbed mass increase of more than 5 kg seemed unlikely.

To evaluate the "identifiability" of these different parameters, the amount of change linked to what seemed realistic variations was computed using the cost function on modal frequencies (4.8) and the logLS cost function (3.12) based on transfer functions used for the new update method that will be detailed in section 4.4.

Table 4.1: Sensitivity of the update cost functions (error measured between the initial and modified models) to a standard change in parameters to be updated.

Parameter	Initial Value and standard change	Change in modal frequency cost	Change in logLS cost
Link I_1	2 10^{-11} m^4 (+100%)	18.00	514.80
Link I_2	10^{-11} m^4 (+100%)	131.60	2734.21
Link A	10^{-5} m^2 (+100%)	0.90	0.70
Mirror mass	2.224 Kg (+500 g)	10.26	3816.10
Distributed plate mass	0.970 Kg (+500 g)	7.46	3437.50

From Table 4.1, the sensitivity of the system response to the link axial stiffness (link A) is clearly so low that only unrealistically large variations of the parameter would lead to modifications of the system response that could be distinguished from the residual model error. This parameter thus cannot be identified from the considered test. Both the link bending stiffnesses (link I_1 and I_2), however, produce effects that are significant enough to be used (see details in section 4.4).

The two mass changes are given as the addition of 500g (but one is a concentrated mass at the mirror location and the other a mass distributed on the edge of the plates). The sensitivity is very large so that they are "identifiable" perturbations. However their effects on the global system response are almost identical, so that the two modifications cannot in fact be distinguished in terms of the measured response in the modal test (see more details in section 4.4).

4.3. Reduced Order Predictive Models

The last necessary element to create a practical update algorithm is the ability to easily predict the quantities needed for the error criterion (i.e. modal frequencies and shapes or transfer functions from existing actuators to existing sensors) for the different values of the design parameters. Of course, as in Chapter II, one is only interested in low frequency response predictions were the system is tested, but the dependence of this low frequency response must be properly characterized for significant variations of design parameters.

Conceptually the full FE model could be used as a predictive model, but in reality this would be excessively expensive (realistic models are large tend to grow faster than computer capabilities, so that this problem will not disappear in the near future). Furthermore, it is not necessary to recompute the low frequency normal modes of the large model, since one is interested for update purposes in evaluating the response of a model that is relatively close to the nominal solution. Perturbation analysis and model reduction are two main approaches used to obtain inexpensive (in terms of needed computations) reduced predictive models.

A first difficulty, detailed in section 4.3.1, is to determine a reduced description of the modifications which will be used by the predictive models. Then perturbation or sensitivity approaches (reviewed in section 4.3.2) use a linearization of the relation (response)$\leftrightarrow$(design parameter) to predict the effects of small changes. FE model condensation methods have sometimes been used to obtain reduced models, but, as pointed out in section 4.1.1 where they were reviewed, these methods are often inappropriate for the complex structural systems considered here. Finally, model truncation as shown in section 2.2 provides a way to obtain reduced models of the low frequency response. Using a Ritz analysis, as shown in section 4.3.3, the initial truncated solution of the full model can be reanalyzed to obtain predictions with higher accuracy than with perturbation approaches. Furthermore, static modes can also be used to improve results of reanalyzed models. Finally, a review of the accuracy obtained with the perturbation and reanalysis methods is done in section 4.3.4 for the IT.

4.3.1. Description of System Modifications

The influence of design parameters on the full system matrices of the model is non-linear in general. However, changes to the full order FE matrices linked to the change Δp of a design parameter p can be represented as additive corrections

$$\begin{aligned} M(p+\Delta p) &\approx M(p)+\alpha_i(\Delta p)M_{\alpha_i}, \\ K(p+\Delta p) &\approx K(p)+\beta_i(\Delta p)K_{\beta_i}, \end{aligned} \tag{4.15}$$

where $M_{\alpha i}$ and $K_{\beta i}$ are normalized incremental mass and stiffness matrices representing a unit change of the scalar coefficients $\alpha_i(\Delta p)$ and $\beta_i(\Delta p)$. For some parameters, such as the material density ρ or Young's Modulus E, the matrices M and K depend linearly on the parameter. In such cases, one can directly use $\alpha_i(\Delta p)=\Delta p$ and $\beta_i(\Delta p)=\Delta p$. For others, such as the plate thickness, the dependence is more non-linear and must be integrated in non-linear functions $\alpha_i(\Delta p)$ and $\beta_i(\Delta p)$, with sometimes the need to define more than one additive matrix for the same parameter (i.e. define a $M_{\alpha 1}$ and $M_{\alpha 2}$). The non-linear terms $\alpha_i(\Delta p)$ and $\beta_i(\Delta p)$ can then be linearized around a nominal value, but this is not always necessary.

The description using additive corrections is fundamentally equivalent to the direct use of design parameters. However, it allows easier formulations of the update problem in many cases (e.g. [ber3, ibr3], or the commercial package of INTESPACE [roy4, roy3]). (For more details on the additive correction description see Ref. [roy3]).

Writing the mass, damping, and stiffness modifications linked to all the modified design parameters as single mass ΔM, damping ΔC, and stiffness ΔK modification matrices, the modified FE model equations (2.1) become

$$\begin{aligned}(M+\Delta M)\ddot{q}+(C+\Delta C)\dot{q}+(K+\Delta K)q &= bu \\ y &= cq\end{aligned} \tag{4.16}$$

The basic assumption, for predictions done with reduced models, is that response of the modified system can still be accurately represented using the projection on the low frequency modes (model truncation) which was valid in the initial configuration. Thus using the same approach as for the normal mode models in section 2.2, the modified systems equations (4.16) are projected onto a truncated set of real vectors ϕ_T (low frequency normal modes and static correction modes)

$$\begin{aligned}(I+\Delta\mu)\ddot{p}+(\Gamma+\Delta\Gamma)\dot{p}+(\Omega+\Delta\Omega)p &= \phi^T bu \\ y &= c\phi p\end{aligned} \tag{4.17}$$

where $\Delta\mu=\phi_T^T\Delta M\phi_T$, $\Delta\Gamma=\phi_T^T\Delta C\phi_T$, and $\Delta\Omega=\phi_T^T\Delta K\phi_T$. Note that if all the modes are kept in ϕ_T, equations (4.16) and (4.17) describe exactly the same response in different coordinate systems (FE DOFs q versus normal mode states p).

The use of the truncated modal model representation (4.17) solves all the difficulties linked to predictions. The truncated damping representation, which is the only one available (see section 2.2.3) can be used. The model being reduced can be handled by available computers. Correction modes can be added in cases where more accuracy is needed (see section 4.3.3). Furthermore, as will be shown in section 5.1, identified quantities can be

used to create a hybrid experimental/analytical model allowing better predictions of the system response.

4.3.2. PERTURBATION AND SENSITIVITY ANALYZES

The traditional engineering solution to evaluate the response of a system after small modifications is to use perturbation analysis (which, in practice, can only use the set ϕ_T of computed low frequency normal modes; no extension has been published to extend the method and use correction modes). The basis of this approach is to consider that although the relation between the low frequency response (normal modes ϕ_T, modal frequencies Ω_T and modal damping matrix Γ_T) and the modifications (ΔM, ΔC, and ΔK) is clearly non-linear, it can be accurately linearized for small changes (a n^{th} order expansion is obviously possible, although even the second order is rarely used).

The basic perturbation theory for normal modes (see also references [elr1, kim1, bal5]) assumes that the modifications on the normal mode frequencies and modeshapes take the form

$$\begin{aligned} \Omega_{jj} &= \omega_j^2 = \omega_{j0}^2 + \Delta\omega_j^2 \\ \phi_{Tj} &= \phi_{Tj0} + \sum_{k \neq j} c_{jk}\phi_{Tk} \end{aligned} \tag{4.18}$$

which, for small modifications (ΔM, ΔC, and ΔK), leads to the approximations (see any of the above mentioned references)

$$\begin{aligned} \Omega_{jj} = \omega_j^2 &= \omega_{j0}^2 + \left(-\omega_{j0}^2\phi_{Tj}^T\Delta M\phi_{Tj} + \phi_{Tj}^T\Delta K\phi_{Tj}\right) = \omega_{j0}^2 + \left(-\Omega_{jj0}\Delta\mu_{jj} + \Delta\Omega_{jj}\right) \\ \phi_{Tj} = \phi_{Tj0} + \sum_{k \neq j} &\frac{-\omega_{j0}^2\phi_{Tk}^T\Delta M\phi_{Tj} + \phi_{Tk}^T\Delta K\phi_{Tj}}{\omega_{j0}^2 - \omega_{k0}^2}\phi_{Tk} = \phi_{Tj0} + \sum_{k \neq j} \frac{-\Omega_{jj0}\Delta\mu_{kj} + \Delta\Omega_{kj}}{\omega_{j0}^2 - \omega_{k0}^2}\phi_{Tk} \end{aligned} \tag{4.19}$$

In the equations (4.19), the notations of the projected system (4.17) are used intentionally to highlight a major point, usually omitted in presentations of perturbation theory. In practice, the set of modes kept for the perturbation analysis is always truncated (ϕ_T), so that the perturbation analysis is an approximation of the projected equations (4.17) and thus only indirectly approximates the full systems equation (4.16). (The direct use of the projected equations (4.17), which will be considered in section 4.3.3, is thus more accurate).

Note that the matrix expressions of the perturbation results (right hand terms in (4.19)) clearly show that the diagonal terms of the perturbation matrices $\Delta\mu$ and $\Delta\Omega$ correspond to changes in the eigenvalues and the off-diagonal terms to changes in the eigenvectors.

A first major limitation of the perturbation analysis is that the expressions (4.19) for the modified normal modes are singular for multiple eigenvalues. Different ways to alleviate this difficulty for multiple poles have been introduced (e.g. Ref. [sha1]), but the problem then becomes that for high modal densities, small changes may lead to multiple poles (see the analysis in Ref. [tri1]). If the initial system does not have multiple poles, multiple pole perturbation analysis cannot be applied, so the range of validity of the perturbation analysis becomes extremely small.

Other limitations are that the expression (4.19) does not allow modification of the damping and does not predict the effects of the modifications on the damped response. These restrictions could be alleviated using perturbation methods for complex modes and could even be extended to non-symmetric systems (for which only parts of the present research apply), but this would lead to a number of distinct procedures, so that it is simpler to use the unique reanalysis approach (proposed in the next section).

For system modifications that are linearly dependent on a parameter ε (i.e. $\Delta M = \varepsilon M_1$ and $\Delta K = \varepsilon K_1$), the expressions (4.19) provide estimates of the derivatives of modal frequencies and modeshapes with respect to the parameter ε

$$\begin{aligned} \frac{\partial \omega_j^2}{\partial \varepsilon} &= \left(-\omega_{j0}^2 \phi_{Tj}^T M_1 \phi_{Tj} + \phi_{Tj}^T K_1 \phi_{Tj}\right) = \left(-\Omega_{jj0} \Delta\mu_{jj} + \Delta\Omega_{jj}\right) \\ \frac{\partial \phi_{Tj}}{\partial \varepsilon} &= \sum_{k \neq j} \frac{-\omega_{j0}^2 \phi_{Tk}^T M_1 \phi_{Tj} + \phi_{Tk}^T K_1 \phi_{Tj}}{\omega_{j0}^2 - \omega_{k0}^2} \phi_{Tk} = \sum_{k \neq j} \frac{-\Omega_{jj0} \Delta\mu_{kj} + \Delta\Omega_{kj}}{\omega_{j0}^2 - \omega_{k0}^2} \phi_{Tk} \end{aligned} \tag{4.20}$$

Such derivatives, traditionally called sensitivities, provide a linearization of the relation $(\varepsilon) \leftrightarrow (\omega, \phi)$ which can be used for incremental predictions, as follows

$$\begin{aligned} \omega_j^2(\varepsilon) &= \omega_{j0}^2 + \varepsilon \frac{\partial \omega_j^2}{\partial \varepsilon} \\ \phi_{Tj}(\varepsilon) &= \phi_{Tj0} + \varepsilon \frac{\partial \phi_{Tj}}{\partial \varepsilon} \end{aligned} \tag{4.21}$$

Unless the sensitivities are recomputed after each step on ε, such predictions are equivalent to the perturbation theory.

When a sensitivity analysis is used for a model update procedure, the relation between modes and design parameters is linearized, which often simplifies the problem formulation and allows direct solutions. Sensitivity approaches were thus used in the early work of Collins, et al. [col1], or in more recent commercial packages such as CORDS [fla1, fla2, fla3] or SSID [has1]. (For further references see the review done by Levine [lev1]).

Higher order (or even exact [elr1] but non-linear) perturbation theories have been developed. But the advantage of simplicity is lost and the results remain approximations of the reduced system model (4.17), with no possibility for appending correction modes to kept normal modes. For accuracy, it thus seems more efficient to use the reduced model (4.17) directly in the reanalysis approach presented in the next section. However, even with these limitations, sensitivity analyses do provide an easily available linearization of the effects of mass and stiffness modifications. A linearization is a major advantage for the implementation of many algorithms, so that the results presented here or their extension are and will remain useful.

4.3.3. Reduced Model Reanalysis

Near a given system configuration (i.e. for a restricted range of possible design parameter values), one can define global shape functions that allow an accurate description of the dynamics. In general such an approach is called a Ritz analysis, but when the shape functions used are normal modes of the initial configuration, the approach is often called *reanalysis*. Using a truncated set of normal modes to reanalyze the system response leads to the reduced model (4.17).

For small modifications, the low frequency normal modeshapes usually form a good basis of Ritz vectors (this is why the sensitivity analyses are valid in a number of cases). However, if the system (and thus the modes) changes significantly, the predictive validity of the reanalysis model becomes less obvious, and one may have to include more information (other Ritz vectors and static correction modes in particular as will be detailed later) which does not modify the predictions in the initial configuration, but increases the range of possible modifications where the model predictions are accurate.

The need to use more Ritz vectors than the set of normal modes of the system in its initial configuration is clearly shown by FE models. The number of base vectors in a FE model is driven by the need to obtain models that represent the local behavior accurately for large ranges of the design parameters. This spatial discretization leads to a higher number of predicted modes, most of which are inaccurate [ben1] (and thus have no more value than Ritz vectors), but are needed to guarantee that the low frequency normal mode predictions remain accurate for large ranges of possible local design parameter values.

The difference between the perturbation and the reanalysis approaches can be interpreted physically as the fact that the perturbation theory tries to follow the modal coordinates (determine the new modal states p corresponding to normal modes of the modified system) where the reanalysis uses the modal states p_0 of the nominal model with

non-diagonal projected modifications. From the reanalysis model (4.17), new modal coordinates can be computed by solving the associated reduced order eigenvalue problem. The perturbation approach uses a first order approximation to evaluate this eigenvalue solution and is thus always less accurate. It is often much less accurate for problems with high modal densities where the definition of modal coordinates is very sensitive to small perturbations (see the example in section 4.3.4).

Another advantage of the reanalysis approach (and of Ritz analyses in general) is that the introduction of correction modes becomes natural. The addition of more normal modes outside the actual bandwidth of interest is the first obvious extension, but static modes (first defined in section 2.2.2 for I/O systems) are also useful. To define static correction modes for FE models, the definition of inputs must be clarified. The modified system equations (4.16) linked to design parameters updates can be rewritten as

$$\begin{aligned} M\ddot{q} + C\dot{q} + Kq &= -\Delta M\ddot{q} - \Delta C\dot{q} - \Delta Kq + bu \\ y &= cq \end{aligned} \tag{4.22}$$

where the mass, damping and stiffness modifications appear respectively as acceleration, velocity, and displacement feedback. In many cases, the correction matrices ΔM, ΔC, and ΔK span a subspace defining a set of inputs described by a matrix F_U. The static input modes corresponding to F_U are used as in section 2.2.2 to generate static correction modes

$$\phi_S = \left(K^{-1} - \sum_{j \in \left\{ \begin{smallmatrix} \text{kept normal modes,} \\ \text{other static modes} \end{smallmatrix} \right\}} \left\{ \phi_j \phi_j^T / \omega_j^2 \right\} \right) F_U . \tag{4.23}$$

In general, the corrections are localized so that the matrix F_U is of small dimensions. In some cases, however, the number of static modes ϕ_S can lead to models with too many states for fast computations of the reduced model response and to numerical conditioning problems for the orthogonalization of the static modes with respect to each other (usually done using a Shmidt orthogonalization). Both restrictions can be alleviated using a mass-orthogonal singular value decomposition and keeping only the modes with the largest singular values as static correction modes.

The eigenvalues Σ_S and eigenvectors Ψ_S of $\phi_S^T M \phi_S$ are the mass-orthogonal singular values and right singular vectors of ϕ_S. The associated left singular vectors that can be used as static mode corrections in the reanalysis are

$$\phi_{SP} = \phi_S \Psi_S \Sigma_S^{-1/2} . \tag{4.24}$$

where only the vectors corresponding to large singular values Σ_{Sjj} are kept. In this research, the improvement in numerical conditioning was the main motivation for the use of these

principal modes (rather than the traditional static correction modes). Other advantages in terms of model reduction would need to be further characterized, but this will not be considered here.

Finally it should be noted that the reanalysis approach is fully compatible and very similar in motivation to Component Mode Synthesis methods [cra3] in which low frequency normal modes and additional correction modes of different components of a system are linked to obtain a full system model.

4.3.4. APPLICATIONS TO THE INTERFEROMETER TESTBED

As an example for evaluating the validity of perturbation and reanalysis approaches for FE updates, the variations of the system response in the 20-60 Hz band linked to changes of the bending stiffness model of the science-plate/truss links will be analyzed for the IT. Since an initial estimate for these design parameters is very difficult to obtain, an update would let them vary over a large range. However, the rate of change of the modal frequencies only becomes significant for a section inertia below 10^{-10} m^4, so that the parameter ranges $I_1 \in [2\ 10^{-11}, 2\ 10^{-10}]$ m^4 and $I_2 \in [10^{-11}, 10^{-10}]$ m^4 are considered here and the low values ($I_1 = 2\ 10^{-11}$ m^4, $I_2 = 10^{-11}$ m^4) are used to create the initial solution (whose modes are the Ritz vectors for the reduced model (4.17)).

The relative errors in the prediction of the change in modal frequencies are shown (Figure 4.3) for the first nine flexible modes of the structure.

The perturbation approach gives obviously inaccurate results for the large parameter range considered here. (It becomes significantly worse than the reanalysis prediction for stiffness increases of more than 25 %, and the expected change (corresponding to the first point shown in the figure) is of the order of a 250% increase.)

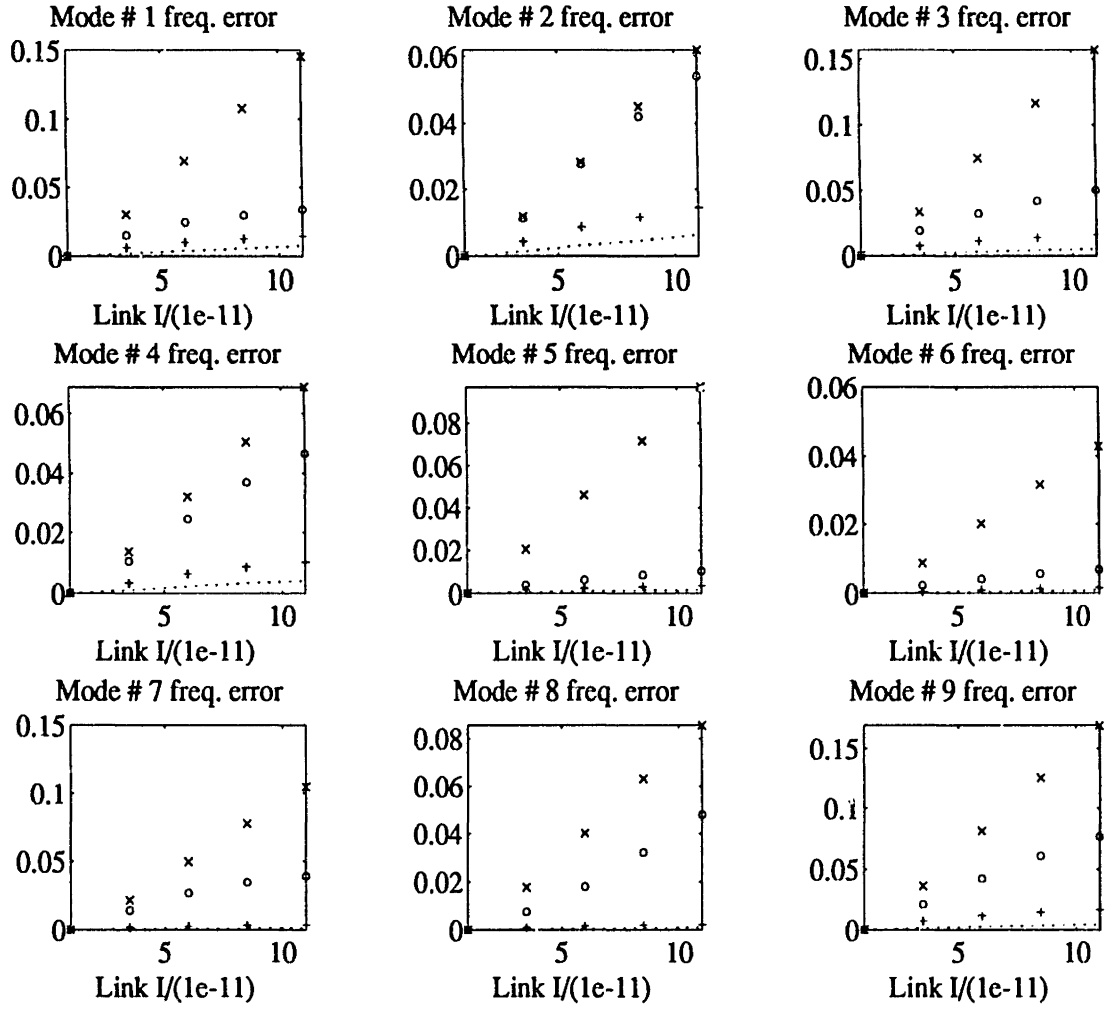

Figure 4.3: Error relative to the full order FEM solution made for the prediction of the first nine modal frequencies of the IT as a function of the link bending stiffness. Results of (x) the perturbation approach with 25 modes, (o) the reanalysis approach with 25 normal modes, (+) the reanalysis approach with 65 normal modes, (····) the reanalysis approach with 25 normal modes and 50 principal components of static correction modes.

The model reanalysis using 25 modes does always better than the perturbation analysis but not significantly better for some modes (mode 2 in particular). These results can be significantly improved by using a larger number of dynamic modes (see in the figure that much better results are obtained for all 9 modes using 65 normal modes of the initial model). The increase of computational cost is usually not a problem for FE update procedures, but might become one for robust control synthesis problems (where it is often desirable to limit the model size, but where parametric variations tend to be smaller so that small truncated models would probably be accurate enough).

In the present, case the modification is distributed (the stiffness of 12 links located in different areas of the structure is modified) so that the addition of static correction modes only improves the global results if more than 50 correction modes (principal components of the 72 static modes initially defined for the problem as shown in section 4.3.2) are kept. Using 25 normal modes and 50 correction modes, the predictions of the reanalysis model are however significantly better than those of the 65 normal mode model, which shows that in many cases the static modes can be more useful for accurate predictions than extending the model bandwidth by adding more dynamic modes.

This first analysis was related to pole predictions, but modeshape predictions are also important. The method developed in this work (see section 4.4) uses frequency response comparisons, so the modeshape accuracy evaluation was first done with frequency response functions. Figure 4.4 plots predictions of the frequency response corresponding to the shaker V accelerometer 1 transfer function for the first point shown in figure 4.3 (link bending stiffness increased by 250%).

The perturbation analysis is clearly not appropriate for this case since the error made on the transfer function prediction is extremely large. Furthermore, conditioning problems, which force a limitation of the number of modes kept, appear very rapidly. For the case considered here, only 20 modes could be kept before obviously inaccurate modes were obtained above the model bandwidth.

The reanalysis with 25 modes is much more accurate, although the predicted frequencies are still somewhat inexact (the peaks are shifted to the right). For parameter variations smaller than this case, the 25 mode reanalysis model would be accurate enough for most purposes. However, if the increased computational time is not a problem (it is usually not), the 65 mode reanalysis model can be used and gives results that significantly reduce this already small error (see the improvement in figure 4.4).

In the plot, the errors on frequencies, which shift the transfer function estimate, are more easily spotted. The small errors made in the modeshapes (seen as errors in the peak heights) should however be noted too. This visual predominance of the frequency error does in fact translate into a higher influence of modal frequency errors for comparison criteria based on transfer functions.

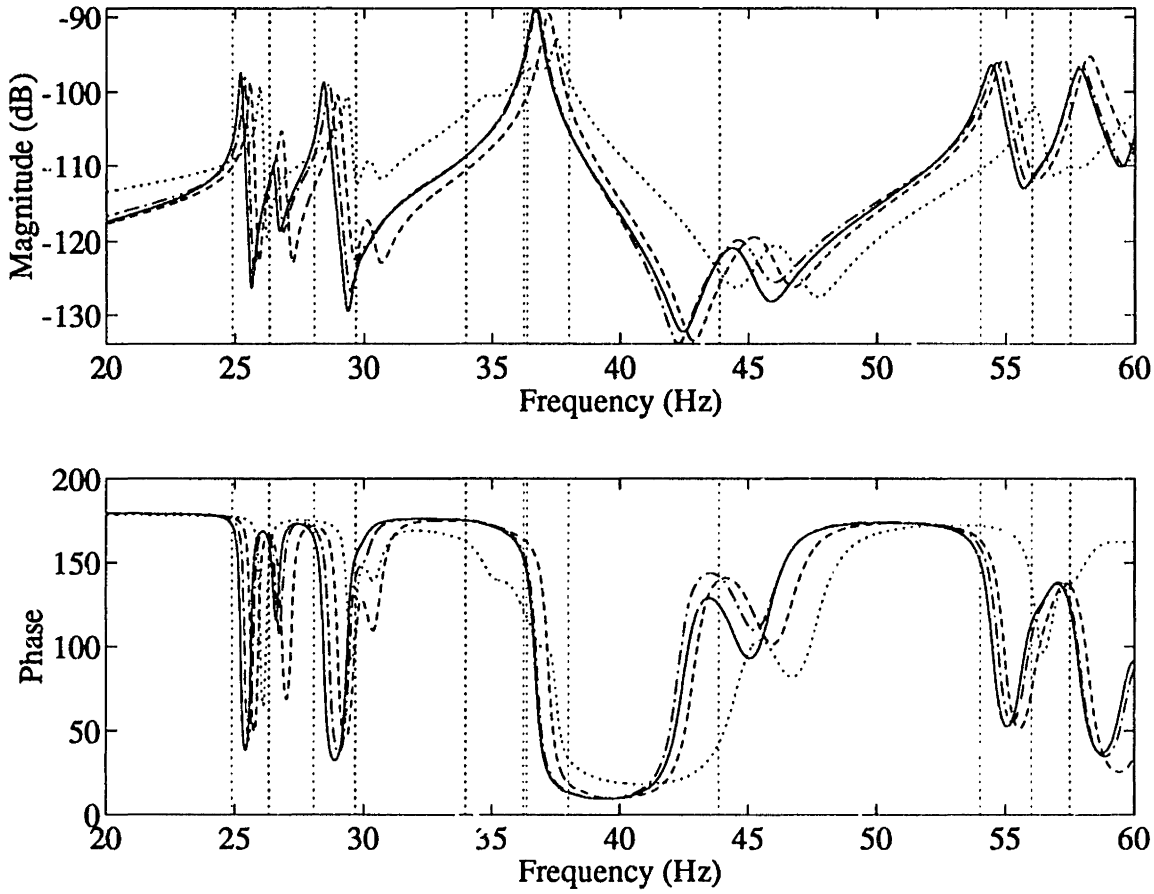

Figure 4.4: Transfer function predictions for a link bending stiffness increased by 250% (—) Full FE solution, (·—·) 65 mode reanalysis, (---) 25 mode reanalysis, (····) perturbation analysis.

The comparison of a single frequency response function does not however provide a good idea of the overall quality of predictive models. Using the 28 transfer function predictions corresponding to the modal test made for the IT, the overall error can be measured using any of the criteria detailed in section 3.1.3. For example, using the logLS cost function with the 28 transfer functions of a test with the shaker on leg V, the prediction error is: 5 10^{+3} using the 65 mode reanalysis model, 1.8 10^{+4} using the 25 mode reanalysis model, and 5.6 10^{+4} using the sensitivity analysis (versus a residual error between the best FE model of the IT and the experiment of 1.3 10^{+4}).

The 65 mode reanalysis model is the only one having a prediction error below the residual FE model error for a link stiffness increase of the considered order (250 %). It would thus probably be the only one appropriate for accurate predictions. However, in practice, this type of reduced model limitation is circumvented by recomputing the full finite

element solution, after the determination of a set of updated design parameters or when the update algorithm calls for excessively large parameter changes.

4.4. Application of the (Reanalysis/logLS) FE Update Algorithm to the Case of the Interferometer Testbed.

In the course of this research a particular update algorithm was developed and coded in the Matlab Toolbox [bal2]. Its main characteristics are the use of:

- A set of measured frequency response functions to characterize the actual system response.
- The Log-Least-Squares cost function (3.11) (introduced in section 3.1.3) to evaluate the model accuracy by comparing measured and predicted frequency response functions.
- The additive matrix representation of the effect of design parameter changes, introduced in section 4.2, as a parametrization for the update model.
- The reanalysis approach, introduced in section 4.3, to evaluate frequency response functions for different values of the updated design parameters.
- A standard simplex algorithm, after a rapid estimation of the optimum location based on a maximum descent algorithm, for the minimization of the logLS cost.

Outside the fact that criteria based on transfer functions are easier to use than modal criteria (see section 4.1.3), the proposed algorithm are probably essentially circumstantial. In fact, it is the opinion of the author that, in practice, the choice of parameters to be updated is an issue of much greater importance than the choices made to create a given update algorithm. Therefore, the analysis presented here will thus not focus on demonstrating the advantages of the chosen method, but will rather use the history of the IT FE model update to highlight difficulties linked to the update of particular design parameters. In particular, it will be shown that the incomplete update of only some of the inexact properties may lead to inexact results, that different parameters sometimes cannot be updated simultaneously, and that the effects of the damping model were negligible for the update of the IT with the proposed algorithm.

In Figure 4.5, the comparison of a measured frequency response function (actuator V sensor 1) with predictions of different versions of the FE model shows that the application of the proposed approach did lead to significant improvements of the IT model by the

successive correction of the plate/truss link stiffness and of the mass distributed around the science plates.

A first step leading to the "initial" FE model (dotted line in Figure 4.5) was to refine the analytical models of the plates. It was then assumed, as usually done, that the mass distribution was correctly represented. A sensitivity analysis of the response to modifications of design parameters led to the conclusion that the only improperly characterized parameters, with enough influence to account for variations of modal frequencies of several percent (initial errors in modal frequencies varied between 1% and 5% for modes below 60 Hz), were the bending stiffness of the beam elements used to represent the plate/truss links (see section 4.2.2).

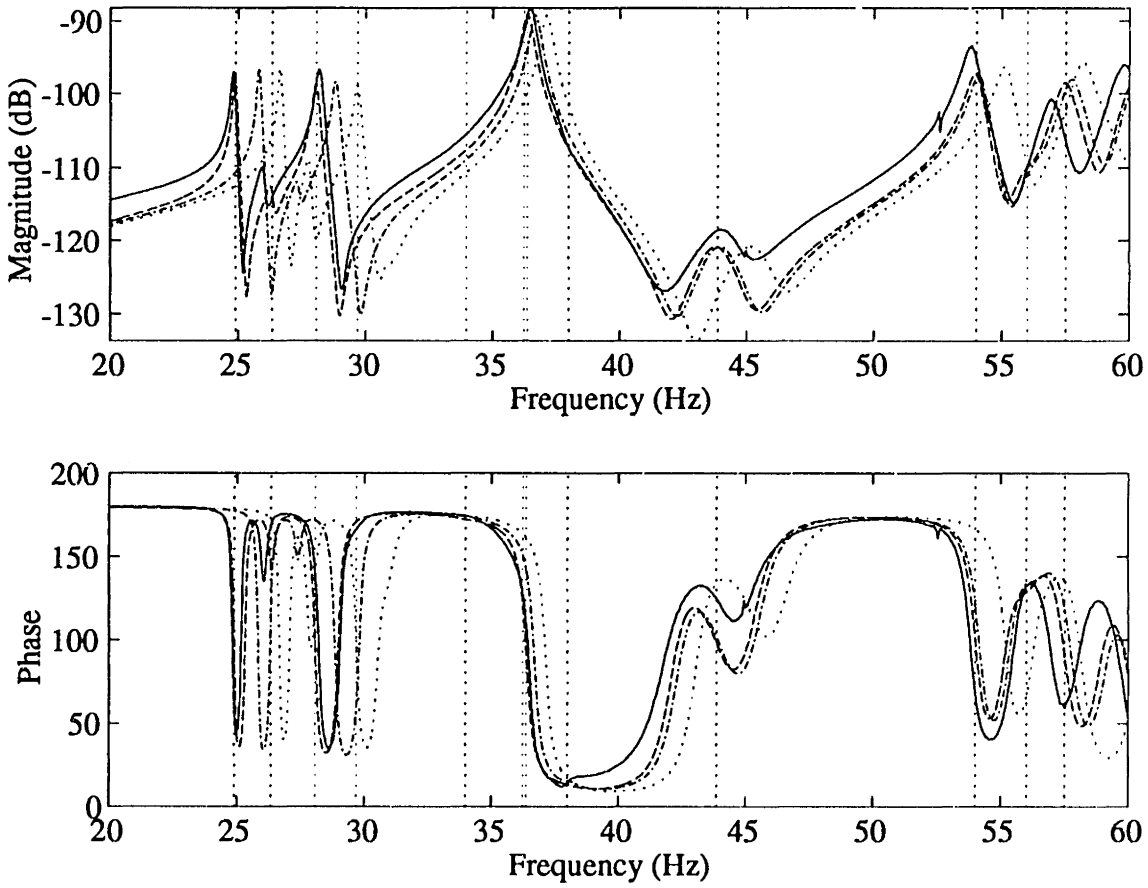

Figure 4.5: Comparison of transfer functions (shaker V sensor 1): (—) measurement, (····) initial FE model, (·—·) FE model with updated link stiffness, (---) FE model with updated plate mass and link stiffness.

The section inertia of these links, initially assumed to be very stiff ($I_1 = I_2 = 10^{-10}$ m^4), was thus updated. As apparent in Figure 4.5, for a lower stiffness ($I_1 = I_2 = 10^{-11}$ m^4

shown as a dot-dash line), all the modes except the first four give very good estimates of the modal frequencies.

The actual optimum of the minimization of the logLS cost function for the 28 transfer functions of the test on leg V was obtained for $I_1 = I_2 = 8\ 10^{-12}\ m^4$, but was rejected because of physical considerations. A number of local plate modes (mostly linked to local vibrations of the plate which couple with the rest of the truss) exist above 50 Hz, but a section inertia at $8\ 10^{-12}\ m^4$ led to almost twice the actual number of modes. This (as well as the frequencies of the 9th and 10th modes (at 44.2 and 53.8 Hz) predicted too low) was corrected by using the value $I = 10^{-11}\ m^4$.

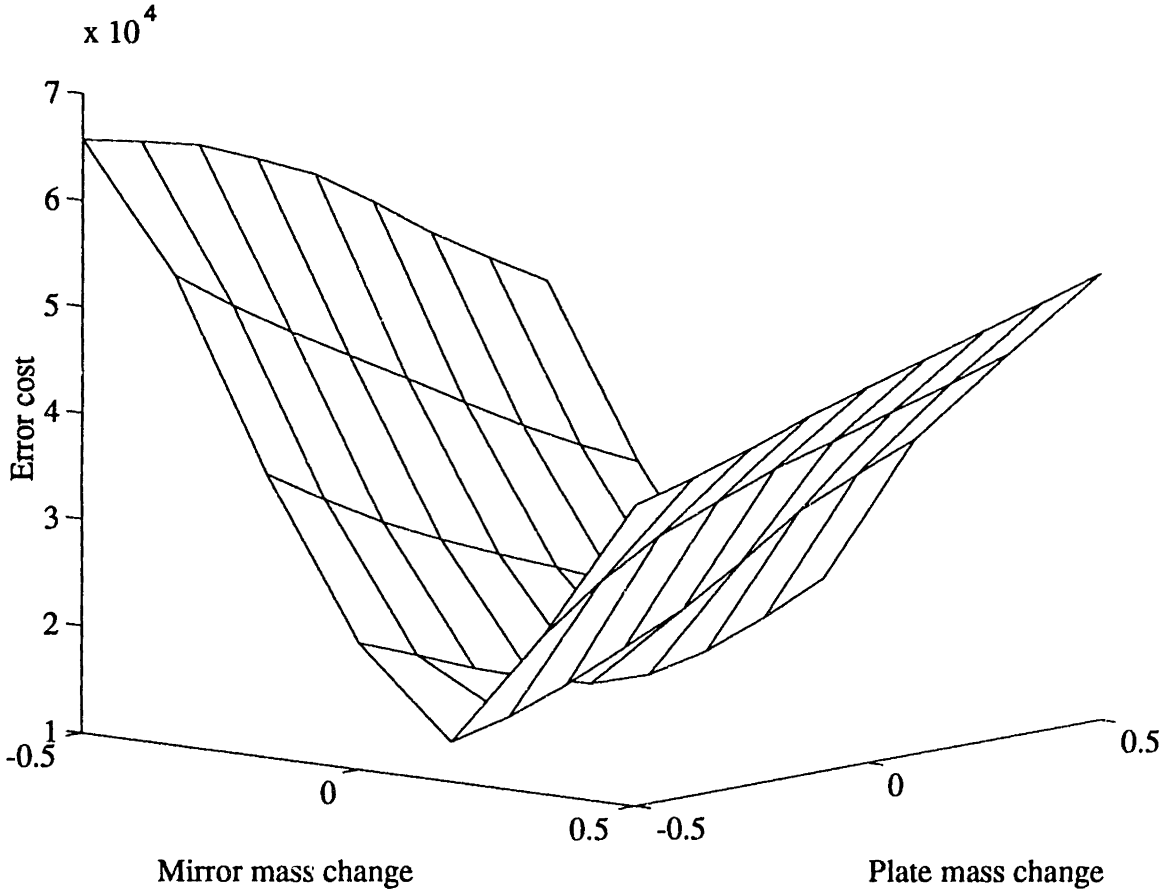

Figure 4.6: Map of cost values as function of mirror and distributed plate mass changes.

Since the agreement was still unsatisfactory, but could not be related to a stiffness error, the mass distribution was questioned. Assuming a simple concentrated mass error at the mirror locations, the update algorithm was used and it converged to an error of 1.05 kg at each of the mirrors. The mass of the different elements constituting the plates could be carefully measured, so it was soon found that an error of approximately 920 g had been

made in modeling the mass of the support plate. (A number of wires, attachments, etc., and a significant portion of the plate surface located outside the points of attachment (and thus with little contribution to the overall stiffness) had been omitted).

The error determined through the component test (measure of weights) was not the error found during the update. (The true error was a mass distributed on the support plates, rather than concentrated at the mirror). This highlights the general problem of demonstrating the uniqueness of the solution for FE update methods.

The uniqueness problem can be easily seen when considering maps of the update costs as functions of the updated parameters. In the present case, a map of the overall update cost, as function of the two design parameters (mirror and distributed masses), was computed and is shown in Figure 4.6. From this map, it appears that the cost remains extremely close to its actual minimum on a line of constant total mass. Thus the considered test cannot distinguish where the mass error is located (at the mirror or on the plate), and a reliable solution can only come from a component test establishing at least one of the masses correctly.

The last update done for the IT model was to do a second update of the link stiffness, which had been made too soft in an effort to compensate for the mass error. More work could be done particularly to update the model of the fourth vertex (see appendix) and the detail of the cat-eye mirror mounts. The properties of those components could not be updated using global system data in the 20-60 Hz range, since they do not have a sufficient influence on the response. These studies were not performed, because the predictions of the current updated model were found to be sufficiently accurate for the creation of hybrid experimental/ analytical models (see Chapter V, and section 5.1 for a better evaluation of the actual agreement) and because no further testbed design phase required greater accuracy.

A last important question in evaluating the usefulness of the presented FE updating methodology is the sensitivity to the damping model. The underlying assumption for updates based on comparisons of frequency response functions is that the effects of damping models are decoupled from mass and stiffness effects. This property was easily shown for simple 1 or 2 DOF systems such as the example presented in section 5.2.2. In general however, this assumption could not be motivated by more rigorous arguments than noting that the damping matrix Γ influences the system response without changing the normal modes (so that the errors in damping lead to fundamentally different discrepancies between measurement and model which should not significantly deteriorate the predictions of the mass/stiffness distribution).

For the IT update, a proportional damping model with measured damping ratios for the poles in the 20-60 Hz band and 1% damping for other modes was generally used. For the leg V shaker, the discrepancy between the predictions of this model and that of one with an identified non-proportional damping matrix were of $1.5\ 10^{+3}$ (as measured by the logLS cost), which is significant when compared to sensitivities to other parameters (shown in Table 4.1).

Two tests showed that this discrepancy had no effect on the update results. The optimum link bending stiffness updates were computed for two different models (the first using modal damping, the second an identified non-proportional damping model). As expected, the two results for the link update were identical (to the accuracy of the optimization, i.e. approximately 1% optimal change). Using analytically generated frequency response from a nominal but non-proportionally damped model, an update of the different parameters considered (bending link stiffness, plate mass, etc.) was performed using a proportionally damped model. Again, as expected, the update procedure indicated that no parameter change was needed.

4.5. CONCLUSIONS

A classification of FE update procedures was proposed using four categories: data used, criterion used to evaluate the agreement between model and data, parametrization of the model, and algorithm used for the update. The compatibility of experimental and analytical modeshape predictions was discussed, reviewing in particular methods of experimental modeshape expansion. Criteria based on modes were reviewed, and the need for a damping representation was discussed for criteria based on I/O response data. The procedure leading to the choice of parameters to be updated was discussed and detailed for the IT case, showing in particular that not all parameters can be updated. The underlying principles of perturbation and reanalysis approaches were analyzed, and applications to the IT case showed that the normal mode model reanalysis leads to the most accurate predictions. The use of static correction modes in the reanalysis approach has been discussed. The update of the IT model using a new algorithm, based on the minimization of the logLS cost function and the use of reanalyzed models, was detailed. Finally, the uniqueness and validity of the update results and the influence damping were discussed for the IT case.

Chapter V

Experimental/Analytical Predictive Models

The experimental models identified in Chapter III are limited to the tested actuator/sensor and system configuration, so that the only predictions that can be made are those linked to these loops (e.g. closing feedback loops using the test sensors and actuators). Analytical FE models allow all the predictions of interest, but lack the accuracy of identification results. This chapter will focus on combining the advantages of these two approaches to create hybrid experimental/analytical models.

The reanalysis approach, presented in section 4.3.3, showed that truncated modal models could be used to accurately predict the response of non-tested system configurations (i.e. modification of sensor/actuator architecture, addition of damping treatments, modification of the mass and stiffness properties). However, most of these predictions can not be obtained with experimental models, because the modeshapes are only known at the tested sensor and actuator locations. To resolve this limitation, it is proposed to use experimental normal modeshapes that are expanded using the solution of the undamped FE model (section 4.1.1). In section 5.1, the creation of such models is detailed, and experimental and analytical evaluations of the accuracy obtaincd are discussed for the Interferometer Testbed (IT).

The truncated normal mode models also allow a good description of the model uncertainty, capturing in particular the effects on non-proportional damping and high modal densities. This description is analyzed in section 5.2, using a two-mode example for a qualitative analysis and the case of the Interferometer Testbed (IT) for quantitative results.

5.1. Experimental/Analytical Predictive Models

The construction of hybrid (i.e. using both experimental and analytical results) predictive models is first introduced in section 5.1.1. Then, to demonstrate the validity of the approach, analytical (in section 5.1.2) and experimental (in section 5.1.3) examples derived from the IT case are detailed.

5.1.1. CONSTRUCTION OF EXPERIMENTAL/ANALYTICAL PREDICTIVE MODELS

After the finite element model update (see Chapter IV), it is known that the agreement of modal frequencies and normal shapes is relatively good (although non-negligible errors remain). It thus becomes useful to do a final "complete update" of the analytical normal mode model much in the way that complete matrix corrections where first introduced for finite element update problems (see Refs. [wei1, ber2, ber4, ber6, kab1, bar1], etc.). This update is done on the damping representation, the normal mode frequencies, and the normal modeshapes.

As discussed in section 2.2.3 and demonstrated in section 3.3, the truncated non-proportional viscous damping matrix allows an accurate representation of complex damping mechanisms at a system level. For an undamped analytical normal mode model, one can therefore construct a damping model by simply using the estimated damping Γ from a global system test. This estimate can be constructed:

- assuming proportional damping and using the damping ratios of estimated poles (Γ is then diagonal with each term of the form $2\zeta\omega_j$ where ζ_j is the damping ratio of the pole) or
- using a full identified damping matrix Γ without the assumption of proportional damping. (Note that a significant contribution of this research is to allow the identification of a non-proportional damping matrix as seen in section 3.3).

For modes that are not (or not accurately) measured, but need to be kept for predictions (such as the static correction modes and other dynamic modes), arbitrary values such as the mean damping ratio of the measured poles can be used effectively. As discussed in section 2.2.3, the damping coupling terms (non-proportional damping) with the accurate dynamic modes of the model should be set to zero, since their effects cannot be properly characterized and are generally small enough to be neglected.

The second step uses measured modal frequencies instead of the less accurate analytical values. As for the damping, the unmeasured modal frequencies (or those that cannot be correlated with the experiment) are kept unchanged.

The third and final step addresses the modeshapes. One could obviously use the analytic modeshapes, but slightly better predictions can be made using the expanded modeshapes introduced in section 4.1.1.

These update steps lead to a truncated modal model of the form

$$\begin{aligned} I\ddot{p} + \Gamma_c \dot{p} + \Omega_c p &= \phi_c{}^T b_c u \\ y &= c_c \phi_c p \end{aligned} \tag{5.1}$$

which uses:

- an experimental modal stiffness matrix Ω_c (diagonal), which has the measured normal frequencies squared for the modes in the model bandwidth and other somewhat arbitrary frequencies for other appended modes needed for predictions.
- an experimental modal damping matrix Γ_c : either the diagonal matrix $2\zeta\omega_j$ (with measured pole damping ratios) if proportional damping is assumed, or the identified full matrix. Somewhat arbitrary terms for correction modes (average damping ratio for additional dynamic modes, or critical damping for static modes).
- a set of expanded modeshapes ϕ_c (mixed experimental/analytical) defined at all the FE DOFs corresponding to the identified normal modes and the other correction modes.
- analytic input and output shape matrices (c_c and b_c) derived from the FE geometry and actuator/sensor calibration.

With the model (5.1), the response of untested loops can be predicted by defining the corresponding analytical input b_c and output c_c shape matrices (see the example in section 5.1.2).

The system matrices have been implicitly updated by using experimental values, so that more accurate results are expected than with the nominal model. Since the updated full order model is not known, modifications of the mass, damping, and stiffness properties cannot be incorporated directly. However, their effects can be predicted using a model reanalysis (first introduced in section 4.3.3) as follows.

For system modifications ΔM, ΔC, ΔK described in the initial full order FE DOF system, reduced mass $\Delta\mu = \phi_c^T \Delta M \phi_c$, damping $\Delta\Gamma = \phi_c^T \Delta C \phi_c$, and stiffness $\Delta\Omega = \phi_c^T \Delta K \phi_c$ modifications are defined and can be added to the reduced system equations (5.1) to obtain a prediction of the modified system response (see the examples in section 5.1.2)

$$\begin{aligned} (I + \Delta\mu)\ddot{p} + (\Gamma_c + \Delta\Gamma)\dot{p} + (\Omega_c + \Delta\Omega)p &= \phi_c{}^T b_c u \\ y &= c_c \phi_c p \end{aligned} \tag{5.2}$$

which can be used in this form or transformed to the new modal coordinates of the modified system (model of the form (5.1)).

The set of expanded modeshapes ϕ_C can be complemented by adding other purely analytical modeshapes (modes beyond the experimental model bandwidth for example). A limitation however appears if static correction modes are needed. As presented in section 2.2.2, static correction modes correspond to the residual static response after subtraction of the static effects of retained dynamic modes. Static correction modes for a hybrid model should thus be the residual static response after subtraction of the effects of the true modeshapes (rather than the analytical ones), and practical ways of obtaining such vectors could be the object of further research (it will be shown in section 5.1.3, that a direct use of the analytical static correction mode may not lead to accurate results).

5.1.2. THEORETICAL EVALUATION OF THE HYBRID MODEL VALIDITY

Non-tested sensor actuator architectures, mass/stiffness modifications, and damping augmentation modifications are changes to the system that should be predicted by a hybrid model. To demonstrate the ability of hybrid models to make such predictions with no interference from other errors, a hybrid was created using an early version of the IT FE model (before the mass and stiffness update) as the analytic model and the frequencies and modal observabilities (at the 27 non-collocated sensors of the modal test) of the updated FE model as the pseudo-experimental part.

This hybrid model uses

- the exact proportional damping model
- the exact modal frequencies (of the recent FE model)
- modeshapes geometrically expanded (equation (4.7) in section 4.1.1) with the full modeshapes of the old FE model and the exact modal observabilities (of the recent FE model).

A first evaluation of the hybrid model quality is linked to the accuracy of the expanded modeshapes. To analyze this accuracy, the modal controllabilities for the shaker location on leg V were predicted using the expanded modeshapes. As shown in Figure 5.1, the hybrid model predictions of the modal controllabilities (based on the expanded modeshapes) are almost indistinguishable from the true controllabilities. In fact, the overall open-loop model agreement is extremely good (using the usual logLS cost function on the 28 transfer functions of the modal test, the error made by the hybrid model is $0.5\ 10^{+3}$ versus $8.8\ 10^{+3}$ for the initial FE model).

As the accuracy of initial modeshapes used for the expansion can generally not be ascertained without a very accurate FE model, the refinement and parametric update of FE models was discussed in Chapter IV. However, if before the update residual modeshape

errors made in the FE model are mostly related to frequencies, the hybrid model predictions using the modeshapes of a somewhat inaccurate model will still be accurate. For the case of the IT, it can thus be verified that the hybrid models using different versions of the FE model (initial, with update link stiffness, with updated plate mass and link stiffness) are almost identical.

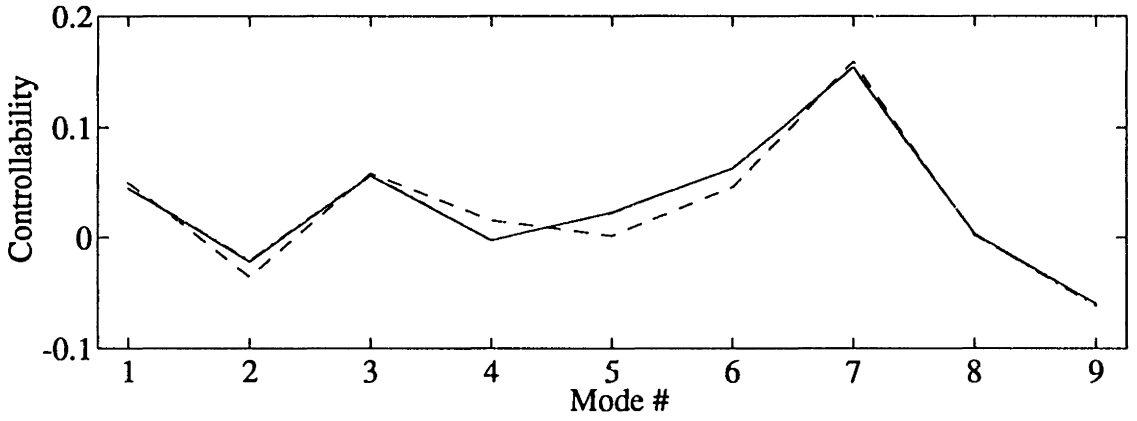

Figure 5.1: Comparison of the first 9 modal controllabilities $\phi_j^T b$ for the leg V shaker location. (—) "true" FE model, (---) initial FE model, (·—·) hybrid model.

For many controlled structures applications, one adds to the base structure damping treatments (such as the Honeywell D-strut used for the IT) whose effects must be predicted accurately for a good design of the damping treatment. A simple description of the D-strut can be obtained using displacement and velocity feedback (see Ref. [and1]). For a measurement y of the relative axial extension of a standard strut, the effect of the D-strut can be described as a relative force feedback of the form

$$F = -k_V \dot{y} - k_P y \tag{5.3}$$

where for the present case k_P=-6.8 10^{+6} (which corresponds to the fact that the D-strut is less stiff than the regular struts), and k_V=1.9 10^{+5} (which models the dissipation in the D-strut).

The prediction of the response for the hybrid model thus takes the form

$$\begin{aligned} I\ddot{r} + \left[\Gamma_C - \phi_C{}^T b_{Cs} k_V c_{Cs} \phi_C\right]\dot{r} + \left[\Omega_C - \phi_C{}^T b_{Cs} k_P c_{Cs} \phi_C\right] r = \phi_C{}^T b_C u \\ y = c_C \phi_C r \end{aligned} \tag{5.4}$$

where b_{Cs} is the input shape function for the relative axial force input and c_{Cs} the output shape function for the relative displacement measurement at the considered location (note that $b_{Cs} = c_{Cs}^T$).

In the analysis presented below, two cases will be considered: k_P=*0* and k_V=1.9 10^{+5} to consider in the damping properties (damping augmentation) k_P=-11.2 10^{+6} and k_V=*0*, to consider a change in the stiffness properties (broken strut).

For each case two series of hybrid models are considered: with just 26 modes and 26 modes + a static correction mode (added to obtain a statically correct model for the axial relative force input on the strut). For the two series of models (26 and 26+1 modes), partial updates are also considered to determine the influence of different parameters. The different columns of Tables 5.1 and 5.2, thus correspond to the pure FE model, a model with updated modal observabilities and controllabilities (derived from expanded modeshapes rather than FE modeshapes), a model with the FE modeshapes but updated frequencies, a model with expanded modeshapes and updated frequencies but a reduced damping matrix computed using the FE modeshapes, and finally the fully update hybrid presented in section 5.1.1.

As a first case, velocity feedback (damping modification) is considered assuming k_P=*0* and k_V=1.9 10^{+5}. (Strut *601* just behind plate *B* (see the appendix) was used, because it is a high strain location where the damping effects are maximized)

Table 5.1: Damping modification. Measures of overall accuracy (logLS cost) for FE and hybrid models with combinations of updated modal observabilities $c\phi$, controllabilities $\phi^T b$, frequencies Ω_C, and damping perturbation $\Delta\Gamma_C$.

Type of model	FE model	Obs. Cont.	Freq.	Obs. Cont. Freq.	Obs. Cont. Freq. Pert.
26 flexible modes	9.41 10^{+3}	7.01 10^{+3}	2.94 10^{+3}	0.70 10^{+3}	0.61 10^{+3}
26 flex. + 1 static	9.44 10^{+3}	7.00 10^{+3}	2.90 10^{+3}	0.69 10^{+3}	0.65 10^{+3}

As shown in Table 5.1, predictions show an extremely significant improvement for both series of models as more elements of the hybrid model are updated. A reduction of the logLS cost by a factor of 2 would already imply a very significant reduction of the model error and a factor of 15 is obtained for the fully updated hybrid model. Furthermore, the partial update of only some of the model properties also improves the predictions, although not as much as the complete update used to generate the hybrid model proposed in section 5.1.1.

As a second case, displacement feedback (stiffness modification) is considered assuming k_P=-11.2 10^{+6} and k_V=*0* (which corresponds to a broken strut). (The results shown assume that strut *143* on leg IV (see the appendix) has no stiffness, but do not introduce a damping modification). (This stiffness modification is representative of the analysis of the position feedback term in (5.3), but the need to use a static mode is smaller for the D-strut stiffness decrease, so that a broken strut was preferred for this example).

Table 5.2: Broken strut. Measures of overall accuracy (logLS cost) for FE and hybrid models with combinations of updated modal observabilities $c\phi$, controllabilities $\phi^T b$, frequencies Ω_C, and stiffness perturbation $\Delta\Omega_C$.

Type of model	FE model	Obs. Cont.	Freq.	Obs. Cont. Freq.	Obs. Cont. Freq. Pert.
26 flexible modes	1.52 10^{+4}	1.47 10^{+4}	1.05 10^{+4}	1.06 10^{+4}	0.95 10^{+4}
26 flex. + 1 static	1.25 10^{+4}	1.21 10^{+4}	1.40 10^{+4}	1.04 10^{+4}	1.27 10^{+4}

In Table 5.2, the first series of predictions for models created using 26 flexible modes (of the inaccurate FE model) shows that the error can be somewhat reduced by using the proposed hybrid model (or even by only updating some of the properties). The relatively large error obtained for the full hybrid model can be easily explained by the fact a static correction mode (see sections 2.2.2 and 4.3.3) is necessary to correctly predict the response after a large stiffness modification such as a broken strut (in particular the predicted modal frequencies remain too high without a static correction mode).

The construction of the hybrid model, introduced in section 5.1, does not provide a proper way of defining static correction modes, since the corresponding complete stiffness matrix is unknown. The second line of Table 5.2 assumes that the static correction mode generated from the FE model can also be used with expanded experimental modeshapes, and the poor results obtained clearly show that this is not a valid option. Without further developments that could be the object of further research, the hybrid models introduced here are therefore limited to modifications that do not necessitate the use of static corrections.

5.1.3. Predictions for the Test Configuration of the Interferometer Testbed

For predictions using a hybrid experimental/analytical model, the important analytical quantity is the accuracy of the FE modeshape predictions. The modeshape accuracy can only be verified *a posteriori* from identification results. For the best FE model, the modal observabilities, at the 28 sensor locations of the IT modal test, are compared in Figure 5.2

with an average of the identified modal observabilities. The figure clearly indicates a relatively good initial agreement between the prediction and the measurement.

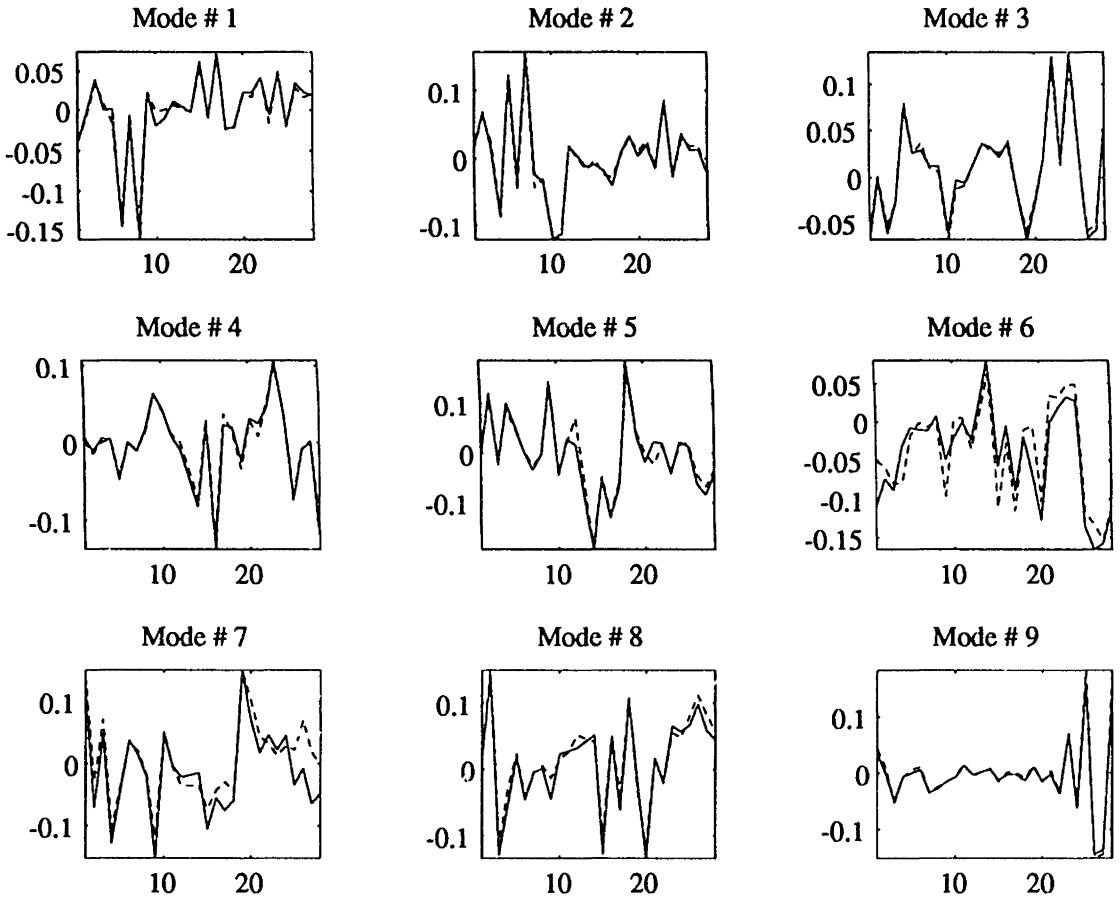

Figure 5.2: For modes $j=\{1\cdots 9\}$, comparison of the scaled normal mode observabilities $c\phi_j$ (in meters, y-axis in the figures) at the 28 sensors of the modal test (x-axis in the figures). (—) mean identified. (---) best FE model.

As shown in figure 5.3, the expanded modeshapes of the hybrid model, which combine these FE modeshapes and the measured observabilities, lead to relative errors that are significantly lower than those done by the FE model. (The mean value for 28 sensors and 9 modes of $c\phi_{FE}/\overline{(c\phi)}_I$ is three times higher than the mean value of $c\phi_{Ex}/\overline{(c\phi)}_I$). Furthermore, the errors made by the hybrid modeshapes are for most sensors below the levels of variation between the different identification results.

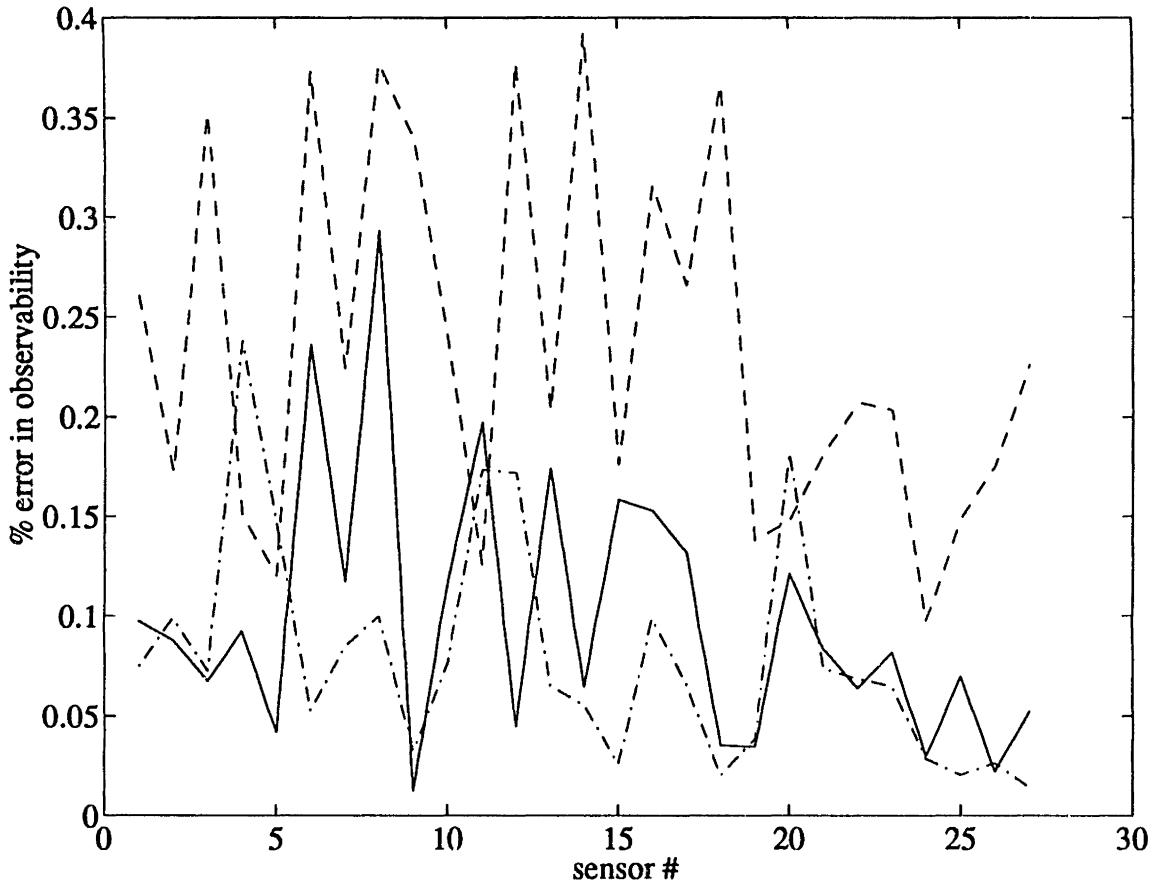

Figure 5.3: Average (for modes $j = \{1 \cdots 9\}$) percent error in modal observabilities at the 27 sensor locations. (—) $\sigma_{(c\phi)_j} / \overline{(c\phi)_j}$ sample standard deviation for the 6 different ID results. (---) $c\phi_{FE} / \overline{(c\phi)_j}$ for best FE model. (·—·) $c\phi_{Ex} / \overline{(c\phi)_j}$ for hybrid model.

The improvement of the predictions (when using expanded modeshapes rather than the FE modeshapes) comes from the fact that the FE modeshapes span the correct subspace but tend to be combination of the true modes, a problem which is corrected using the experimental modeshape expansion. For example, modes 6 and 7 are extremely close in frequency (36.1 and 36.5 Hz), so that small FE modeling errors lead relatively large errors clearly apparent in Figure 5.2. These errors are due to a significant recombination of the two true modes and a rotation by 22° within the constant subspace of the two initial modes (see Ref. [bal6]) reduces the mean error made on the observabilities by a factor of 3 (leading to errors similar to those seen for the other modes). (This large effect of a small error in a structure with a high modal density is analyzed for a simple two-mode example in section 5.2.2).

A first use of a hybrid model is to predict the response of the same system but for a different sensor/actuator configuration. To demonstrate the ability of the IT hybrid model to make such predictions, an hybrid model was created without using the leg V test. With this hybrid model, the untested modal controllabilities $\phi^T b$ linked to the test on leg V were computed and the frequency response functions of that test were generated. (It was chosen to predict the response of one of the tests to allow a comparison with test data).

As an example of the accuracy achieved, Figure 5.4 shows how this prediction correctly captures the system response near modes 6 and 7. Clearly, the hybrid model matches both the magnitude and phase extremely well, even though the underlying FE model is much less accurate and non-proportional damping has a significant influence on this part of the transfer function.

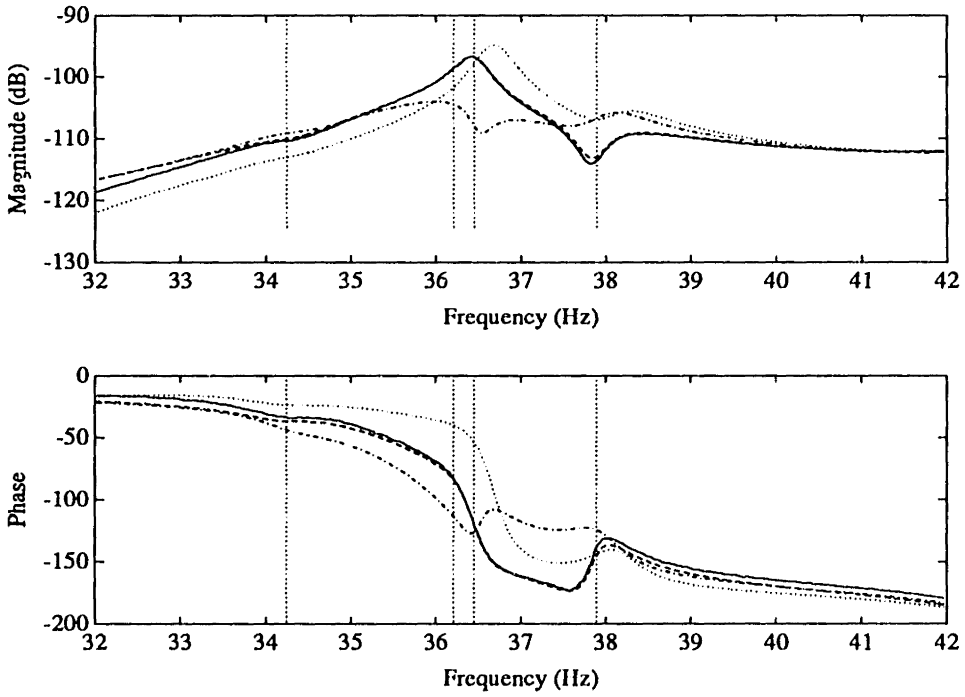

Figure 5.4: Comparison of leg V accelerometer 1 transfer functions. (—) Measured, (---) hybrid model, (·—·) proportionally damped hybrid model, (····) FE model.

The comparison of a single transfer function does not however ascertain the overall validity at all possible measurement points. As an average measure of the prediction accuracy at different points of the structure, the logLS cost function (3.11) and the mean error of RMS prediction (average of the difference between the predicted and the corresponding measured RMS responses) for 1200 points linearly spaced in the 20-50 Hz

frequency band and the 28 measured transfer functions were computed and are shown in Table 5.3.

Table 5.3: Measures of overall accuracy for different predictive models.

Type of model	logLS cost	Mean error of RMS prediction
Hybrid model	$1.35\ 10^{+3}$	0.7 %
Hybrid model, proportionally damped	$1.68\ 10^{+3}$	11.7 %
Finite element model, proportionally damped	$2.41\ 10^{+3}$	17.1 %
Identified normal mode model, non-prop. damped	$1.87\ 10^{+3}$	0.5 %

From Table 5.3, it clearly appears that the use of the hybrid model instead of the FE model significantly improves the accuracy of predictions as measured by the two different cost functions. Furthermore, the use of a non-proportional damping model plays an important role, particularly for predictions of RMS responses (which are critical for many studies such as damper placements [and2]).

The RMS responses are extremely well predicted by the identified normal mode model, which is not surprising as this model is identified using a quadratic criterion on the transfer functions which is strongly related to the RMS prediction. The logLS error for the identified normal mode model, however, is worse than that made with the hybrid models. The improvement obtained with hybrid models can easily be related to the fact that they incorporate FE predictions for higher frequency modes (particularly mode 10 at 54 Hz) which have a significant impact on the log magnitude of the transfer function above 40 Hz but little on the RMS, since the amplitudes are very small in the 40-50 Hz region.

As will be shown in section 5.2.2, partial reassemblies of the testbed have led to a significant evolution of the system dynamics after the complete modal test used in this work. Predictions of tested structural modifications (e.g. addition of D-struts, removal of a strut) were thus not very accurate, but the quality of agreement for analytical tests, such as those presented in section 5.1.2, indicate that this was mostly due to the evolution of the testbed dynamics.

5.2. Error and Uncertainty

Uncertainty is an estimated measure or bound on how much error can exist in a prediction of the response. As seen in Chapters III and IV, measures of model error are defined trough choices in two main areas: the measured data and the cost function used to

compare data and predictions. Thus, to different choices of data and cost functions correspond different definitions of the model uncertainty, which may or may not be appropriate for other purposes, such as robust controller synthesis.

The predictions of the models considered here should not, even for a perfect model, reproduce direct time domain measurements on the real system. Noise characteristics, high frequency dynamics, non-linearities, and time-varying parameters have not been included in the models and should thus appear as prediction errors.

Noises and high frequency unmodeled dynamics can be easily treated using a transfer function representation of the system response. For the structural systems considered here, where noise levels are low, an almost noise-free estimate of the frequency domain response can be obtained under the realistic assumption that noises and inputs are uncorrelated (see section 3.1.1). High frequency unmodeled dynamics can be addressed in more detail using the methods developed for control applications [ath1], or can be simply truncated by considering frequency response functions in the frequency range of the model. (Note that this truncation also applies to additional model dynamics (such as static correction modes) used to obtain predictions over a larger parametric range, see section 4.3).

Non-linearities and parametric time-variations cannot be properly treated, since transfer functions are only defined for linear time-invariant systems. The identification and linearization of time-varying weakly non-linear systems using linear frequency response function estimators and linear identification techniques is an interesting subject (see [ozg1] for example), but too broad for the scope of the present work.

Assuming that the representation of the system by transfer functions is valid and that the important properties of the system are captured by a comparison in the bandwidth where the model is accurate, a description of parametric model uncertainty based on the hybrid model form (5.1)-(5.2) will be introduced in section 5.2.1. In section 5.2.2, using a simple two-mode example, the proposed description of uncertainty will be shown to efficiently capture effects seen in structures with non-proportional damping and high modal densities. Finally in section 5.2.3, a quantitative evaluation of uncertainty in the IT model will be discussed.

5.2.1. Choice of a Parametrization to Describe Uncertainty

Errors can be described in any parametrization, since exact transformations exist between different parametrizations. However, uncertainties describe sets of models within which the actual system is "guaranteed" to be (or "likely" to be for statistical descriptions of

the set). Simple descriptions of sets in a given parametrization do not usually translate into simple descriptions for other parametrizations. Thus, as uncertainty descriptions are only useful if they are simple, it is important to determine a description that is both simple and does not introduce to much conservatism.

The truncated normal mode form, or the equivalent hybrid model form (5.1)-(5.2), lead to a natural description of uncertainty, in the following form

$$\begin{aligned}(I)\ddot{p}+(\Gamma_C+\Delta\Gamma)\dot{p}+(\Omega_C+\Delta\Omega)p&=(\phi_C{}^T b_C+\Delta b)u\\ y&=(c_C\phi_C+\Delta c)p\end{aligned} \tag{5.5}$$

where uncertainties can appear as parameter errors on the truncated modal damping $\Delta\Gamma$, stiffness $\Delta\Omega$, controllabilities Δb, and observabilities Δc. The parametrization of uncertainty (5.5) is appropriate for different reasons.

First, as shown in section 2.2., truncated normal mode models are minimal representations of the system properties in the considered bandwidth. Clearly, some parameters of an over-parametrized model could be arbitrarily uncertain, since they do not represent physical and measurable properties of the system. (This, in particular, is a good reason not to use FE design parameters to describe uncertainties, since some design parameters may have little or no influence on the system response in the frequency range where the FE model is meaningful).

Second, the normal mode description appropriately distinguishes the contributions of the mass and stiffness distribution (which can be established with high accuracy), from those of damping mechanisms (fully described by the modal damping matrix Γ), which are difficult to measure and are thus quite uncertain.

The third and perhaps the most important reason is that, for an appropriate definition of the states p in the parametrization (5.5), small modifications of the system only result in small parameter changes, or, in other words, that small errors can be represented by small uncertainties. The proper choice of states is still an open issue, but the following comments can be done.

If, as done in perturbation analyzes (see section 4.3), the states p are chosen to be the normal mode states of the true system, by definition of these states $\Delta\Omega$ would be diagonal. This choice clearly minimizes the number of uncertain parameters but can induce unnecessarily large uncertainties in the modal controllability Δb, and modal observability Δc. This large sensitivity of the system normal modes to small system changes has been well studied as a phenomenon called localization (e.g. [lev2, che1]), which can be shown [bal6] to appear for any pair of modes that are close in frequency when compared to the

perturbations. An example will be treated in section 5.2.2 and the importance of this phenomena for the IT will be shown in section 5.2.3.

The unnecessary sensitivity of the modal observability and controllability matrices obtained with perturbation analyses can theoretically be avoided using a fixed definition for the states p (however, work is needed to define how this could be done to account for experimental errors). In this case, uncertainties or modifications on the system dynamics appear as uncertainties ($\Delta\Gamma$ and $\Delta\Omega$) in the modal damping and stiffness matrices, and uncertainties in the sensor actuator architecture as uncertainties (Δb and Δc) on the modal controllability and observability matrices. Small uncertainties on the system dissipation will be represented as small $\Delta\Gamma$ matrices. Small uncertainties on the mass and stiffness errors as small but generally full $\Delta\Omega$ matrices (note that uncertainties on the mass will also generate uncertainties on the b and c matrices). Small uncertainties in the sensor/actuator architecture will be represented as small Δb and Δc matrices.

5.2.2. Qualitative Effects of Error. A Two-Mode Example.

The advantage of using the proposed description of uncertainty (5.5) is that it gives a good understanding of how small modifications of the system can lead to large uncertainty descriptions in some parametrizations. The following two-mode example will be used to highlight these properties

$$\begin{bmatrix} \dot{p}_1 \\ \dot{p}_2 \\ \ddot{p}_1 \\ \ddot{p}_2 \end{bmatrix} = \left[\begin{array}{cc|cc} 0 & 0 & 1 & \\ 0 & 0 & & 1 \\ \hline -1 & & -0.04 & \\ & -1.21 & & -0.022 \end{array}\right] \begin{bmatrix} p_1 \\ p_2 \\ \dot{p}_1 \\ \dot{p}_2 \end{bmatrix} + \begin{bmatrix} 0 \\ 0 \\ 1 \\ 1 \end{bmatrix} u \qquad (5.6)$$

$$\begin{bmatrix} y_1 \\ y_2 \\ y_3 \end{bmatrix} = \begin{bmatrix} 1 & 1 \\ 2 & -1 \\ -2 & 0 \end{bmatrix} \begin{bmatrix} p_1 \\ p_2 \end{bmatrix}$$

The nominal system (5.6) has two proportionally damped modes with frequencies at 1 and 1.1, and respectively 2% and 1% damping. The single actuator excites both modes in the same way, and three sensors measure the response at three different locations.

A first point of interest is the analysis of the influence of non-proportional damping. The following example will show how for a system with constant poles and complex modes, significant variations can be obtained of the complex modes, the damping of zeros and the overall RMS response. To demonstrate this influence the damping coefficient Γ_{12} was defined as an uncertainty coupling the two-modes of the nominally proportionally

damped model (5.6). To obtain a clearer analysis of the results, it was arbitrarily chosen to introduce four other uncertain parameters $\delta\Gamma_1$, $\delta\Gamma_2$, $\delta\Omega_1$, and $\delta\Omega_2$

$$\begin{bmatrix} \dot{p}_1 \\ \dot{p}_2 \\ \ddot{p}_1 \\ \ddot{p}_2 \end{bmatrix} = \left[\begin{array}{cc|cc} 0 & 0 & 1 & \\ 0 & 0 & & 1 \\ \hline -1+\delta\Omega_1 & & -0.04+\delta\Gamma_1 & \Gamma_{12} \\ & -1.21+\delta\Omega_2 & \Gamma_{12} & -0.022+\delta\Gamma_1 \end{array}\right] \begin{bmatrix} p_1 \\ p_2 \\ \dot{p}_1 \\ \dot{p}_2 \end{bmatrix} + \begin{bmatrix} 0 \\ 0 \\ 1 \\ 1 \end{bmatrix} u \tag{5.7}$$

$$\begin{bmatrix} y_1 \\ y_2 \\ y_3 \end{bmatrix} = \begin{bmatrix} 1 & 1 \\ 2 & -1 \\ -2 & 0 \end{bmatrix} \begin{bmatrix} p_1 \\ p_2 \end{bmatrix}$$

which were modified so as to keep the location of the system poles invariant. In this case, one thus has a perfect knowledge of the normal modes and the system poles, but imperfect knowledge of the spatial distribution of damping mechanisms (which appears as the possibility of non-proportional damping).

Figure 5.5 summarizes the different ways of looking at the possible system responses for different levels of non-proportional damping (i.e. values of the coupling coefficient Γ_{12}). For passive structures, a physical constraint is that the matrix Γ be positive definite, so that the possible variations of Γ_{12} are limited to the interval $\Gamma_{12} \in [-0.3, 0.3]$.

In Figure 5.5a is shown the collocated transfer function y_1/u in the extreme possible cases. The proportional damping case appears as an average between two extreme cases where non-proportional damping minimizes dissipation in the structure leading to an undamped zero, or maximizes dissipation leading to a significantly damped zero.

The normal modes are invariant by construction of the example. The scaled complex mode observabilities, shown in Figure 5.5b, indicate that non-proportional damping results in phase and magnitude variations from the line of observabilities found in the proportionally damped case (o) (where the complex modes are proportional to the normal modes as seen in section 2.1.3).

As shown in Figure 5.5c, keeping poles invariant does lead to variations of the normal mode frequencies but these are very small (less than 0.1% variation on the frequency (not the frequency squared)). Note, however, that variations of identified pole frequencies of the order of 0.2% were found to have non-negligible effects on the identification process for the IT case (see section 3.4). It may thus be important to distinguish pole and normal mode frequencies for systems with significant non-proportional damping levels.

Finally, non-proportional damping can induce large variations in the RMS response of different transfer functions (in Figure 5.5d for the collocated transfer function y_1/u, the predicted RMS can vary by almost 10%).

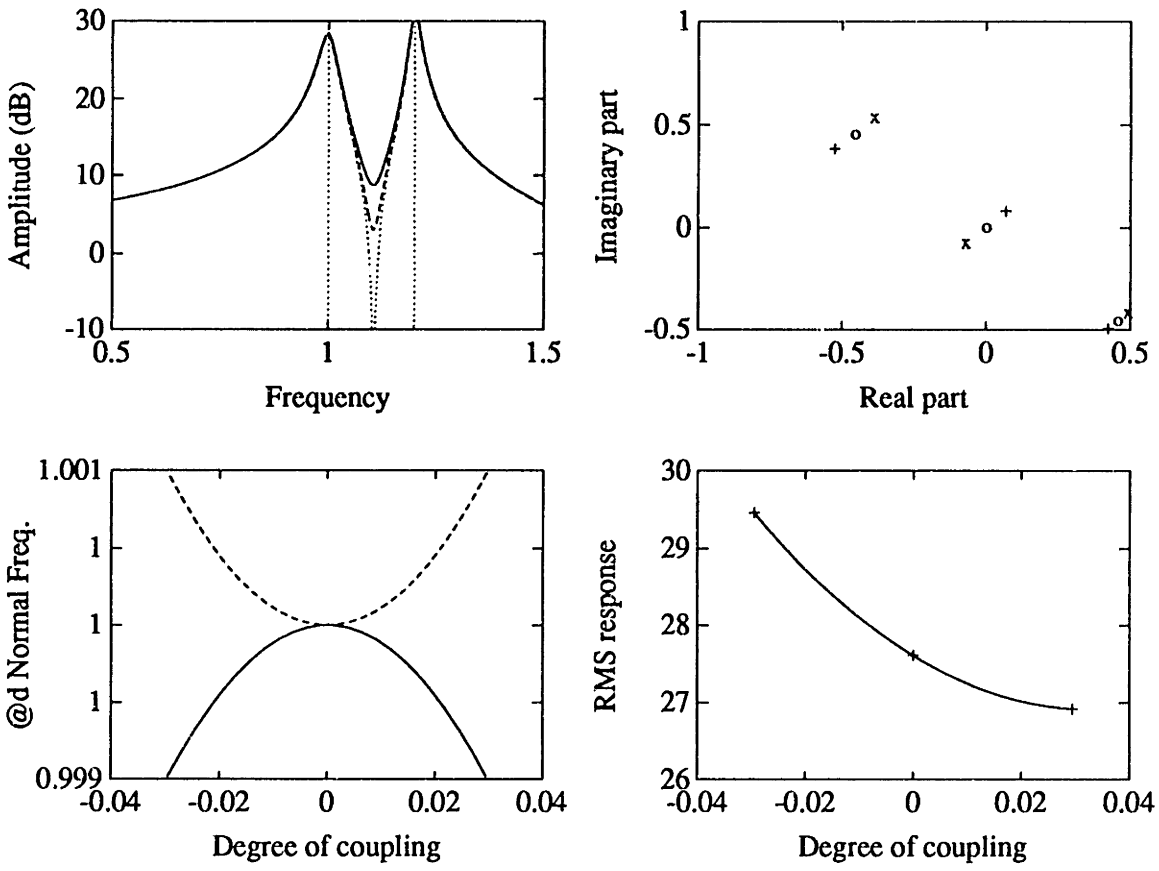

Figure 5.5: Variations linked to non-proportional damping, for a case with constant poles and constant normal modes.
a) Collocated transfer function y_1/u for (—) maximum dissipation, (---) proportional damping, (····) minimum dissipation.
b) Complex residues $c\psi_j$ for (+) maximum dissipation, (o) proportional damping, (x) minimum dissipation.
c) Relative variations of the normal mode frequencies (—) $\sqrt{\delta\Omega_1/1}$ and (---) $\sqrt{\delta\Omega_2/1}$.
d) Variations of RMS for the collocated transfer function y_1/u.

Other studies of non-proportional damping (e.g. [par2, bow1]) have shown that the influence of non-proportional damping increases with damping (and modal density which will not be shown here). To demonstrate this trend for the two-mode example considered here, the maximum variations in the collocated transfer function y_1/u were computed for increasing levels of damping. Using the damping ratio ζ of the first pole as a parameter, the following damping matrix was used:

$$\Gamma = \begin{bmatrix} -2\zeta(1) + \delta\Gamma_1 & \Gamma_{12} \\ \Gamma_{12} & -2(2\zeta)(1.1) + \delta\Gamma_1 \end{bmatrix} \tag{5.8}$$

where Γ_{12} was free to vary within the range where Γ is positive definite, and for each value of ζ the coefficients $\delta\Gamma_1$, $\delta\Gamma_2$ were adjusted to keep the pole constants.

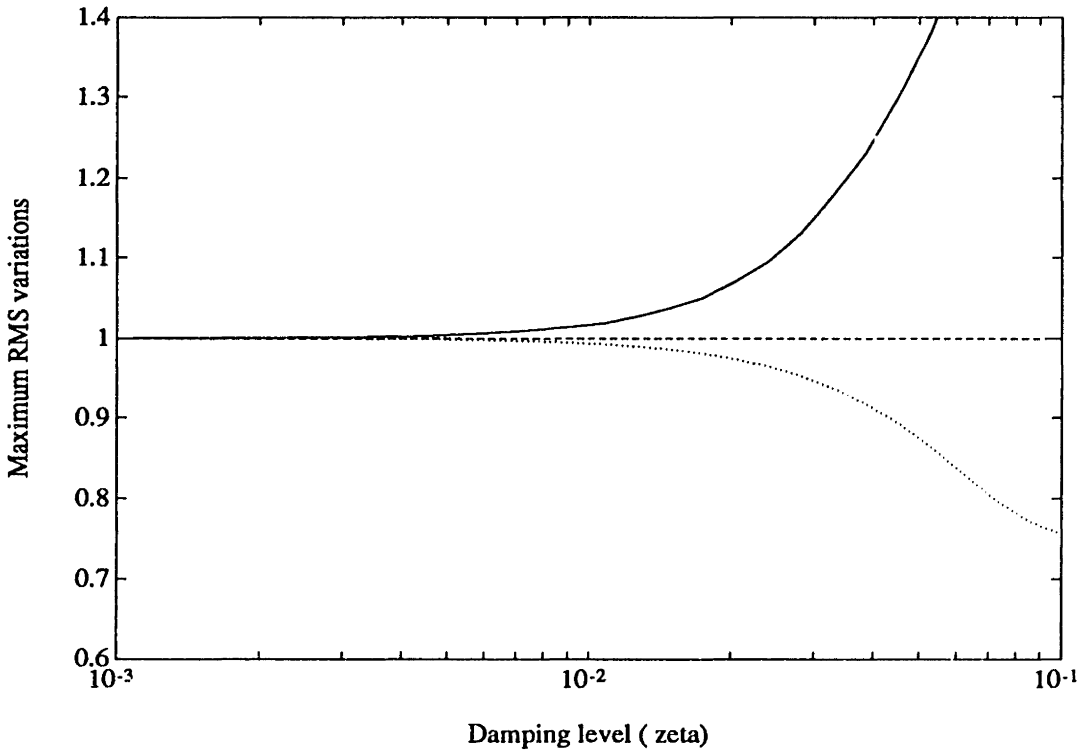

Figure 5.6: Possible RMS difference relative to the proportional damping level (i.e. $\Gamma_{12} = 0$) linked to non-proportional damping for a system with *constant normal* modes as a function of the average pole damping (see definition of the damping matrix as a function of ζ in (5.8)).

As shown in Figure 5.6, the maximum possible influence of non-proportional damping increases almost exponentially with the damping level. As the pole damping increases, the possible interval where Γ_{12} is such that Γ is positive definite also increases, so that the difference between the possible extreme cases becomes more important. Thus, for damping levels of some poles near 2%, the proportional damping estimate can be far from a conservative measure of the actual dissipation in the system.

It must be noted that these results somewhat depend on the chosen transfer function. As appeared in Figure 5.5a., non-proportional damping mostly influences the damping of zeros, and the overall influence of zeros on the RMS response is strongly dependent on the sensor and actuator locations in the structure. The accuracy of a proportional damping model will thus depend on the considered sensor/actuator architecture, on the damping levels, and to a certain extent on the frequency content of inputs used.

A second case of interest is the analysis of small errors in the undamped system dynamics. The following example will demonstrate that the definition of the states is a key to obtain non-conservative descriptions of uncertainty in the model form (5.5).

In this example, stiffness errors were represented in a model of the form (5.5) as an error matrix $\Delta\Omega$ added to the nominally diagonal modal stiffness matrix. A first type of error represented by a $\Delta\Omega$ matrix is simply linked to modal frequencies and induce modifications of the system response which are generally well understood (shift of the resonance and of the zeros to some extent). A second type of error is the apparition of coupling terms between states modeled as uncoupled (off-diagonal terms in the matrix $\delta\Omega$). This type of coupling was considered for the two-mode example of this section, leading to the following model:

$$\begin{bmatrix} \dot{p}_1 \\ \dot{p}_2 \\ \ddot{p}_1 \\ \ddot{p}_2 \end{bmatrix} = \left[\begin{array}{cc|cc} 0 & 0 & 1 & \\ 0 & 0 & & 1 \\ \hline -1+\delta\Omega_1 & \delta\Omega_{21} & -\Gamma_1 & -\Gamma_{12} \\ \delta\Omega_{12} & -1.21+\delta\Omega_2 & -\Gamma_{12} & -\Gamma_2 \end{array}\right] \begin{bmatrix} p_1 \\ p_2 \\ \dot{p}_1 \\ \dot{p}_2 \end{bmatrix} + \begin{bmatrix} 0 \\ 0 \\ 1 \\ 1 \end{bmatrix} u \qquad (5.9)$$

$$\begin{bmatrix} y_1 \\ y_2 \\ y_3 \end{bmatrix} = \begin{bmatrix} 1 & 1 \\ 2 & -1 \\ -2 & 0 \end{bmatrix} \begin{bmatrix} p_1 \\ p_2 \end{bmatrix}$$

where the coupling is described by the coefficient $\delta\Omega_{12}$, the two coefficients $\delta\Omega_1$, $\delta\Omega_2$ are adjusted so as to keep the mode frequencies invariant, and the damping matrix Γ is adjusted to obtain a proportionally damped system for all values of $\delta\Omega$.

A coupling term of the order of 0.1 times the diagonal term is considered small for most structural dynamic applications (orthogonality conditions (4.13) etc.), so the example was treated for $\delta\Omega_{12} \in [-0.1, 0.1]$. Different perspectives on the response predicted by the uncertain model are shown in Figure 5.7.

The magnitude and phase of the non-collocated transfer function y_2/u (shown in Figure 5.7a and 5.7b) indicate that what would be considered small errors in the stiffness lead to significant variations of the response as measured by this sensor. Magnitude changes are important because there is a pole/zero flip (the order of the zero and the second pole changes, see Figure 5.7c), and phase errors are close to 180° because the zero becomes non-minimum phase, and the pole and zero flip.

The normal modeshapes are also very sensitive to these small modifications of the system stiffness properties. As shown in Figure 5.7d, the observabilities of mode 2 have both large variations and sign changes. The invariant property in this case is the overall observability and controllability of the subspace spanned by the two modes, as clearly

apparent in the system equations (5.9), where the modal controllability and observability matrices are kept unchanged. If the states of the model (5.5) were chosen to be the true modal states, the modeshape variations would need to be completely included in the Δb and Δc matrices, which would then be unnecessarily large (and introduce conservatism if the variations are assumed independent). The uncertainty description (5.9) using constant states and a $\Delta\Omega$ matrix, appropriately shows that the actual system properties are not subject to large variations.

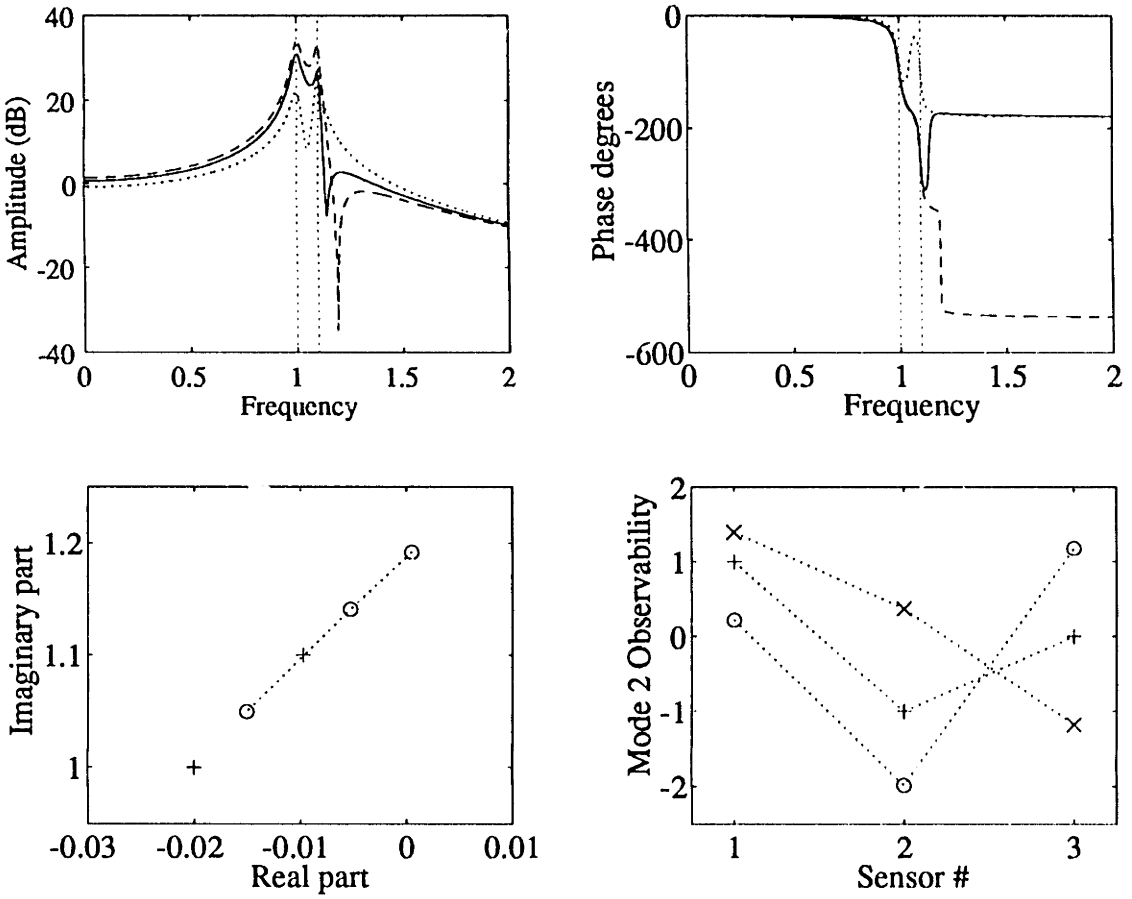

Figure 5.7: Variations linked to a small stiffness error (with proportional damping)
a) Non-collocated transfer function magnitude y_2/u for (—) $\delta\Omega_{12}$=-0.1, (---) $\delta\Omega_{12}$=0, (····) $\delta\Omega_{12}$=0.1
b) Non-collocated transfer function phase y_2/u for (—) $\delta\Omega_{12}$=-0.1, (---) $\delta\Omega_{12}$=0, (····) $\delta\Omega_{12}$=0.1
c) Locations of (+) poles and (o) zero for the non-collocated transfer function y_2/u
d) Normal mode observability at the three sensors for (x) $\delta\Omega_{12}$=-0.1 (o) $\delta\Omega_{12}$=0, (+) $\delta\Omega_{12}$=0.1

A simple parametric analysis for two mode system would show that large effects of small off-diagonal terms become significant if the off-diagonal terms are of the order of the difference between the corresponding diagonal terms ($\Delta\Omega_{ij\ \text{Bound}} = |\Omega_{ii} - \Omega_{jj}|$). The importance of an appropriate choice of state in the parametrization (5.5) therefore increases with the modal density.

However, it can be shown [bal6] that for sufficient modal overlap (half power bandwidth of each pole larger than the frequency separation of the two poles) the transfer functions would in fact become insensitive to the error made on the stiffness. Therefore, above a certain modal density (which depends on the level of damping) the average characteristics of the transfer function can be well known and the choice of states stops being an issue.

5.2.3. Quantitative Evaluation of Model Uncertainty for the Interferometer Testbed

As pointed out in section 3.4, the only available method to evaluate uncertainty is to determine the variations of parameters obtained for different tests of the same system. Clearly such studies are only meaningful if the estimation process is unbiased, a strong condition that must generally be assumed.

Noise models provide a measure of the uncertainty in the measured data, which can be used to generate parametric uncertainty models. For the case of the IT, such studies done in section 3.4 led to the conclusion that uncertainties in the data of a given test had less influence than inconsistencies observed for different tests.

The experimentally identified elements used to construct hybrid models are the normal mode observabilities, frequencies, and damping matrices, so that uncertainty in the hybrid model depend on uncertainty in these parameters, and to a lesser extent on errors in the FE model. Assuming that the variations from test to test, of these measured parameters, are representative of the maximal variations, the sample means and variances can be used as a description of the uncertain model set. This section, as a final validation of the IT model, presents an evaluation of these variations (for the IT case).

To evaluate the variations in modal observabilities (Δc), the means and variances of these terms were computed at the 27 non-collocated sensors of the modal test. Figure 5.8 shows as solid lines the standard deviations for the identified modal observabilities (as fractions of the absolute value of the mean modal observabilities). Most of the identified observabilities have a standard deviation that is no greater that 10% of their mean value,

and it can be verified that most of the large standard deviations correspond to small mean values (which are inherently difficult to identify).

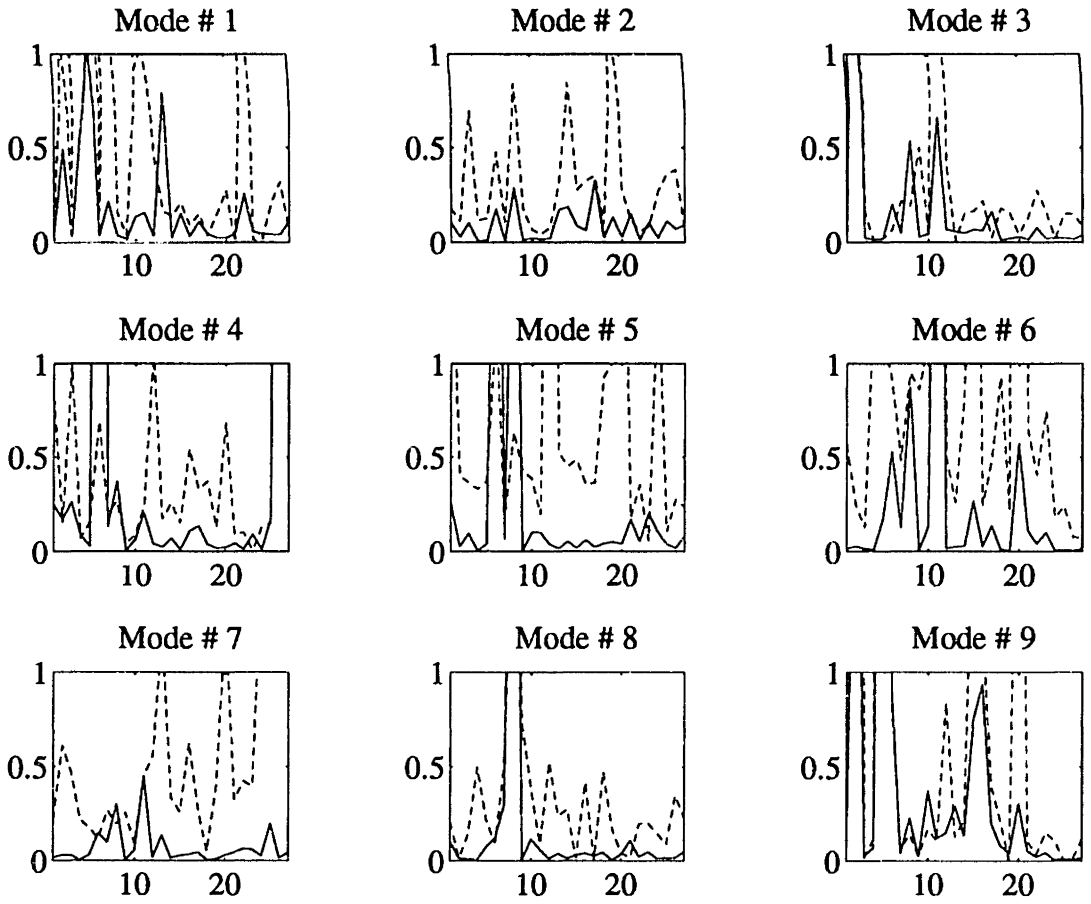

Figure 5.8: Consistency of the modal test, for modes $j=\{1\cdots9\}$. (—) sample standard deviation of the identified modal observabilities $c\phi_j$ (y-axis, plotted as a fraction of the amplitude of the mean observability $\overline{c\phi_j}$) at the 27 non-collocated sensor locations (x-axis). (---) relative error made by the FE model ($\left(c\phi_{FEj}-\overline{c\phi_j}\right)/\overline{c\phi_j}$).

For the IT, a 10% uncertainty level for each of the terms of the normal mode modal observability and controllability matrices thus seems to be a reasonable estimate of the level of errors that can be expected from identification. The FE model has a much larger error (shown as the dashed lines in Figure 5.8), but the hybrid model (constructed with the mean of the identified observability matrices) has an error to the mean observability that is, for most sensors and modes, below the sample standard deviation. This thus gives a strong confidence in the validity of the hybrid model.

Uncertainties in the modal stiffness matrix ($\Delta\Omega$ matrix) come from both errors in the modal frequencies and interaction between close modes (see the example treated in section 5.2.2). As expected, inconsistencies in the identified normal mode frequencies are identical (almost) to inconsistencies on the pole frequencies shown in Table 3.2 (very low error levels, below 0.2%). Realistic estimates for the off-diagonal terms of $\Delta\Omega$ are difficult to determine, since these terms depend on the non-uniquely defined choice of states (which also induces errors the modal observability and controllability matrices).

No generally applicable solution was found to determine these terms, so that only a measure of the error $\Delta\Omega$ made by the FE model could be used. This measure was obtained by computing the stiffness orthogonality condition (4.13) for a set of modes expanded so that the mass orthogonality condition remains verified (application of the expansion formula (4.7) with a unitary pseudo-inverse as first proposed in Ref. [smi1]). Effects are important for off-diagonal terms of the order of the difference between two diagonal terms ($\Delta\Omega_{ij\ \text{Bound}} = |\Omega_{ii} - \Omega_{jj}|$), so that results of the stiffness orthogonality computation are shown in Table 5.3 as fractions of this bound (thus giving non-dimensional evaluation of the parameter influence).

Table 5.4: Evaluation of FE model stiffness error off-diagonal terms, as percentage of the reference levels of significant impact ($\Delta\Omega_{ij\ \text{Bound}} = |\Omega_{ii} - \Omega_{jj}|$).

	12.8	2.3	0.5	1.1	0.4	1.0	0.6	1.0
12.8		5.8	2.4	1.5	0.2	0.5	1.0	0.6
2.3	5.8		5.9	1.6	0.2	0.2	2.4	4.4
0.5	2.4	5.9		2.2	1.6	5.2	1.1	1.7
1.1	1.5	1.6	2.2		7.0	3.6	1.4	0.7
0.4	0.2	0.2	1.6	7.0		**16.2**	**14.3**	3.7
1.0	0.5	0.2	5.2	3.6	**16.2**		**13.7**	1.7
0.6	1.0	2.4	1.1	1.4	**14.3**	**13.7**		2.2
1.0	0.6	4.4	1.7	0.7	3.7	1.7	2.2	

The coupling between modes 1-2, 6-7, 7-8, 6-8 are significant, but these are better indications that the modes of the FE model are linear combinations of the corresponding true modes, than that the model is inconsistent between the different tests. However, a conservative uncertainty model would keep terms that are at least a few percent of the diagonal values. So that in practice, significant effects should be expected for diagonal terms of the modal stiffness matrix separated by a few percent (e.g. between modes 6 and 7).

A last point of interest is to evaluate the accuracy of the non-proportional damping matrix estimation ($\Delta\Gamma$ matrix). Table 5.4 summarizes the main trends that can be derived from the analysis of the 6 identification results.

Table 5.4: Consistency of the experimentally identified modal damping matrices Γ for the first 9 modes of the interferometer testbed.

Mean damping matrix

0.98	-0.02	-0.04	-0.39	0.66	-0.14	0.20	-1.00	-0.87
-0.02	**1.76**	0.13	0.66	0.06	-0.49	-0.85	-1.05	-0.00
-0.04	0.13	**1.80**	-0.06	-0.24	0.13	0.75	1.39	2.13
-0.39	0.66	-0.06	**4.68**	1.10	-1.08	-0.39	-1.78	2.46
0.66	0.06	-0.24	1.10	**6.07**	**-1.69**	0.64	-2.00	-1.41
-0.14	-0.49	0.13	-1.08	**-1.69**	**11.66**	**-3.14**	**4.11**	0.97
0.20	-0.85	0.75	-0.39	0.64	**-3.14**	**3.54**	**-0.61**	-0.12
-1.00	-1.05	1.39	-1.78	-2.00	**4.11**	**-0.61**	**4.56**	1.07
-0.87	-0.00	2.13	2.46	-1.41	0.97	-0.12	1.07	**12.72**

Standard deviation/Mean value in % (terms smaller than 100%)

17.58								
	6.99		96.78					
		10.12					56.78	
	96.78		**27.48**					
				7.88	**37.54**		63.18	
				37.54	**12.57**	**12.88**	**27.56**	
					12.88	**12.20**	**34.03**	
		56.78		63.18	**27.56**	**34.03**	**9.94**	71.64
							71.64	**11.16**

% of positive definiteness bound ($\gamma_{ij\ \text{Bound}} = \sqrt{\gamma_{ii}\gamma_{jj}}$)

	1.4	2.6	18.1	27.3	4.0	10.9	47.5	24.6
1.4		7.1	23.0	1.9	10.8	34.0	37.0	0.0
2.6	7.1		2.0	7.3	2.9	29.8	48.6	44.6
18.1	23.0	2.0		20.6	14.6	9.5	38.6	31.9
27.3	1.9	7.3	20.6		**20.1**	13.8	38.1	16.1
4.0	10.8	2.9	14.6	**20.1**		**48.8**	**56.3**	8.0
10.9	34.0	29.8	9.5	13.8	**48.8**		**15.1**	1.8
47.5	37.0	48.6	38.6	38.1	**56.3**	**15.1**		14.0
24.6	0.0	44.6	31.9	16.1	8.0	1.8	14.0	

The standard deviations show that only a few of the off-diagonal terms are consistently identified, but not surprisingly the well-identified terms are those with a large mean value, and particularly the coupling terms between modes 5-6, 6-7, 6-8, and 7-8 (which clearly

shows that non-proportional damping is an important effect for this group of modes). Significantly better consistency would be obtained by eliminating the worst term of the six tests for each element of Γ, but a justification for the elimination of these terms (such as a large sensitivity to measurement noise in the identification process) would be needed and is not yet available.

The importance of the well-identified non-proportional damping coupling terms can also be seen in the fact that these terms are significant fractions of the largest possible values (the values of off-diagonal terms are limited to $\gamma_{ij\ \text{Bound}} = \sqrt{\gamma_{ii}\gamma_{jj}}$, as it is known that the damping matrix must be positive definite). (Note that the bound argument has no value for not well-identified terms).

From these results, an appropriate damping uncertainty model $\Delta\Gamma$ could have standard deviations of 20 % for the diagonal terms and 20% of the $\sqrt{\gamma_{ii}\gamma_{jj}}$ bound value for the off-diagonal terms (although this is much harder to justify).

For a final validation of this analysis, 12 transfer functions of the modal test on leg V were remeasured one year, and many partial truss reassemblies, after the initial modal test. As shown in Figure 5.9 for one of the transfer functions, the evolution of the structural response was quite significant. To get a better global characterization of this evolution, the two tests were compared using three cost functions (see results in Table 5.4, where for reference the errors made using the hybrid model are also shown). Using the quadratic cost and the accuracy of RMS predictions, the evolution of the testbed response seems significantly larger than the errors made by the hybrid model in the initial case. Using logLS cost function, which is much more sensitive to errors made on low amplitude regions of the transfer functions than the other two measures, emphasizes errors on the zeros by the hybrid model so that the evolution of the testbed seems slightly less important.

Table 5.4: Global measures of error for the hybrid model and corresponding evolution of the testbed between 1991 and 1993.

Error measure using 12 transfer functions in the 20-60 Hz range	Hybrid model	Measurement in 1993
logLS cost	$3.8\ 10^{+2}$	$3.3\ 10^{+2}$
mean error in prediction of RMS	0.3 %	13.0 %
quadratic error	$0.3\ 10^{-8}$	$3.1\ 10^{-8}$

The data of the 1993 test are much more limited than that of the full modal test, so the accuracy achieved for the identified model is not as good. But a rapid assessment of the evolution of the system characteristics gives an average evolution of the pole locations near

0.2% (versus a maximum of 0.2% for the initial modal test), an average evolution of modeshapes of the order of 20 % (versus a conservative estimate of 10% for the modal test), and an evolution of pole damping ratios around 20 % (versus less than 10% for the modal test). No reliable estimate of non-proportional damping coefficients could be obtained as the amount of data available was insufficient.

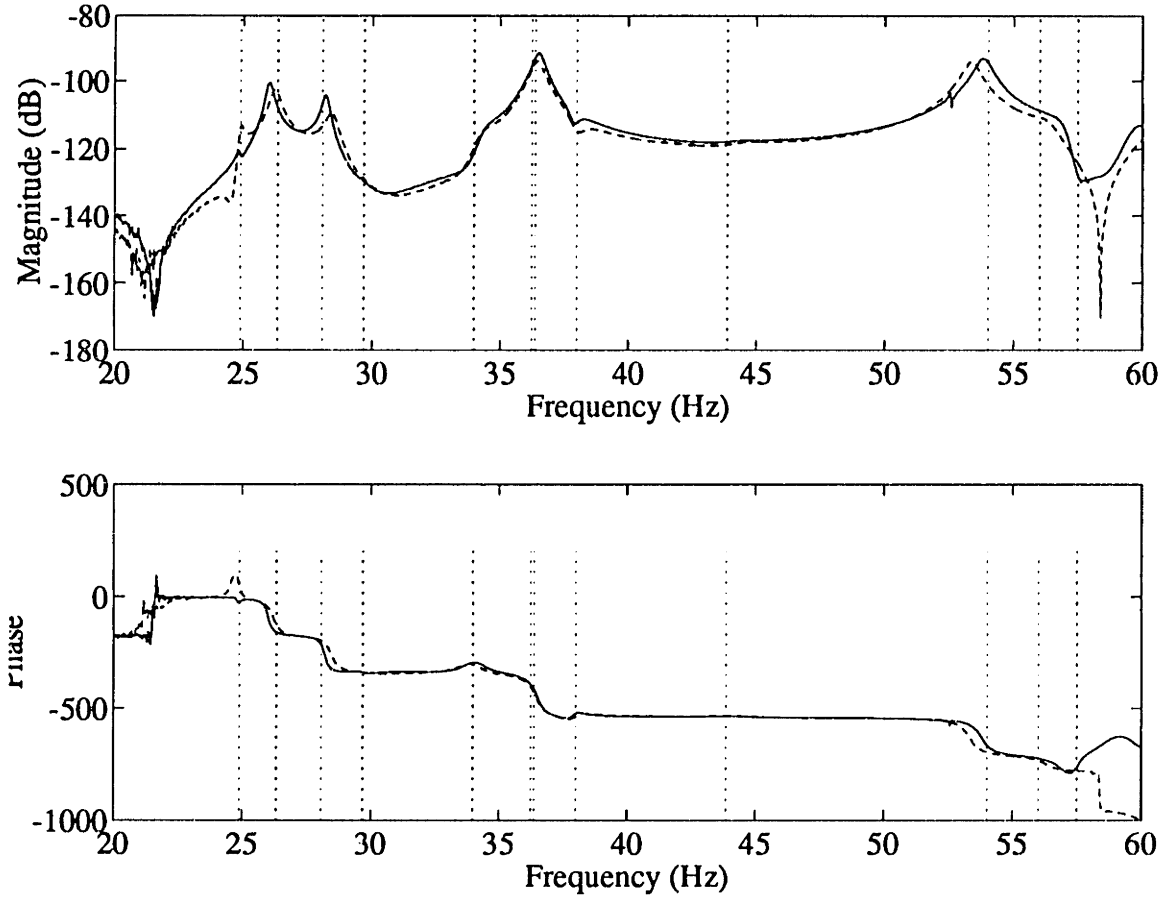

Figure 5.9: Consistency of the modal test. Comparison of a transfer function (leg V sensor 7) measured in (—) January 1993 and (---) December 1991

5.3. CONCLUSIONS

It was shown that hybrid experimental/analytical models can be created using expanded experimental modeshapes combined with experimental modal frequencies and an experimental non-proportional damping matrix. These models allow predictions of the response for arbitrary sensor/actuator architectures, and, through a model reanalysis, the

prediction of the system response after mass, damping, and stiffness modifications which can be described in the full order FE coordinate system. Purely analytical normal modes can be appended to these models with good accuracy, but solutions to introduce static corrections are still needed. The validity of hybrid model predictions was demonstrated using analytical and experimental examples derived from the IT case.

The description of uncertainty in parametric models was addressed. It was shown that the normal mode model form used for the hybrid models is a good parametrization to describe uncertainty. The extent of the maximum effects of non-proportional damping were analyzed, and it was shown that the freedom in defining the model states can lead to unnecessarily conservative descriptions of uncertainty, particularly for structures with high modal densities. Finally, as a validation of the IT model, the variations of identified parameters for different tests have been discussed.

Chapter VI

Conclusions and Recommendations

6.1. SUMMARY

An integrated methodology for the creation of high accuracy predictive models has been presented and demonstrated by application to the case of the MIT/SERC interferometer testbed. The creation of such models implies the simultaneous use of experimental and analytical models, which must first be created independently and then combined as hybrid experimental/analytical models.

For lightly damped structures with high modal densities, the complex mode parametrization must be used to obtain accurate identification results. After the enforcement of the model properness condition, complex mode models can be reparametrized as normal mode models which allow the separate analysis of undamped dynamics (mass and stiffness effects) and of non-proportional damping mechanisms.

Analytical FE models are created using a detailed description of the local component properties and refined to obtain physically significant representations of the local properties (i.e. models with no analytical limitations). Even for physically significant models, initial FE models are generally inaccurate, so the parameters of the model must be updated. The best update method uses component tests, but it is often easier to update parameters using comparisons of the global model agreement (which can be characterized using identified modal models or by direct comparison with measured responses). Comparisons of global system responses do not generally allow the identification all the model parameters, so care must be taken to update only parameters whose influence can be differentiated from expected residual errors and from contributions of other unknown parameters.

Combining experimental and analytical results into small hybrid models, better predictions than those obtained with FE models can be made of arbitrary untested sensor/actuator configurations, for the nominal system or after known modifications of the mass, damping and stiffness properties. Model uncertainty can also be characterized both qualitatively and quantitatively using these models, which appropriately capture the effects of non-proportional damping and high modal density.

6.2. CONTRIBUTIONS

New methods have been introduced to identify scaled complex mode modal observability and controllability matrices. A new algorithm allows a cost-effective and very accurate identification of complex mode poles and residue matrices. The algorithm efficiently handles MIMO tests with large numbers of sensors as well as structures with high modal densities and local modes. The algorithm optimizes solutions found by other methods and generally allows significant improvements of the models. A new method, based on the singular value decomposition of the identified residue matrix, leads to a determination of the modal multiplicity and to accurate scaled estimates of the modal observability and controllability matrices.

A new method has been introduced to identify non-proportionally damped normal mode models from complex mode models. The assumption of a truncated non-proportional modal damping matrix was shown to correspond to a properness condition on the complex modeshapes. An algorithm to enforce this condition on the complex modes was proposed and the then exact transformation between the complex and normal mode parametrizations was detailed. The application of this method to the case of the interferometer testbed led to the first experimental characterization of non-proportional damping for a relatively complex structure and demonstrated the effectiveness of the new methods proposed to identify both complex and normal modes.

A new classification of FE modeling methods was made, clearly indicating how choices at different levels lead to a given update algorithm. A particular algorithm, combining the advantages of comparing frequency responses with the log-least-squares cost and using reduced order predictive modal models, was introduced. The history of its use for the update of the interferometer testbed model was detailed, and allowed an analysis of inherent limitations of all FE update procedures.

It was then shown how experimental and analytical models can be combined to create extremely accurate predictive models. These models incorporate the very accurate experimental description of non-proportional damping and modal frequencies and use identified modal observabilities to define updated full order modeshapes. Because the modeshapes are defined at all the FE degrees of freedom, these models can be used to predict, with much better accuracy than the FE model, the system response at untested sensors or actuators after arbitrary (but known) mass, damping, or stiffness modifications. The validity of the approach was demonstrated with experimental and analytical examples on the interferometer testbed.

Finally, the description of error in the proposed models was discussed. Effects of errors in the damping, and mass/stiffness models were analyzed qualitatively for a two mode example, showing in particular the limits of non-proportional damping effects and the influence of modal density. Then, for the interferometer testbed, a quantitative evaluation of the model error was made and led to the conclusion that variations in time of the testbed properties were of the same order or even greater than errors made with the best model.

6.3. RECOMMENDATIONS

The present work was limited to linear time-invariant symmetric systems. The extension to asymmetric systems (e.g. systems with aeroelastic coupling or gyroscopic damping) could be easily done, although the existence of distinct left and right complex modes (modal controllabilities and observabilities) would lead to more stringent requirements in terms of number of actuators for the identification of experimental models. The identification and modeling of weak non-linearities should also be further addressed considering non-linear models of non-linear components (see Refs. [mas1, web1, kar1]) or using linear tools to obtain equivalent linear models (see ref. [ozg1]).

The new identification methodology proposed in this work should be extended. The use of other types of data and other criteria should be considered (as done by Jacques [jac1] using the logLS cost function or Liu using time domain data). Other optimization algorithms, using more efficiently the computed gradient information, could be considered for the few cases where the proposed approach does not give satisfactory results. Finally, a model optimization in the normal mode form could be useful to improve some results. Using the sensitivity approach developed in section 3.4, this optimization would also provide a better evaluation of the sensitivity of identified parameters (in the normal mode parametrization) to measurement noise and consequently a better analysis of the quality of results.

Multiple SIMO tests lead to multiple measurements of all the parameters (modal observabilities, frequencies, and non-diagonal normal mode damping matrix) which can be used to obtain both better averaged properties and estimates of uncertainty linked to the identification process. Truly MIMO tests, which were not possible here for purely material reasons, would allow even more accurate measurements by reducing the inconsistencies generally present between different SIMO tests. Using MIMO frequency response function estimators (e.g. ref. [cob1]) providing completely consistent estimates of the MIMO transfer function matrix, all the elements of the parametric modal model (poles, complex

modal observabilities and controllabilities) would have to be adjusted for at least as many transfer functions as actuators, which should provide much more accurate models.

In the case of the interferometer testbed, uncertainties in the model parameters depend more on the variations of the system from test to test than on noise in the measurement. As similar properties could be expected for most structures, approaches using noise models to determine parametric uncertainty (see section 3.4) may thus only be appropriate to determine the accuracy of a given identification procedure, but not for other purposes such as robust control design.

The description of uncertainty defined in this work was chosen because it allows representation of small physical changes by small uncertainties. The choice of the model states, however, appeared as an important factor, particularly for structures with high modal densities (since the size of effects on modes and transfer functions depends on the relative size of the physical modifications and the modal frequency separation). Furthermore, the number of uncertain parameters introduced is too large to be practically used by current robust controller synthesis methods (see the reviews done Refs. [howl, hag1]). It would thus be more efficient to define measures of the closed-loop robustness directing the selection dominant parametric uncertainties for which controllers would be specifically designed.

Theoretically, the determination of a non-proportional damping matrix allows a characterization of the spatial distribution of damping mechanisms. It should be investigated whether such studies can be practically done with sufficient precision, but a spatial characterization of damping, particularly if extended to cases with gyroscopic damping, could have many analysis and design applications.

For the generation of accurate FE models, the present work has highlighted the importance of accurate local models. The tools available for analyses of the influence of local parameters on the global system response exist, but are quite cumbersome to use. An effort should be made to create FE codes allowing such analyses more easily. The update of local model parameters using system tests is used because the data is available (such tests are performed to validate the FE models and usually show discrepancies which the user tries to correct). The method presented alleviates the difficulties linked to "pairing" inaccurate modes and allows efficient computations through the use of the reanalysis approach. Little work was done on determining the most appropriate optimization strategy. However, this would only become a major limitation if simultaneous update of large numbers of parameters was envisioned, which is clearly not realistic since the uniqueness and thus the validity of the solution can currently only be demonstrated for cases with few parameters.

Appendix

The MIT/SERC Interferometer Testbed

7.1. Testbed Description

The Interferometer Testbed (IT) (see ref. [bla1]) is an integral part of SERC's research program in Controlled Structure Technology (CST). This 3.5 meter testbed shown in Figure 7.1 was designed to capture the essential configuration, physics and performance metric of an actual high precision observatory spacecraft. The testbed serves as a focus for a research program on the different phases of controlled structural system design, and provides a versatile environment for the demonstration and comparison of active and passive CST developments. In particular, the relevance and effectiveness of the methods developed in this research was demonstrated using experimental data measured on the IT.

The 3.5 meter naked tetrahedral truss structure was first tested, and the modeling problems linked to this configuration of the system have been previously addressed in references [bal5, bal4]. The present work considers the phase B testbed, where the four science plates supporting the laser metrology system for the optical tetrahedron have been added. In Figure 7.1, the so-called "fourth" vertex (see Figure 7.3 for component names) supporting the laser source and other measurement optics is in the center (back). The three other vertices of the optical tetrahedron (called science plates A-C) are placed at different positions along the span of the truss legs non-adjacent to the fourth vertex.

The fourth vertex bucket initially contributed significant dynamics around 130 Hz, but these where pushed at higher frequencies by the addition of two stiffeners, so that the flexibility of the fourth vertex is not relevant to the presented study of modes in the 20-60 Hz band (the inertia is very important but could be accurately measured).

The science plates are 6.3 mm thick aluminum plates. They are linked to the truss by U-shaped aluminum elements screwed to the plate and the truss ball joints (three of the screws are clearly visible in the figure). On the main plate, the mirror assembly (on the right) is composed of a back plate, stiffened by two "legs" (made of the aluminum tubes used for the basic truss), which supports a three axis active cat-eye mirror mount (two the piezoelectric stacks between white plastic screws are visible in the figure) and a triax accelerometer block (on the back of the plate).

The mass of the science plates is a significant fraction of the total testbed mass (approximately 4 % each) and modes in the 20-60 Hz range are very sensitive to errors in the mass estimate (see section 4.4). The stiffness of in particular the main plate and the links plate/truss also have a strong influence on the response.

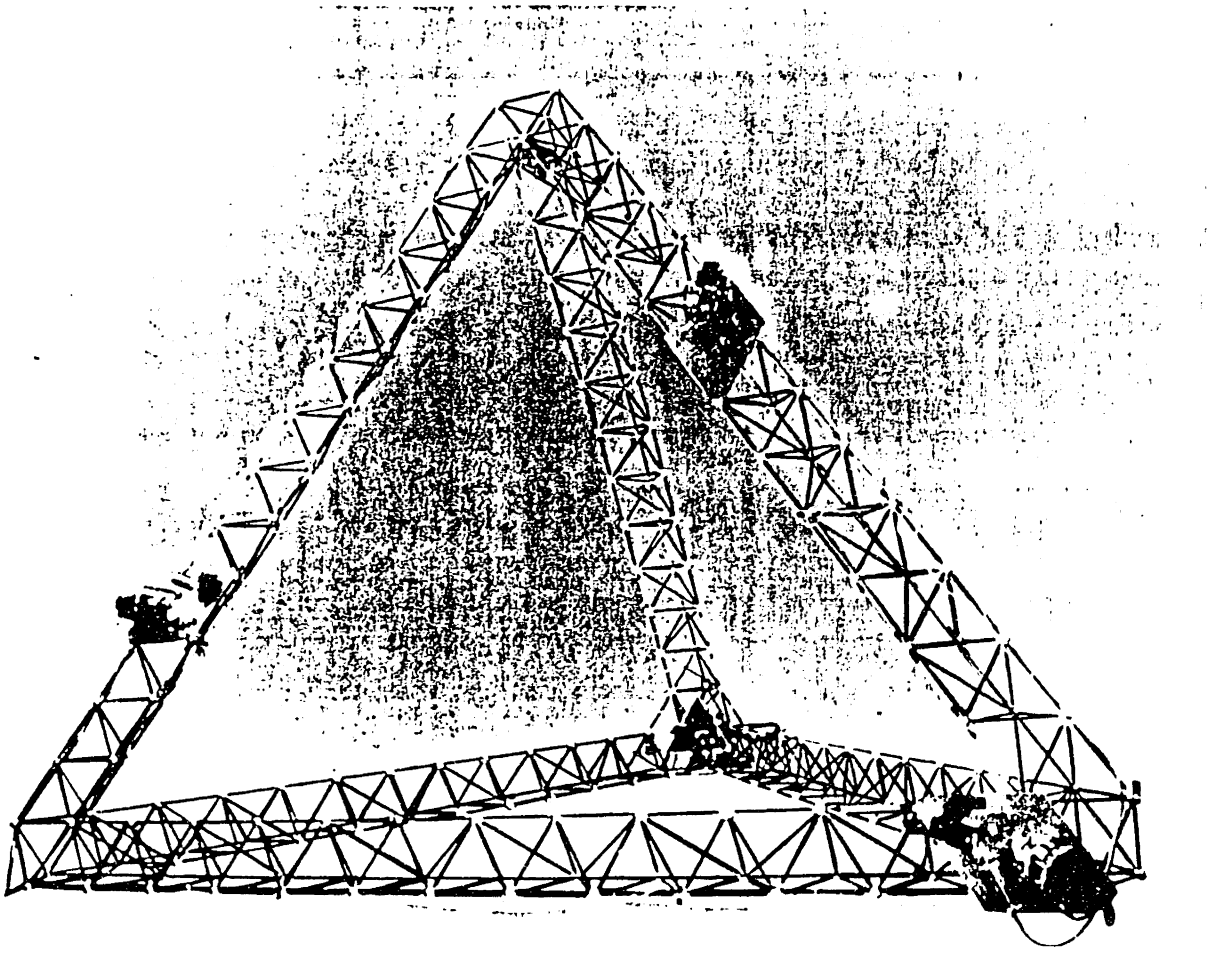

Figure 7.1: The MIT/SERC interferometer testbed.

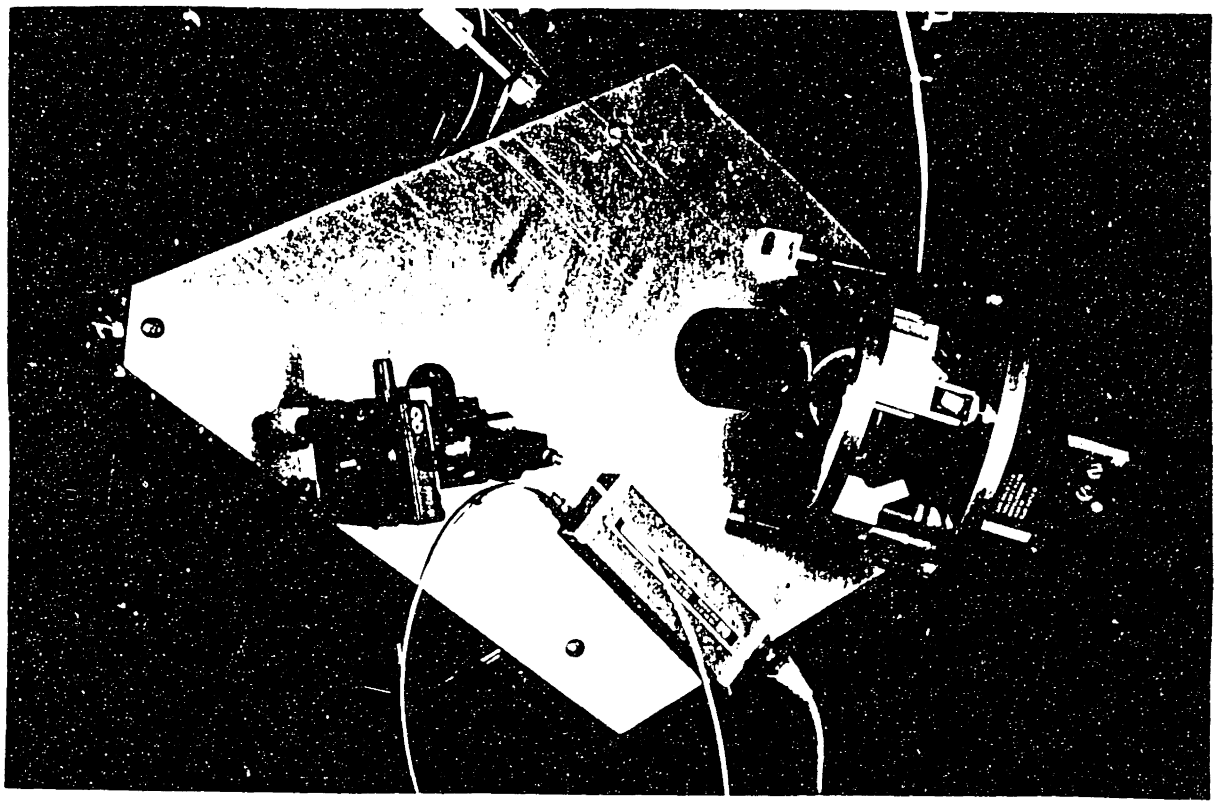

Figure 7.2: Science plate C of the interferometer testbed.

7.2. Modal Test of the Interferometer Testbed

The present work uses experimental data from a modal test performed on the IT. An external shaker, suspended from a crane so as to obtain very low shaker resonances and linked to the truss by a flexible stinger, was used to test the response. Six tests were performed with the shaker placed on each of the truss legs (indicated as ▲ in Figure 7.3). As part of the modal test, the response of 27 accelerometers distributed on the truss (indicated as ● in Figure 7.3), the force input, and the collocated acceleration (at the stinger attachment point to the truss) were measured. The same 27 accelerometers were used for the 6 tests, which allowed, as presented in this thesis, a good correlation of the identified modeshapes for the different tests (see Chapter V).

The measurements were obtained using broadband inputs, but it was verified for a few frequency response functions, that a sine sweep only resulted in minor changes.

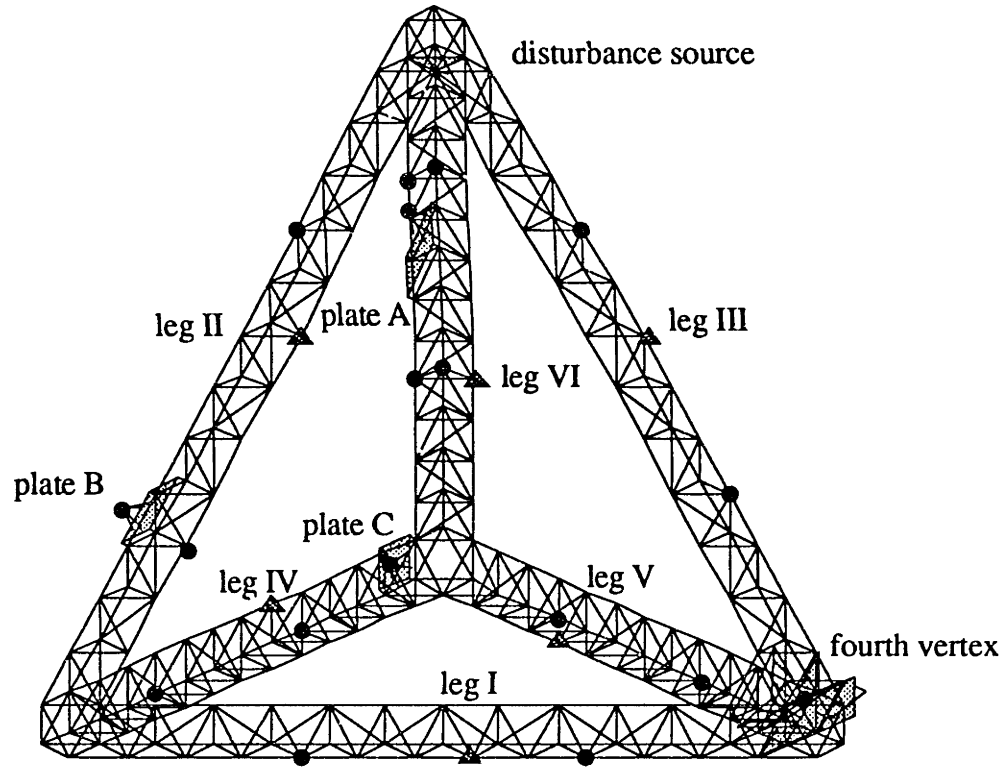

Figure 7.3: Configuration of the MIT/SERC interferometer testbed modal test. ● accelerometer locations, ▲ shaker locations. Leg numbering scheme and science plate names.

7.3. ABOUT THE FINITE ELEMENT MODEL

The FE model of the IT truss uses one beam element per strut with axial stiffness adjusted to represent both the joint and the actual strut stiffness. As discussed in Refs. [bal5, bal4], the axial stiffness used (7.77 N/μm for the short struts and 11.2 N/μm for the long struts) were derived from independent component tests including the actual joint flexibility. The test/model agreement for the naked truss was found to be extremely good with less than 2% error in the frequency prediction for all the modes up to 150 Hz.

The different science components (fourth vertex, three science plates, disturbance source) were modeled separately with 3 node (18 DOF) plate elements, beam elements to represent different instruments and concentrated mass/inertia where needed.

Different models are available on SERC's computer network in the directory */home2/interf/adina*. The subdirectory */plates* contains

- commented *.m* files with the descriptions (geometry, mass distribution, formatted input for the ADINA finite element code [adi1]) of all the components added to the bare truss model (fourth vertex, three science plates, disturbance source).
- component models ADINA input *name.in* and output *name.out* files for verification of the local models.

After a verification of the validity of the component models (check that the low frequency modes are not significantly modified by a mesh refinement of the model), the component models and the truss model were linked using beam elements to connect the truss and component attachment points.

The latest model is *inter5* (the *.in* file contains the ADINA input, the *.out* the ASCII output, the *.mat* the frequencies and modeshapes in MATLAB format, the *_mx.mat* the skyline mass and stiffness matrices, the *_mxi.mat* the decomposition of the stiffness matrix for uses in static response computations).

Between *inter4* and *inter5* the masses of the science plate were corrected and the link stiffness were adjusted (see section 4.4 for details on this update). *inter40* is a version of *inter4* with the initial (very stiff) link stiffness.

The input files are commented, so that any other information can be easily obtained when scanning the file. For uses of the FE model for predictions of the response, control design, etc., the Toolbox [bal2] for MATLAB developed as part of this research provides a complete set of routines.

Bibliography

adi1 ADINA, *A Finite Element Program for Automatic Dynamic Incremental Nonlinear Analysis*, ADINA R&D, Inc., 71 Elton Avenue, Watertown, MA, 02172, USA

all1 Allemang, R.J., Brown, D.L., "Multiple-Input Experimental Modal Analysis - A Survey," *IJEAMA*, 1986, **1**-1, pp. 37-44

all2 Allemang, R.J., Rost, R.W., Brown, D.L., "Dual Input Estimation of Frequency Response Functions for Experimental Modal Analysis of Aircraft Structures," *IMAC*, 1982

alv1 Alvin, K.F., Peterson, L.D., Park, K.C., "A Method for Determining Minimum-order Mass and Stiffness Matrices from Modal Test Data," *IMAC*, 1993, pp. 1287-1293

alv2 Alvin, K.F., Park, K.C., "A Second Order Structural Identification Procedure via State Space Based System Identification," *AIAA Guidance, Navigation and Controls Conference*, Hilton Head, SC, 1992

and1 Anderson, E., *Actuator Placement for Structural Control*, MIT PhD thesis, 1993

and2 Anderson, E.H., Hagood, N.W., "The Effect of Model Error on Actuator and Damper Placement for Structural Control," *SPIE North American Conf. on Smart Structures and Materials*, Albuquerque, NM, 1993

ard1 Arduini, C., "Spectral Condensation: A New Concept in Numerical Structural Dynamic Analysis," *ESA Journal*, 1984, **8**

arr1 Arruda, J.R.F., "Objective Functions for the Nonlinear Curve Fit of Frequency Response Functions," *AIAA Journal*, **30**-3, pp. 855-857

ath1 Athans, M., *Multivariable Control Systems*, MIT Course 6.233-6.234 (course notes)

bal1 Balmès, E., Crawley, E.F., "Designing and Modeling Structural Dynamics for Control. Applications to the MIT/SERC interferometer testbed," *1st SMAC conference*, Nice (France), December, 1992

bal2 Balmès, E., "Experimental and Analytic Structural Dynamic Analysis Toolbox," *(A toolbox for MATLAB™, The MathWorks, Inc., 21 Eliot St., South Natick, MA 01760, USA)*, 1993

bal3 Balmès, E., "Integration of Existing Methods and User Knowledge in a MIMO identification algorithm for structures with high modal densities," *IMAC*, 1993, pp. 613-619

bal4 Balmès, E., "A Finite Element Updating Procedure Using Frequency Response Functions. Applications to the MIT/SERC Interferometer Testbed," *IMAC*, 1993, pp. 176-182

bal5 Balmès, E., *Modeling Structural Dynamics for Control*, MIT MS Thesis, SERC report #14-91, 1991

bal6 Balmès, E., "High Modal Density, Curve Veering, Localization: A Different Perspective on the Structural Response," *Journal of Sound and Vibration*, 1993, **161**-2

bar1 Baruch, M., "Optimization Procedure to Correct Stiffness and Flexibility Matrices Using Vibration Tests," *AIAA Journal*, **16**-11

ben1 Bennighof, J.K., Meirovitch, L., "Eigenvalue Convergence in the Finite Element Method," *Int J. Num. Meth. Eng.*, **23**, pp. 2153-2165

ber1 Berman, A., "System Identification of Structural Dynamic Models - Theoretical and Practical Bounds," *AIAA-Paper 84-0929*, 1984

ber2 Berman, A., Nagy, E.J., "Improvement of a Large Analytical Model Using Test Data," *AIAA Journal*, 1983, **21**-8, pp. 1168-1173

ber3 Berger, H., Ohayon, R., Barthe, L., Chaquin, J.P., "Parametric Updating of Finite Element Model Using Experimental Simulation - A Dynamic Reaction Approach," *IMAC*, 1990, pp. 180-186

ber4 Berman, A., Flannelly, W.G., "Theory of Incomplete Models of Dynamic Structures," *AIAA Journal*, 1971, **9**-8

ber5 Bert. C.W., "Material Damping: An Introductory Review of Mathematical Models, Measures, and Experimental Techniques," *Journal of Sound and Vibration*, 1973, **29**-2, pp. 129-153

ber6 Berman, A., Wei, F.S., Rao, K.V., "Improvement of Analytical Dynamic Models Using Modal Test Data," *SDM, AIAA-80-0800-CP*, 1980

bis1 Bisplinghoff, R.L., Ashley, H., *Aeroelasticity*, Dover Pub. Co., New York, 1975

bla1 Blackwood, G., Miller, D.W., Jacques, R., Hyde, T., "MIT Multipoint Alignement Testbed: Technology Development for Optical Interferometry," *SPIE conference on Active and Adaptative Optical Systems*

bou1 Bouhaddi, N., Cogan, S., Fillod, R., "Dynamic Substructuring by Guyan Condensation, Selection of the Master DOF," *IMAC*, 1992

bow1 Bowden, M., Dugundji, J., "Joint Damping and Nonlinearity in Dynamics of Space structures," *AIAA Journal*, 1990, **28**-4, pp.740-749

bre1 Breitbach, E., "A Semi-Automatic Modal Survey Test Technique for Complex Aircraft and Spacecraft Structures," *Proc. IIIrd Testing Symposium*, Frascati, Italy, 1973, pp. 519-529

cae1 Caesar, B., "Updating System Matrices Using Modal Test Data," *IMAC*, 1987

car1 Carne, T.G., Mayes, R.L., Levine-West, M.B., "A Modal Test of a Space-truss for Structural Parameter Identification," *IMAC*, 1993, pp. 486-494

cau1 Caughey, T.K., "Classical Normal Modes in Damped Linear Dynamic Systems," *ASME J. of Applied Mechanics*, 1960, pp. 269-271

che1 Chen, W.J., Pierre, C., "Exact Linear dyanmics of Periodic and Disordered Truss Beams : Localisation of Normal Modes and Harmonic Waves," *SDM*, 1991

cob1 Cobb, R.E., Mitchell, L.D., "A Method for the Unbiased Estimate of System FRF in the Presence of Multiple Correlated Inputs," *IJEAMA*, 3-4, pp. 123_128

coll Collins, D.J., Hart, G.C., Hasselman, T.K., Kennedy, B., "Statistical Identification of Structures," *AIAA Journal*, 1974, **12**-2

copl Coppolino, R.N., Stroud, R.C., "A Global Technique for Estimation of Modal Parameters from Measured Data," *IMAC*, 1986, pp. 674-681

cral Craig, R.R. Jr., Kurdila, A.J., Kim, H.M., "State-Space Formulation of Multi-Shaker Modal Analysis," *IJEAMA*, 1990, **5**-3

cra2 Craig, R.R. Jr., Blair, M.A., "A Generalized Multiple-Input, Multiple-Ouptut Modal Parameter Estimation Algorithm," *AIAA Journal*, **23**-6, pp. 931-937

cra3 Craig, R. R. Jr., "A Review of Time-Domain and Frequency Domain Component Mode Synthesis Methods," *Int. J. Anal. and Exp. Modal Analysis*, 1987, **2**-2, pp. 59-72

crol Crowley, J.R., Rocklin, G.T., Hunt, D.L., Vold, H., "The Practical Use of the Polyreference Modal Parameter Estimation Method," *IMAC*

cro2 Crowley, S.M., Allemang, R.J., "Applications of the Polyreference Technique in Experimental Modal Analysis," *IMAC*, 1984, pp. 111-117

elrl Elred, M.S.,Lerner P.B., Anderson, W.J., "Higher Order Eigenpair Perturbations," *AIAA Journal*, 1992, **30**-7, pp. 1870-1876

ewil Ewins, D.J., *Modal Testing: Theory and Practice*, John Wiley and Sons, Inc., New York, NY, 1984

flal Flanigan, C.C., "Correlation of Finite Element Models Using Mode Shape Design Sensitivity,"

fla2 Flanigan, C.C., "Test/Analysis Correlation of the STS Centaur Using Design Sensitivity and Optimization Methods," *IMAC*, 1987

fla3 Flanigan, C.C., "Test-Analysis Correlation Using Design Sensitivity and Optimization - Does It Work ?," *SAE paper 0148-7191/88/1003-1531*

fral Franklin, G.F., Powell, J.D., Workman, M.L., *Digital Control of Dynamic Systems*, Addisson-Wesley, 1990

frel Freed, A.M., "A Comparison of Test Analysis Model Reduction Methods," *IMAC*, 1990

full Füllekrug, U., "Survey of Parameter Estimation Methods in Experimental Modal Analysis," *IMAC*, 1987

gill Gilpin, K., *Identification of a Lightly Damped Structure for Control/Structure interaction*, MIT MS thesis, SERC #11-91, 1991

girl Girard, A., "Modal Effective Mass Models in Structural Dynamics," *IMAC*, 1991, pp. 45-50

gorl Gordis, J.H., "An Analysis of the Improved Reduced System (IRS) Model Reduction Procedure," *IMAC*, 1992

grel Gregory, C.Z. Jr., "Reduction of Large Flexible Spacecraft Models Using Internal Balancing Theory," *J. Guidance*, 1984, **7**-6

hagl Hagood, N.W., *Cost Averaging Techniques for Robust Control of Parametrically Uncertain Systems*, MIT PhD Thesis, 1991

hasl Hasselman, T.K., Chrostowski, J.D., Ross, T.J., "SSID/PDAC Theoretical Manual (Version 1.0)," *NASA TR-91-1152-1*, 1991

hej1 He, J., Ewins, D.J., "Compatibility of Measured and Predicted Vibration Modes in Model Improvement Studies," *AIAA Journal*, 1991, **29**-5, pp. 798-803

hob1 Ho, B.L., Kalman, R.E., "Effective Construction of Linear State-Variable Models from Input/Output Data," *Proc. of 3rd Annual Allerton Conference on Circuit and System Theory*, 1965, pp. 449-459

how1 How, J.P., *Robust Control Design with Real Parameter Uncertainty using Absolute Stability Theory*, MIT PhD Thesis, 1993

hun1 Hunt, D.L., Vold, H., Peterson E.L., Williams, R., "Optimal Selection of Excitation Methods for Enhanced Modal Testing," *SDM*, 1984

ibr1 Ibrahim, S.R., "Computation of Normal Modes from Identified Complex Modes," *AIAA Journal*, 1983, **21**-3, pp. 446-451

ibr2 Ibrahim, S.R., "Dynamic Modeling of Structures from Measured Complex Modes," *AIAA Journal*, 1983, **21**-6, pp. 898-901

ibr3 Ibrahim, S.R., D'Ambrogio, W., Salvini, P., Sestieri, A., "Direct Updating of Nonconservative Finite Element Models Using Measured Input Output," *IMAC*, 1992, pp. 202-210

imr1 Imregun, M., Ewins D.J., "Realization of Complex Mode Shapes," *IMAC*, 1993, pp. 1303-1309

jac1 Jacques, R.N., Miller D.W., "Multivariable Model Identification From Frequency Response Data," *Submitted to the 32nd CDC*, 1993

jeo1 Jeong, W.B., Nagamatsu, A., "A New Method for Poly-Reference Identification of Modal Parameters in Modal Testing," *IMAC*, 1992, pp. 153-158

jua1 Juang, J.N., Pappa, R.S., "An Eigensystem Realization Algorithm (ERA) for Modal Parameter Estimation and Model Reduction," *J. Guidance, Control, and Dynamics*, 1985, **8**-5, pp. 620-627

jua2 Juang, J.N., Pappa, R.S., "Effects of Noise on Modal Parameters Identified by the Eigensystem Realization Algorithm," *J. Guidance, Control, and Dynamics*, 1986, **9**-3, pp. 620-627

kab1 Kabe, A.M., "Stiffness Matrix Adjustment Using Mode Data," *AIAA Journal*, **23**-9

kal1 Kalman, R.E., "Irreductible Realizations and the Degree of a rational Matrix," *J. SIAM*, 1965, **13**-2

kam1 Kammer, D.C., "Optimum Approximation for Residual Stiffness in Linear System Identification," *AIAA Journal*, 1988, **26**-1, pp. 104-112

kar1 Karlov, V.I., *Physical Identification for Control of Flexible Structures*, Short course notes, 1993

kim1 Kim, K.O., "Improved Calculations of Modal Design Sensitivities," *Computers & Structures*, 1990, **29**-5, pp. 777-780

law1 Lawson, C.L., Hanson, R.J., *Solving Least-Squares Problems*, Prentice-Hall, 1974

lee1 Lee, H.G., Dobson, B.J., "The Direct Measurement of Structural Mass, Stiffness, and Damping Properties," *Journal of Sound and Vibration*, 1991, **145**-1, pp. 61-81

leu1 Leuridan, J.M., Brown, D.L., Allemang R.J., "Direct System Parameter Identification of Mechanical Structures with Application to Modal Analysis," *SDM, AIAA-82-0767 CP*, 1982

lev1 Levine-West, M.B., "High Fidelity Predictive Models of Structures on Orbit," *Report No. JPL D-10113*

lev2 Levine-West, M.B., Salama, M.A., "Mode localization experiments on a ribbed antenna," *Proceedings of the AIAA/ASME/ASCE/AHS 33nd SDM Conference*, Dallas, Texas, 1992

lew1 Lewis, R.C., Wrisley, D.L., "A System for the Excitation of Pure Natural Modes of Complex Structures," *J. Aero. Sci.*, 1950, **17**, pp. 705-722

lia1 Liang, Z., Tong. M., Lee, G.C., "Complex Modes in Damped Linear Dynamic Systems," *IJEAMA*, 1992, **7**-1, pp. 1-20

lie1 Lieven, N.A.J., Ewins, D.J., "A Proposal for Standard Notation and Terminology in Modal Analysis," *IJEAMA*, 1992, **7**-2, pp. 151-156

lie2 Lieven, N.A.J., Ewins, D.J., "Spatial Correlation of Modeshapes, The Coordinate Modal Assurance Criterion (COMAC)," *IMAC*, 1988

lie3 Lieven, N.A.J., Ewins, D.J., "Error Location and Updating of Finite Element Models Using Singular Value Decomposition," *IMAC*, 1990

lin1 Link, M., "Survey of Selected Updating Procedures," *Proc. 11th Int. Seminar on Modal Analysis Workshop*, Leuven, Belgium, 1986

lin2 Lin, C.S., "Location of Modeling Errors Using Modal Test Data," *AIAA Journal*, 1990, **28**-9

lju1 Ljung, L., "System Identification: Theory for the User," *Prentice-Hall*, 1987

lms1 , *LMS CADA-X, the System Solution for Integrated Test Laboratory*, Leuven Measurements & Systems, Leuven, Belgium, 1990

lon1 Longman, R.W., Juang, J.N., "A Variance Based Confidence Criterion for ERA Identified Modal Parameters," *AAS Paper 87-454*

lyo1 Lyon, *Statistical Energy Analysis of Dynamic Systems*, The MIT Press

mac1 Maciejowski, J.M., *Multivariable Feedback Design*, Addison-Wesley, 1989

mas1 Masters, B.P., Crawley, E.F., "Multiple Degree of Freedom Force-State Component Identification," *SDM, AIAA Paper 93-1654*, 1993

mei1 Meirovitch, L., *Elements of Vibration Analysis*, MacGraw-Hill Inc., New York, N.Y., 1989

mor1 Morand, H.J.-P., "A Modal Hybridization Method For The Reduction of Dynamic Models in the Medium Frequency Range," *personal communication*

nat1 Natke, H.G., Robert, D., "Determination of Normal Modes from Indentified Complex Modes," *Z. Flugwiss. Weltraumforsh.*, 1985, **9**-2, pp. 82-88

nef1 Nefske, D.J., Sung, S.H., "Power Flow Finite Element Analysis of Dynamical Systems," *Winter Annual Meeting of ASME NCA-Vol 3*

nie1 Niedbal, N., "Advances in Ground Vibration Testing Using a Combination of Phase Resonance and Phase Separation Methods," *2nd Int. Symp. on Aeroelasticity and Struc. Dynamics*, Aachen, FRG, 1985, pp. 523-528

oca1 O'Callahan, J.C., "Comparison of Reduced Model concepts," *IMAC*, 1990

oca2 O'Callahan, J.C., Avitabile, P.A., Riemer, R., "System Equivalent Reduction Expansion Process (SEREP)," *IMAC*, 1989, pp. 29-37

oca3 O'Callahan, J.C., "A Procedure for an Improved Reduced System," *IMAC*, 1989

ott1 Otte, D., Debille, J., Leuridan, J., "Enhanced Force Vector Appropriation Methods for Normal Mode Testing," *IMAC*, 1993, pp. 1310-1316

ozg1 Ozguven, H.N., Imregun, M., Kuran, B., "Complex Modes Arising from Linear Identification of Non-Linear Systems," *IMAC*, 1991, pp. 644-650

pap1 Pappa, R.S., Ibrahim, S.R., "A Parametric Study of the ITD Modal Identification Algorithm," *Shock and Vibration Bulletin*, 1981, **43**-7, pp. 43-72

pap2 Pappa, R.S., "Close-Mode Identification Performance of the ITD Algorithm," *AIAA Paper 83-0878*

par1 Park, K.C., Alvin, K.F., Perterson, L., "Extraction of Undamped Normal Modes and Nondiagonal Modal Damping Matrix from Damped System Realization Parameters," *SDM*, 1993

par2 Park, S., Park, I., Ma, F., "Decoupling Approximation of Nonclassicaly Damped Structures," *AIAA Journal*, 1992, **30**-9, pp. 2348-2351

paz1 Paz, M., "Dynamic Condensation," *AIAA Journal*, 1984, **22**-5, pp. 724-727

ray1 Rayleigh, J.W.S., *The Theory of Sound*, Dover Publications, New-York, NY, 1945 (reedition)

red1 Red-Horse, J.R., et al., "System Identification of the JPL Micro Precision Interferometer Truss: An Overview," *Proceedings of the third International Conference on Adaptive Structures*, San Diego, CA, 1992

ric1 Richardson, M.H., Formenti, D.L., "Global Curve Fitting of Frequency Response Measurements Using the Rational Fraction Polynomial Method," *IMAC*, 1985, pp. 390-397

ric2 Richardson, M.H., Formenti, D.L., "Parameter Estimation from Frequency Response Measurements using Rational Fraction Polynomials," *IMAC*, 1982

roy1 Roy, N.A., Girard, A., Bugeat, L.P., Bricout, J.N., "A Survey of Finite Element Updating Methods," *Proc. of Int. Symp. on Environmental Testing for Space Programs- Test Facilities and Methods, ESTEC*, Noordwwijk, The Netherlands, June 26-29, 1990

roy2 Roy, N.A, Girard, A., Bugeat, L.-P., "Expansion of Experimental Modeshapes - An Improvement of the Projection Technique," *IMAC*, 1993, pp. 152-158

roy3 Roy, N.A., Girard, A., Bugeat, L.-P., "Enhanced Updating of Finite Element Models Using an Energy Approach," *IMAC*, 1993, pp. 655-660

roy4 Roy, N.A., Girard, A., Dupuis, P.-E., "A Direct Energy Approach for Updating Finite Element Models," *IMAC*, 1991, pp. 51-57

ses1 Sestieri, A., Ibrahim, S.R., "Analysis of Errors and Approximations in the Use of Modal Coordinates," *IMAC*, 1993, pp. 425-433

sha1 Shaw, J., Jayasuria, S., "Modal Sensitivities for Repeated Eigenvalues and Eigenvalue Derivatives," *AIAA Journal*, 1992, **30**-3, pp. 850-852

shi1 Shih, C.Y., Tsuei, Y.G., Allemang, R.J., Brown, D.L., "A Frequency Domain Global Parameter Estimation Method for Multiple Reference Frequency Response Measurements," *IMAC*, 1988, pp. 389-396

ske1 Skelton, R.E., "A Tutorial On Model Error Concepts In Control Design,"

smi1 Smiley, R.G., Patrick, G.B., Sohaney, R.C., "Automated Methods of Frequency Response Function Quality Evaluation," *IMAC*, 1986, pp. 107-112

smi2 Smith, S.W., Beattie, C.A., "Simultaneous Expansion and Orthogonalization of Measured Modes for Structure Identification," *Dynamics Specialist Conference*, AIAA-90-1218-CP, 1990, pp. 261-270

spa1 Spanos, J.T., Mingori, D.L., "Newton Algorithm for Fitting Transfer Functions to Frequency Response Measurements," *Journal of Guidance, Control, adn Dynamics*, 1993, **16**-1

tin1 Ting, J.M., Crawley, E.F., "Characterization of Damping of Materials and Structures from Nanostrain Levels to One Thousand Microstrain," *AIAA Journal*, 1992, **30**-7, pp. 1856-1863

tri1 Triantafyllou, M.S., Triantafyllou, G.S., "Frequency coalescence and mode localization phenomena: a geometric theory," *Journal of Sound and Vibration*, 1991, **150**, pp. 485-500

web1 Webster, M.S., *Modelling Beam-Like Space Trusses with Nonlinear Joints with Application to Control*, MIT PhD Thesis, 1991

wei1 Wei, F.S., "Mass and Stiffness Interaction In Analytical Model Modification," *AIAA Journal*, **28**-9

wei2 Wei, M.L., Allemang, R.J., Brown, D.L., "Real Normalization of Measured Complex Modes," *IMAC*, 1987

wil1 Williams, R., Vold, H., "Multiphase-Step-Sine Method for Experimental Modal Analysis," *IJEAMA*, 1986, **1**-2

wil2 Williams, R., Crowley, J., Vold, H., "The Multivariate Mode Indicator Function in Modal Analysis," *IMAC*, 1985, pp. 66-70

you1 Yousuff, A., Skelton, R.E., "Controller Reduction by Component Cost Analysis," *IEEE Transactions on Automatic Control*, 1984, **29**-6

zan1 Zang, L., Kanda, H., Lembregts, F., "Some Applications of Frequency Domain Polyreference Modal Parameter Identification Method," *IMAC*, 1986, pp. 1237-1245

zha1 Zhang, Q., Lallement, G., "New Method of Determining the Eigensolutions of the Associated Conservative Structure from the Identified Eigensolutions," *IMAC*, 1985, pp. 322-328